NBSIR 86-3353 (NASA)

A Comparative Study of the Structure and Mechanical Properties of Polyethylene Films Used in Heavy Lift Balloons

F. Khoury
J.M. Crissman
J.D. Barnes
B.M. Fanconi
H.L. Wagner
C.M. Guttman
J.R. Maurey
C.A. Harding
L.H. Boiz

NBSIR 86-3353 (NASA)

A COMPARATIVE STUDY OF THE STRUCTURE AND MECHANICAL PROPERTIES OF POLYETHYLENE FILMS USED IN HEAVY LIFT BALLOONS

F. Khoury
J.M. Crissman
J.D. Barnes
B.M. Fanconi
H.L. Wagner
C.M. Guttman
J.R. Maurey
C.A. Harding
L.H. Bolz

Abstract

Aspects of the mechanical properties and structure of three types of polyethylene film (I, III and Bl) used by NASA in helium filled heavy lift balloons have been investigated and compared. An additional film (Fl) which has as yet not been used in heavy lift balloons was also studied. The following are among the features which have been investigated:- Biaxial deformation behavior under inflation at 23°C and -73°C, biaxial creep under inflation at 23°C and -73°C, tensile properties at 23°C of unoriented specimens prepared by compression molding multilayers of the films, film shrinkage upon melting. The preferred orientation characteristics of the crystalline regions in the films were determined from pole figures coupled with small angle x-ray diffraction data. The possible morphological origins of the various orientation characteristics exhibited by the films are discussed with reference to three 'model' orientations and combinations thereof. Numerical simulations of the experimental pole figures were attempted in an effort to compare differences in orientation among the films quantitatively. Finally, the following features which had been determined for films I, III and Bl in a previous study have been determined for the 'newer' film Fl: Chain branching, molecular weight and molecular weight distribution, intrinsic viscosity, melting/crystallization, density/crystallinity, birefringence, and tensile properties at 23°C (uniaxial extension in the machine and transverse directions).

(ii)

Table of Contents

A. Introduction

The work described in this report is a continuation of an earlier exploratory study [1] sponsored by the National Aeronautics and Space Agency (NASA). It is part of an ongoing investigation undertaken by NASA to determine the causes of the catastrophic failure of helium filled 'heavy-lift' balloons in which the helium is contained by low density polyethylene film. The thickness of the polyethylene film is usually in the range 13μm - 25μm. The balloons are used to raise instrument payloads of up to about 2500 Kg to elevations of over 35 Km for various research projects. The capacity of the balloons at float attitude can be as large as 1.16×10^6 cu. meters.

Since 1980 there has been an increased incidence of catastrophic balloon failures during ascent at elevations between 12 Km and 18 Km where the ambient temperature is about -70°C. The causes of the increased failures of this type from 1980 to the present as compared to the performance of balloons prior to 1980 have been elusive. Limitations inherent in the design characteristics of the balloon coupled with trends to higher payloads, inadvertent flaws which may occur in the process of balloon assembly (construction), and changes in the raw polymer and/or the processing conditions used in the production of the polyethylene films prior to and since 1980 are among the possible causes investigated by NASA.

The overall purpose of our earlier study [1] and the present investigation was to examine and compare various aspects of the structure and mechanical properties of proprietary films representative of those used in heavy lift balloons prior to and since 1980. The goal was to determine whether there are significant differences among the films which are not covered by present acceptance criteria and which might have a bearing on film

performance in balloons. Five films (denoted I, II, III, V and B1) were investigated in our earlier study [1]. Film III was the only one representative of films used prior to 1980. Similarities as well as differences between various features of the films were identified.

Among the close similarities between the films were the following: methyl group content ($2CH_3$/100 carbon atoms, crystallinity (46.2%-48.2%), and peak melting temperature (105.5°C-107.1°C). All the films were negatively birefringent, i.e., $n_M-n_T<0$ where n_M and n_T are the refractive indices parallel to the machine (M) and transverse (T) directions respectively. The birefringence was low in all the films and fell in the range - 0.0009 to -0.0019. Wide angle x-ray diffraction patterns obtained with the x-ray beam parallel to M, T and N (normal to the film) respectively indicated that there were qualitative similarities between the preferred orientations of the microcrystalline regions in the various films. The indications were (1) that the a-axis tended to be oriented preferentially parallel to the MT plane and preferentially parallel to M in that plane, and (2) that the b-axis tended to be preferentially oriented parallel to the NT plane and preferentially parallel to N in that plane. A possible working model consistent with these features was suggested.

Differences among the films were revealed in two main features, namely in the molecular weights of the polymer, and in the balance of the strain to break behavior in the machine direction relative to that in the transverse direction. Thus, films II and III (the latter being the only one representative of films used prior to 1980) had relatively higher molecular weights than the other films, whereas B1 film had the lowest. Concerning mechanical properties, films II, III and IV exhibited in uniaxial deformation experiments higher average extensions to break parallel to T than

to M at both 23°C and -70°C. In contrast, the average strains to break in both directions for film I were essentially the same at 23°C, furthermore at -70°C the extension to break was higher in the M direction. The extension to break behavior of the Bl film in the M relative to the T direction was similar to that of the film I at 23°C and to that of films II, III and IV at -70°C. In addition, although the average strain to break in the M and T directions in each of the five films met the NSBF specification that the strain should not be less than 250% in both the M and T directions at -70°C, film III was the only one for which none of the measurements fell below 250%.

The present study has been limited to three of the films investigated previously, namely films I, III, and Bl, to which an additional film (denoted Fl) of interest to NASA has been added. Films I and Bl are currently used in heavy lift balloons. Film III is, as pointed out earlier, representative of films used prior to 1980. Film Fl has not been used by NASA in heavy lift balloons. Various characteristics which had been previously [1] determined for films I, III and Bl were also determined for the Fl film during the period covered by the present report. The results which include measurements of molecular weight distribution, intrinsic viscosity, density (crystallinity), peak melting temperature, birefringence, and uniaxial (tensile) deformation behavior at 23°C are presented collectively in Appendix B. The main part of the report is concerned with a description and discussion of the results of a study of the following aspects of the films:-

- Deformation behavior of the four films under inflation (bubble geometry) at 23°C and -73°C.

- Uniaxial deformation behavior at 23°C of unoriented specimens made by melting and remolding films I, III and Bl.

- Shrinkage upon melting.

- A more detailed study and comparison of the preferred orientation characteristics of films I, III and B1. Our earlier probings [1] have been supplemented with the determination of (200), (020) and {110} pole figures. In addition, small angle x-ray diffraction (SAXD) patterns have been obtained with the x-ray beam parallel to the N, M and T directions respectively. Similar pole figure and SAXD data were obtained for the additional F1 film.

The results (covered in the present and in our earlier investigation [1]) on films I, III, B1 and F1 are examined collectively at the end of this report.

B. <u>Mechanical Properties</u>

(1) <u>Biaxial Deformation Behavior Under Inflation at 23°C and -73°C:</u>
<u>Deformation to Near Failure (Films I, III, B1 and F1)</u>

The first experiments described below are the inflation behavior of the four films at room temperature (23°C). It is instructive however before describing the results to dwell in more detail on some of the characteristics of the inflation experiment which we mentioned in our previous report [1]. For this purpose we have chosen as an example the inflation of a thin sheet of dentaldam rubber which remains stable (under inflation) up to quite large deformations. Prior to inflation, two sets of twelve ink marks, six on either side of the pole spaced 0.50 cm apart, were placed at 90° to one another on the flat sheet. The sheet was then inflated until its shape was approximately that of a hemisphere. While the sheet was held at constant internal pressure, the strain was determined between each set of adjacent marks. The results are presented in Fig. 1 where the numbers shown represent the percent strain between each set of marks. Over that portion of the sheet where marks were placed the strain, in a radial direction, varies by a factor of about two. Close to the pole the deformation is equalbiaxial, whereas it

approaches pure shear near the clamping ring. The average strain over the portion of the surface examined was 67 percent. In anticipation of procedures to be described below in Section B2 it should be noted that the deformation is fairly uniform over the central region out to about the third mark away from the pole (radius of 1.5 cm).

Following the same procedures used for the rubber, a series of experiments was carried out at 23°C on samples from each of the four films under investigation. In each case the film was inflated slowly to a condition just short of failure, at which point the pressure was reduced slightly to prevent rupture. The strain was then determined between each adjacent set of marks. The results are summarized in Figs. 2-5. For film I (Fig. 2) one can see that in the region between the first set of marks on either side of the pole, where the deformation is greatest, both the machine and transverse directions have deformed an equal amount (145%). A similar result was observed for film B1 shown in Fig. 3 where in the region nearest the pole it can be seen that this film has also deformed almost an equal amount in both the machine (170%) and transverse (180%) directions. No evidence of necking was observed in either of these two films. Based upon the inflation experiments both films I and B1 appear to be rather well balanced.

In comparison, film III showed a different behavior, as can be seen in Fig. 4. As the inflation progressed a necked region appeared (Fig. 4a), which upon further inflation widened in the transverse direction and eventually several other necks appeared in the region of the pole. Upon reaching the condition shown in Fig. 4b just prior to rupture, it can be seen that in the region of the pole the film has elongated significantly more in

the transverse direction (200%) than in the machine direction (135%). Film

F1   also exhibited necking as can be seen in Fig. 5a. In this case

however, the neck formed well away from the pole between the second and third

marks. The necked region lies along the same direction as that found for

film III. Upon further inflation the condition shown in Fig. 5b was reached.

For this film it was observed that once the neck developed almost all of the

subsequent deformation occurred within the small region between the first

and second marks on the right hand branch.

A comparison of the results obtained from the bubble inflation

experiment with those obtained from the elongation at break measurements in

uniaxial extension (Table 10, reference [1], and Appendix B in this report

for film F1) is presented in Table 1. The values shown represent the ratio

of the deformation in the transverse direction to that in the machine

direction. For films I, III, and B1 the values shown from the inflation

experiment represent the average value of the strain between the first set of

marks on either side of the pole at a condition just prior to rupture. In

the case of the film F1 the neck did not occur in the region nearest the

pole. Therefore the value shown was obtained by taking the average

deformation over all twelve marks in both the machine and transverse

directions. For the most part there is a rather good correlation between the

two sets of results which indicate that films I and B1 are well balanced

with regard to deformation in the machine relative to the transverse

directions, whereas films III and F1 are unbalanced.

Inflation experiments were also done at -73°C using a low temperature

chamber which will be described in Section B(3). In this case no

determination of the strain was made over localized areas of the film since

such measurements were found difficult to perform inasmuch as opening the

chamber even for a short period of time resulted in rapid heating and failure of the film specimen. Films from each category were visually monitored as the pressure was gradually increased up to the point of failure. As was the case at room temperature, films I and B1 deformed uniformly and did not exhibit necking, whereas multiple necks appeared in film III, and a single neck occurred in film F1. The occurrence, both at 23°C and -73°C, of multiple necks in film III and of a single neck in the film F1 would appear to be a characteristic feature which distinguishes these two films from one another.

(2) Biaxial Creep Under Inflation at 23°C (Films I, III, B1)

The creep behavior under inflation of films I, B1, and III was examined at 23°C. In the previous subsection it was observed that in the case of the dentaldam rubber under inflation the deformation was fairly uniform in the region near the pole out to about the third mark away from the pole. This condition was also true for the polyethylene films provided necking did not occur and the strain did not exceed about 20 percent. In the present set of experiments ink marks were placed 1.5 cm on either side of the pole, one set parallel to the machine direction, and one set parallel to the transverse direction. The measured strain, then, represents an average strain over the 3.0 cm diameter portion of the bubble surrounding the pole. Three sets of experiments were done in which the applied pressure was set at one of three values (5000, 7000, and 9000 Pa). The thickness of each specimen was determined from the thickness profile data provided by NASA. Since the film thickness varied from .0017 cm to .0021 cm the pressure was adjusted in such a manner than each film specimen was normalized to a   thickness of .0018 cm (0.7 mil). [i.e., the pressure was adjusted such that $P(h/.0018)$ was set equal to one of the three values noted above, h being the actual profile thickness.] The results are shown in Fig. 6. It can be seen that, with one

exception, the behavior of all three films at each level of applied pressure is nearly indistinguishable. The one specimen of the B1 film tested at 9000 Pa extended to a strain of nearly 0.70 before failure. No great significance should be assigned to the relatively higher deformation exhibited by this specimen. Its different behavior may be associated with the large variations in thickness in the specimen. At pressures higher than 9000 Pa all of the films, immediately upon application of the pressure, extended to a strain of more than 0.25 and the bubble quickly became unstable losing its spherical symmetry. In these instances, the films either ruptured or took the shape of a <u>tube</u> at which point the experiment was stopped.

In Table 2 are shown values of the true stress (in the region of the pole) as determined using the following equation:

$$\sigma_T = \frac{P}{2} \frac{r}{h} \lambda^2 \tag{1}$$

where P is the inflation pressure, r is the radius of curvature, h is the initial film thickness, and λ is the stretch ratio given by $\lambda = 1 + \varepsilon$, ε being the strain. Equation (1) is applicable only in the region near the pole, and when the material remains stable and the strain does not exceed 0.40 - 0.50. The left hand numbers in the columns in Table 2 represent the minimum value and the right hand number the maximum value of stress measured during each creep experiment. It can be seen that at the lower levels of pressure the experiment is one in which the true stress remains essentially constant, a consequence of the fact that very little creep is occurring with time. At a given pressure there is very little difference in the values of true stress from film to film. From these measurements it would appear that all of the films remain stable under inflation at 23°C for values of true stress up to about 16 MPa.

(3) Biaxial Creep Under Inflation at -73°C (Films I, III, B1)

A low temperature chamber was assembled to examine the low temperature creep behavior of the films using the same bubble geometry described in the previous two sections. The low temperature chamber was equipped with a window to allow visual access to the film with a cathetometer. The window was constructed from two sheets of PMMA separated by a narrow air gap. In order to prevent frosting of the window, a steady flow of dry air was maintained across the outer surface of the window. The chamber was cooled by maintaining a pool of liquid N_2 in a foil pan covering the bottom of the chamber. A proportional controller and heating element was used to supply sufficient heat to hold the temperature constant at the desired temperature in the vicinity of the film. The air inside the chamber was circulated by means of a blower which had a capacity of 1.53 cubic meters per minute (54 cubic feet per minute). As a matter of convenience, all the low temperature measurements were carried out at -73°C. At -73°C, it was found that in the vicinity of the inflation apparatus the temperature could be held constant to within ±1°C over a period of from one to two hours.

Since no suitable extensometer was available and the chamber could not be opened at low temperature once the experiment was started, the strain had to be estimated by indirect means. This was accomplished by first carrying out a set of experiments at 23°C in which both the radius of curvature of the bubble and the strain were determined directly. The radius of curvature was determined by measuring the height of the bubble with a cathetometer. The strain was monitored by placing two sets of marks on the film, one set along the machine direction and one along the transverse direction. Each set of marks was separated by 3 cm (1.5 cm on either side of the pole). The film was then inflated by increasing the pressure in small

steps. Between each step increase in pressure the radius of curvature and the strain in both directions were measured. The two measures of strain were then averaged and the resulting strain was plotted versus the radius of curvature. Such a plot is shown in Fig. 7 where the filled circles correspond to the experimentally determined values. The crosses shown in Fig. 7 are the values of the strain which would be predicted using the known values of the radius of curvature and by assuming that the deformation is uniform over the surface of the bubble. It can be seen that, for this special case where the marks have been placed approximately 40 percent of the distance from the pole to the clamping ring, the predicted values of strain determined using only the radius of curvature agree rather well with the actual data determined using the marks.

A set of creep experiments was then carried out at -73°C in which the strain was determined from the radius of curvature measurement. An additional assumption being made is that the inflation characteristics of the bubble at -73°C do not differ significantly from those at 23°C. The results for films I, III, and Bl are presented in Fig. 8. It can be seen that all three films show a quite similar behavior. At a pressure of 34 kPa all three films failed in three minutes or less. On the other hand, at 33 kPa none of the films failed after one hour. Table 3 indicates the range of values of the true stress at each level of applied pressure at -73°C. These data indicate that all three films remain stable over a period of time of one hour or more for values of true stress at least as high as 50 MPa.

We have also examined the situation in which the film is subjected to a deformation history under inflation at 23°C and then is cooled slowly to -73°C at constant pressure. One piece of film from each of the three film categories was inflated gradually at 23°C until it reached an average strain

of 20%. While holding the pressure constant the bubble was then cooled

slowly to -73°C and the radius of curvature, r, monitored as a function of

decreasing temperature. For all three film categories it was found that the

radius of curvature did not change appreciably during cooling, and, within

experimental error, remained constant throughout the experiment. Upon

reaching -73°C the internal pressure was quickly doubled and, again, no

change was observed in r for any of the three films. The maximum value of

the true stress observed in all three experiments was about 49 MPa, which

from Table 3 can be seen to be still below the levels required for failure to

occur after one hour.

(4) Tensile Properties at 23°C of Unoriented Specimens Prepared by the

Compression Molding of Multi-Layers of Films I, III and B1

In work summarized in reference [1], it was shown that clear differences

exist between the various films in their molecular weight and molecular weight

distribution. Comparison of the normalized chromatograms revealed that

film III contained a larger proportion of high molecular weight species

than did the other films and, on a relative basis, had the highest M_w,

followed in decreasing order of molecular weight by film I and film B1.The

question remains open as to whether specific information can be derived

concerning the contribution of differences in molecular weight and molecular

weight distribution between the films to differences in their mechanical

performance. The influence which differences in molecular weight can have on

the tensile creep behavior of initially unoriented high density linear

polyethylenes was illustrated in our earlier report [1]. Ideally,

determination of the effect of molecular weight differences per se on the

mechanical properties of the oriented films would require the availability of

films made from resins of different molecular weights but processed under

identical conditions (i.e., same blow ratio, draw ratio, cooling history, etc.). In the absence of such films, we have, as background information, examined the possible effect of differences in the molecular weight of the polymer in films I, III, and B1 by studying the mechanical properties of specimens of the unoriented material. The specimens were prepared by remolding material taken from each of the three categories of film.

Specimens of the unoriented polymer were prepared as follows: sheets of film were folded repeatedly into stacks approximately four centimeters on a side, each containing 128 layers of film. The stacks were then placed in a press and subjected to a pressure of 100 MPa (14500 psi) in order to remove as much air as possible and to fuse the layers together. The stacks were next placed in a mold which consisted of an aluminum frame and two one centimeter thick aluminum plates coated with teflon[*]. The frame had an opening 15 cm long and 5 cm wide. The press was preheated to 130°C and the mold placed in the press under light contact pressure for a period of ten minutes. The pressure was then increased to 15 MPa (≡2200 psi) and the heat turned off. The mold was cooled in the press at a rate of about 1°C per minute to a temperature below 75°C before removal from the press. Sheets prepared in this manner were nominally about one millimeter thick. Specimens were cut from each sheet using one of two different dies depending upon the experiment to be done.

In the first set of experiments the tensile behavior was investigated under conditions of constant rate of clamp separation at 23°C. For this purpose, the same specimen geometry chosen earlier to study the film

---

[*]Certain commercial materials and equipment are identified in this paper in order to specify adequately the experimental procedure or materials. In no case does such identification imply recommendation or endorsement by the National Bureau of Standards, nor does it imply necessarily the best available for the purpose.

specimens was used [1]. As before, the gage length was set at 0.60 cm. The specimen width was 0.30 cm. One of two different test machines was used depending upon the properties to be measured. Determination of the yield stress and strain at yield were accomplished using the same servo controlled hydraulic test equipment described in our previous report [1]. However since this machine has only 15 cm of actuator travel, it was found necessary to determine the strain at break and tensile strength using a screw driven machine having a much greater crosshead travel. In all cases the rate of clamp separation was the same as that used in our previous study of the film specimens (991% per minute).

Table 4 presents the test results for 23 specimens taken from the three categories of film. A minimum of three specimens was used to determine each property. Table 5 summarizes the average values for each property. It is apparent from Table 5 that, on average, there is no great difference in properties from film to films. Film III does exhibit the greatest average value for tensile strength while the film Bl exhibits the smallest value, although the observed differences cannot be considered large. The values for the elongation at break require special attention. The values quoted represent the elongation at break as determined from the clamp separation, and do not represent the actual elongation within the original gage section, as is discussed in the following paragraph.

For two specimens, marks were placed 0.5 cm apart on the initial exposed portion of the specimen. During the course of the experiment the stretching process was interrupted periodically long enough to measure both the clamp separation and the distance between marks. This process was continued until fracture occurred. Fig. 9 shows a plot of the strain, as determined from the clamp separation, versus the strain, as determined using the marks. It can

be seen that at strains up to $\varepsilon=4$ ($\lambda=5$) essentially all of the deformation occurs within the gage section. However, at yet greater elongations, a significant amount of material is being drawn out from inside the clamps. By the time the clamp separation has reached a stretch ratio, λ, of 15 it is estimated that up to 60% of the total amount of material exposed has been drawn out of the clamps. Therefore the values shown should be scaled down by a factor of two, or more. In spite of the fact that a considerable amount of material is drawn out of the clamps during this type of experiment, it appears that, on average, all three categories of film behave in a very similar manner. The stress-strain curves for all three categories of film were identical in character and it is unlikely that, among them, any significant differences in behavior occurred in the original gage section alone.

Comparison of the results for the remolded material (Tables 4 and 5) with similar tests done on specimens of the balloon films at 23°C (Tables 10a and 12 in reference [1]) shows the following similarities and differences. The yield stress is slightly higher for the initially unoriented remolded materials than for the films. On the other hand, the tensile strength for the three categories of balloon film is about 65% higher than for the corresponding unoriented samples.

In addition to the experiments described above the creep behavior of the remolded material at 23°C was examined. Of particular interest in this regard is the region of deformation beyond the yield point where cold drawing and ultimate fracture occur. Under these conditions, any contributions to the cold-drawing and failure behavior due to differences in molecular weight may become more apparent than in tests carried out a constant rate of clamp separation. For this phase of the work a different specimen geometry was

used from that used for the constant rate of clamp separation experiments.
In the present case dumbbell shaped specimens having a straight section 3.0
cm long and a width of approximately 0.30 cm were cut with a die from the
compression molded sheets. Marks were placed on the specimen approximately
2.5 cm apart, and during the creep experiment the length within the gage
section was monitored with a cathetometer. For each type of film creep
experiments were done at each of three levels of applied stress, 10, 12.5,
and 15 MPa.

The results are presented in Fig. 10. All three specimens tested at 10
MPa did not fail after 10^4 minutes at which point the experiment was stopped.
For the other six specimens the times to failure are given in Table 6. At
the higher levels of applied stress (12.5 and 15.0 MPa) it was found
necessary to apply the load rather slowly initially in order to prevent rapid
heating of the specimen and premature failure. It can be seen from Fig. 10
that all six specimens tested at these stresses attained nearly all of their
ultimate elongation in a time less than one minute. For the three specimens
tested at 10 MPa there are some differences in the early time creep behavior
($<10^2$ minutes). However, no great significance should be placed on these
differences, since factors such as how rapidly the specimen was loaded or
local variations in thickness may well influence the early time behavior.

As it relates to differences in molecular weight or molecular weight
distribution, the most significant differences in behavior among the
unoriented specimens remolded from the three types of films would appear to
be in the maximum strain attained prior to failure or termination of the
experiment. In Table 7 a comparison of the maximum strain attained prior to
failure is shown for the three materials at 23°C. Since the three specimens
tested at 10 MPa did not fail within 10^4 minutes, the values shown are those

corresponding to a creep time of 10^4 minutes. At all three levels of applied stress it can be seen that film III material exhibits the least amount of creep, while the film Bl exhibits the greatest amount prior to failure. We have previously reported [1] that the film III had the highest molecular weight and film Bl the lowest. It appears, then, that the differences in molecular weight observed between the various categories of film are reflected in the creep behavior of the unoriented remolded materials, the order being the higher the molecular weight the lesser the amount of creep prior to failure, as might have been expected. The small differences observed in the tensile strength may also be a manifestation of the differences in molecular weight.

(C) Film Shrinkage

By virtue of affecting the orientation characteristics and fine texture in films, differences in draw ratio and blow ratio used in film production are reflected in differences in the shrinkage behavior which the films exhibit in the transverse relative to the machine direction upon melting. Examination of shrinkage behavior is thus a useful, if qualitative, method for probing the existence and possible origins of intrinsic differences between films due to processing, even though interpretation of the results in the present case is complicated by differences among the proprietary films in the molecular characteristics (molecular weight distribution, branching) of their constituent polymers.

Film shrinkage is a highly temperature-sensitive and time-dependent phenomenon and care must be taken to ensure that each piece of film is exposed to the same melting conditions. In the present case pieces of film were cut into the shape of a square 6 cm on a side with adjacent sides parallel to the machine and transverse directions respectively. Each piece

of film was floated on hot silicon oil (140°C) for a period of ten minutes.
After ten minutes each piece of film was removed from the oil, allowed to
cool, and was then wiped dry. The new dimensions were recorded and the ratio
of the initial to final dimensions calculated (R_M or R_T). At least two
pieces of film from each roll or sheet were examined. The four films of
primary interest in the present phase of this investigation are the films I,
III, B1, and F1. However, for completeness we have included shrinkage data
obtained on films II and IV which were investigated in the earlier phase of
our work [1]. Films I - IV and B1 all exhibit peak melting points near
107°C, whereas the F1 melting peak is in the 122-123°C range (see Appendix
B(d)).

Shrinkage data for 58 pieces of film from the six different categories
of film are presented in Table 8. The results for films I - IV are presented
in chronological order of manufacture. Since four of the specimens of film
III were taken from rolls of a thicker 1.0 cm cap material, their shrinkage
results will be excluded from further consideration in this discussion. The
average values of the shrinkage ratios for each film category are given in
Table 9. Excluding for the moment the film F1, it can be seen that overall
the films IV and II show the greatest shrinkage in the machine direction, I
and B1 the least, and film III falls intermediate. In the transverse
direction films I and B1 show the greatest shrinkage, IV and II the least,
and film III again is intermediate. In both the machine and transverse
directions the shrinkage of film III represents very closely the average
value of the shrinkage ratio for all five film categories. All five films
show significantly greater shrinkage in the machine direction than in the
transverse direction.

Film Fl shows quite different shrinkage characteristics from any of the other five films (see Table 9). On average, the Fl film shrinks by a factor of nearly 12 in the machine direction, whereas in the transverse direction it has actually expanded. These results would suggest that of the four films of primary concern in this phase of the work (I, III, Bl, and Fl) the Fl film is the most highly oriented in the machine direction (see later Section D).

(D) Orientation Characteristics in Films I,III, Bl and Fl

Supplementing our earlier limited probing of the orientation characteristics of the crystalline regions in films I, III, Bl and other films, we present and compare in this section the results of the determination of the (200) (020) and {110} pole figures exhibited by these three films as well as film Fl, coupled with a consideration of the small angle x-ray diffraction patterns obtained from these films with the x-ray beam parallel to the M, T and N film directions. This section of the report is divided into three subsections. Some experimental details, as well as a brief description of the method of displaying the pole intensity distributions relative to the M, T and N directions in the pole figures, are given in subsection D(i). The pole figure and small angle x-ray diffraction results are described, compared and discussed in Section D(ii) with reference to "working models" the elements of which are described in detail in Appendix A. Surface replicas of film Fl were briefly examined. Some limited observations derived from this examination are included at the end of Section D(ii). Finally, the results of an initial attempt to simulate numerically the (200) and (020) pole intensities of the four films are presented in subsection D(iii).

(i) Experimental Details and Description of Pole Figure Projections

The specimens prepared for the pole figure determinations consisted of

about 70-90 parallel strips of film stacked on top of one another (total

thickness ~1.5 mm). The sides of the strips which coincided with the M and T

directions, were ~8 mm and 1.5 mm long respectively. A special procedure using

templates was used to facilitate the stacking of the strips as closely

parallel to one another [i.e. with as small deviations in the M, T and N

(normal) directions as possible throughout the stack].

An automated wide angle x-ray diffractometer, equipped with a four

circle goniometer sample holder, and operated in the transmission mode was

used to determine the (200), (020) and {110} pole figures of the polyethylene

films. A pole figure is a planar projection of the dispositions of the

points of intersection (poles) of the normal to a given type of

crystallographic plane [e.g. (200)] in the variously oriented

microcrystalline regions of the specimen with the surface of a reference

hemisphere which is concentric with the center of mass of the specimen. An

example of the azimuthal equidistant projection of the reference hemisphere

in relation to the M, T and N directions of a film specimen is shown in

Fig. 11 in which M is normal to the plane of the projection. The radial

lines and concentric circles in Fig. 11 are, respectively, the projections of

the longitudes ϕ and the latitudes χ of the hemisphere. The spherical

coordinates (ϕ,χ) specify the disposition of a pole on the surface of the

hemisphere and hence the spacial orientation of the corresponding plane

normal relative to the M, T, and N axes in the specimen. The coordinates of

plane normals which are parallel to M, T and N are as follows: Parallel to

M: $(\chi=90°)$; parallel to T: $(\phi=0°, \chi=0°)$ or $(\phi=\pm180°, \chi=0°)$; parallel to N:

$(\phi=90°, \chi=0)$ or $(\phi=-90°, \chi=0)$.

Briefly, the experiments consist of systematically varying the orientation of the specimen relative to the incident monochromatic x-ray beam (Cu Kα radiation) and recording the relative intensities of the x-rays diffracted by a chosen type of crystallographic plane [e.g (200)] at each orientation. The corresponding variations in intensity of the (200) poles as a function of (ϕ, χ) are displayed in projection in the corresponding pole figure as contour lines which serve to delineate the spatial distribtuion in the orientation of the (200) plane normals relative to M, T and N in the specimen.

Small angle x-ray diffraction (SAXD) patterns were recorded photographically using a pin-hole collimated small angle camera. Ni filtered CuKα radiation from a rotating anode source was used. The same specimens as those used in the pole figure experiments were used to obtain the SAXD patterns with the x-ray beam parallel to either N or T. For obtaining SAXD patterns with the beam parallel to M the template system mentioned above was used to prepare stacks of parallel film strips which were ~1.5 mm thick in the M direction. Details concerning some experiments involving optical and electron microscopy are given later in the text.

(ii) Results and Discussion

The (200), (020) and {110} pole figures exhibited by films I, III, B1 and F1 are shown in Figs. 12-15 respectively. To facilitate comparisons between the films their respective (200) pole figures are shown together in Fig. 16; their (020) and {110} pole figures are shown in Fig. 17 and Fig. 18. The plotting of the relative pole intensity variations which are delineated by eight contour lines (#s 1-8) in each pole figure is based on a scale consisting of nine intensity levels. The intensity increment between each successive level is equal to $\Delta I/9 = (Imax-Imin)/9$, where Imax

and Imin are respectively the highest and lowest intensities among all the data recorded for each pole figure. Intensities in the lowest level range i.e. Imin to (Imin+ΔI/9) are circumscribed by contour line #1. Intensities in the highest level i.e. in the range Imin+8ΔI/9 to Imax are circumscribed by contour line #8. The intensities in regions bounded by contour lines #4 and #5 fall in the range (Imin+4ΔI/9) to (Imin+5ΔI/9), and so on. The values of the ratio (Imax/Imin) for each pole figure are listed in Table 10. For ease in identifying the regions of highest pole intensity (circumscribed by contour line #8), these have been shaded in Figs. 12-15, and Figs. 16-18. The SAXD patterns taken with the x-ray beam parallel to each of the M, T and N reference directions in the films are shown in Figs. 19-23.

Many considerations which guided the examination and interpretation of the pole figures and SAXD patterns listed above and discussed below stem from, or were prompted by, several previous studies on polyethylene films [2-11]. The papers of Lustig and Lindenmeyer [6] and Keller and Machin [7] were particularly relevant in this connection. Various limitations and/or ambiguities in interpretation which arise in the determination of preferred orientations (in low density polyethylene films having broad orientation distributions) from pole figures, are discussed in both papers [12]. In addition, the discussion by Keller and Machin [7] on the origins of the manifestation of preferred a-axis orientation parallel to the machine direction (M) in polyethylene films, and the row structure models they proposed in this connection, were particularly pertinent as will become evident later.

It is evident from even a cursory examination of the pole figures in Figs. 16-18 that the (200), (020), and {110} pole intensity distributions in film F1 differ significantly from those in Films I, III and B1. In what

ensues we shall first examine and compare the results on Films I, III and Bl collectively, and speculate (with reference to the "Transcrystalline" and "Row" type model orientations described in Appendix A) on the possible morphology-related origins of both the preferred orientation characteristics these three films exhibit in common (see later), and the differences which distinguish film Bl from films I and III. We shall then discuss film Fl.

Confining ourselves at this stage to a consideration of only the (200) and (020) pole figures exhibited by films I, III and Bl (Figs. 16-17), the following similarities between these films may be noted: - First, the (200) pole intensity in each film is higher in and close to the MT plane (ϕ=0°,χ=0° to 90°; ϕ=±180°,χ=0 to 90°) than elsewhere, and is highest in and close to the M direction (χ=90°). Second, the (020) pole intensity is higher in and close to the NT plane (ϕ=0° to ±180°,χ=0°) than elsewhere and is highest in and close to the N direction ($\phi = \pm90°$, $\chi = 0°$). These similarities confirm the qualitative deductions we reported previously [1] concerning the preferred a-axis and b-axis orientations in the films. However, the pole figures reveal the additional information that the distribution of the a-axis orientation [i.e. the (200) poles] in the NT plane in the Bl film differs from those in Films I and III, the latter two films being closely similar to one another.

Thus, as can be seen from Fig. 16 the decrease in the (200) pole intensity in the MT plane from the maximum at and around M to its lowest level (in that plane), which is at and around T in all three films, is relatively less pronounced in film Bl than in films I and III. The ratios of the (200) pole intensity at and around M to the intensity at and around T are as follows: Film Bl (1.3_6-1.5_4), film I (2.3-3), and film III (2.2-2.7).

Note in this connection (Fig. 16) that the (200) pole intensity at T is in the range (Imin+5ΔI/9) to (Imin+6ΔI/9) in film B1, whereas it is in the range (Imin+2ΔI/9) to (Imin+3ΔI/9) in films I and III.

As for the distributions of the (020) the pole intensities in the NT plane (see Fig. 17), the decrease in pole intensity from the maximum at and around N to its lowest level (in that plane), which is at and around T, is relatively more pronounced in the B1 film than in films I and III. The ratios of the (020) pole intensity around N to the intensity around T for the three films are as follows: - Film B1 (3.2-4.4), films I and III (2-2.4). Note that the intensity around T is in the range Imin to (Imin+ΔI/9) in film B1, whereas it is in the range (Imin+2ΔI/9) to (Imin+3ΔI/9) in films I and III.

We turn at this juncture to a preliminary consideration of the possible origins of the above mentioned preferred a-axis and b-axis orientation characteristics which films I, III, and B1 display in common relative to M, T, and N. Referring to the idealized (200) and (020) pole figures corresponding to the three morphologically-based "preferred-orientation-models" described in Appendix A (Figs. 26, 28, 29), and shown collectively in Fig. 30, the following may be noted:-

First, superposing the (200) pole figure of the lamellar Transcrystalline orientation upon that of either the Row(ac), the Row(a), or the combined Row(ac) and Row(a) orientations, yields in each case a composite pole figure in which the overall (200) pole intensity distribution is qualitatively consistent with those exhibited by the three films (I, III, B1, Fig. 16): i.e. the (200) pole intensity in the composite pole figure is higher in the MT plane than elsewhere, and is highest parallel to M. As can be seen from Fig. 30, the later feature is due specifically to any one, or a

combination of both, Row orientations. The ratio of the (200) pole intensity
at M relative to that at T, would be expected to be relatively smaller the
lower the content of Row oriented as compared to Transcrystalline oriented
material in a film. Accordingly, the appreciably smaller value of this ratio
of intensities in film Bl as compared to films I and III, considered in terms
of the composite working model(s) envisaged above, would indicate that Bl
contains relatively less Row oriented material.

Second, returning to Fig. 30, it can be seen that superposing the (020)
pole figure of the lamellar Transcrystalline orientation upon that of either
(or a combination of both) Row orientations yields a composite pole figure in
which the overall (020) pole intensity distribution is qualitatively
consistent with those exhibited by the three films (Fig. 17): i.e. the (020)
pole intensity in the composite pole figure is higher in the NT plane than
elsewhere, and is highest parallel to N, the latter feature being due
specifically to the Transcrystalline orientation. The fact that the ratio of
the intensity at N to that at T in the (020) pole figure of film Bl is
appreciably larger than in films I and III indicates that there is
relatively less Row oriented than Transcrystalline material in Bl than in
films I and III.

In summary, comparisons of both the (200) and the (020) pole figures
exhibited by films, I, III and Bl in terms of a working model based on the
Transcrystalline and Row orientations described in Appendix A, lead to the
same conclusion, namely that film Bl contains relatively less Row oriented
relative to material with Transcrystalline orientation as compared to Films I
and III. With this apparent difference among the three films as background,
we proceed below to a discussion of their {110} pole figures (Fig. 18) and

the small angle x-ray diffraction patterns (Figs. 19-21, 23). Both sets of results have a bearing on the question of whether the Row oriented material in the composite model is predominantly Row(ac) or Row(a).

We start with a consideration of a composite orientation model consisting of the Transcrystalline and Row(a) orientations. As pointed out in Appendix A these two types of orientation correspond respectively to the 'populations' in the hypothetical model envisaged in our previous report [1] (Figs. 25a, b, reference [1]). It can be readily surmised from Fig. 30 that superposing the idealized {110} pole figures corresponding to these two preferred orientations yields a composite {110} pole figure exhibiting maximum pole intensity where the arcs due to the Transcrystalline orientation overlap the circle (latitude $\chi=34°$) due to Row(a) material, i.e. at ($\phi=+90°$, $\chi=34°$) and ($\phi=-90°$, $\chi=34°$). This is in close agreement with the dispositions of the regions of highest pole intensity (circumscribed by contour line #8) in the {110} pole figures of the three films (I, III, and B1) shown in Fig. 18. However, referring again to Appendix A and Fig. 30, the combination of the Transcrystalline, Row(a), and Row(ac) {110} pole figures also yields maximum pole intensity at ($\phi=+90°$, $\chi=34°$) and ($\phi=-90°$, $\chi=34°$) where all three pole distributions overlap. Indeed, it is not possible to distinguish with any certainty from the maxima in the experimental {110} pole figures or from the character of the overall spread of pole intensities in these figures whether the films contain, in addition to the Transcrystalline component, only Row(a) or both Row(a) and Row(ac) oriented material. A distinction between these alternatives can however be made from a consideration of the small angle x-ray diffraction patterns exhibited by the films. This is discussed below.

As pointed out in Appendix A the fine textures associated with the Transcrystalline, Row(ac) and Row(a) models are lamellar in character as is the case in the spherulitic structures from which they derive. At the local level crystalline lamellae and disordered layers are packed in an alternating fashion (see Fig. 25c) with the c-axis in the lamellar crystals oriented normal to the plane of the lamellar crystals as well as to the intervening disordered layers. It is the essentially regular (periodic) variation in electron density associated with this layer-like disposition of crystalline and disordered regions at the local level which gives rise to discrete x-ray diffraction maxima at small angles. As additional background we point out that the conditions for diffraction to occur are governed to a good approximation [16] by Bragg's law, $\lambda = 2d\sin\phi$ where $\lambda = 0.15418$ nm is the wavelength of incident x-rays, d=interlamellar spacing, θ=angle between the incident x-ray beam and the plane parallel to the alternating crystalline and disordered layers.

For an interlamellar spacing which is usually of the order of 10 nm $\theta \leq 0.44°$, i.e. only those regions in the films in which the crystalline and intervening disordered layers are almost parallel to the x-ray beam will given rise to discrete diffraction. Since the c-axis in the crystalline lamellar layers is oriented preferrentially at right angles to these layers as well as to the intervening disordered layers, it follows that only the locally layered regions in the films in which the c-axis is oriented at close to 90° to the incident beam will be appropriately oriented to diffract. This criterion will be used below for comparing the observed SAXD patterns with those which would be expected based on the respective preferred c-axis orientation characteristics (relative to M, T and N) in the Transcrystalline, Row(ac) and Row(a) models and combinations thereof.

The small angle x-ray diffraction patterns (Figs. 19-21) obtained from the three films exhibit the following features. The patterns obtained with the x-ray beam parallel to N, Figs. (19-21)a, exhibit a diffuse but nonetheless distinguishable diffraction ring which is more intense in the M direction than in the T direction. This latter feature is however perceptively less pronounced in the Bl film than in films I and III as can be seen in Fig. 23 where the patterns from these three films are shown side by side. The periodicity in the fine texture (interlamellar spacing) calculated from the angular displacement of the diffraction ring from the center of the patterns, and assuming Bragg's law, is about 15.5 nm ($\theta=0.28°$) in the three films. The patterns obtained with the x-ray beam parallel to M, Figs. (19-21)b, all exhibit a pair of diffuse diffraction spots which lie along an axis parallel to the T direction in the films. The patterns obtained with the x-ray beam parallel to T, Figs. (19-21)c, exhibit a pair of diffuse diffraction spots which lie along an axis parallel to the M direction. The periodicity in fine texture corresponding to the diffraction spots in Figs. (19-21)b, and Figs. (19-21)c is also approximately 15.5 nm. (The intense streaks which extend from the beam stop along an axis parallel to the N direction in Figs. (19-21)b,c may be attributed to interstrip scattering from the stacked strips of films which constituted the specimens used to obtain the diffraction patterns.)

Using the interrelated diffraction criteria pointed earlier concerning the orientation of the crystalline and disordered layers, and hence the c-axis in the crystalline lamellae relative to the incident x-ray beam, we proceed to an examination of the characteristics of the experimental SAXD patterns in terms of the three model orientations.

We start with a consideration of the SAXD patterns which would be expected from the three models with the incident <u>x-ray beam parallel to N.</u> In the case of the Transcrystalline model, the c-axis in the lamellae is oriented preferentially parallel to the MT plane and is randomly oriented in that plane (Table 11). Accordingly, the corresponding SAXD pattern would be expected to exhibit a diffraction ring of uniform circumferential intensity. In the case of the Row(ac) model, there is a preferential orientation of the c-axis parallel to M (Table 11). The corresponding SAXD pattern would be expected to exhibit discrete intensity maxima along an axis parallel to M. As for the Row(a) model, the c-axis is oriented preferentially in the NT plane and is randomly oriented in that plane (Table 11). In this case only those portions of the lamellar fine texture having the c-axis oriented nearly parallel to T will diffract giving rise to intensity maxima (spots) which lie along an axis parallel to T.

It follows from the considerations outlined in the previous paragraph that, with the incident x-ray beam parallel to N, the Transcrystalline and Row(a) orientations combined would yield a composite SAXD pattern exhibiting a diffraction ring (due to the Transcrystalline component) in which the intensity is greater in the T than in the M direction [due to the Row(a) component]. In contrast, the composite SAXD pattern of the Transcrystalline and Row(ac) orientations combined would exhibit a diffraction ring in which the intensity is higher in the M than in the T direction, which is what is observed experimentally in the patterns from films I, III, and Bl (see Fig. 23). In short, viewed in terms of the model orientations depicted in Appendix A, the experimental SAXD patterns taken with the x-ray beam parallel to N indicate that the predominant orientations in films I, III and Bl are the Transcrystalline and Row(ac) orientations. Although the presence of some

Row(a) oriented material is indicated by the {110} pole figures it may be reasonably concluded from the nature of the intensity distributions in the SAXD patterns shown in Fig. 23 that such material is a relatively minor component in the films.

Finally, insofar as the SAXD patterns of films I, III and B1 taken with the incident x-ray beam parallel to N are concerned, it should be noted that these patterns and the pole figure data are consistent with one another in the following respect. In describing the SAXD patterns (Fig. 23) earlier, it was pointed out that although the intensity of the diffraction ring obtained in all three cases was higher in the M than in the T direction, this feature is perceptively less pronounced in the B1 film than in films I and III. On the basis of the foregoing considerations this difference can be reasonably interpreted as indicating that there is relatively less of the Row(ac) as compared to Transcrystalline orientation in the B1 film. As indicated previously (see page 24) comparison of the (200) and (020) pole figures exhibited by the three films leads to a similar conclusion although in the latter case the alternatives among the Row oriented species were not readily distinguishable.

An examination of the SAXD patterns obtained with the incident x-ray beam parallel to M and to T in terms of the criteria discussed above shows that the dispositions of the diffraction spots along the direction parallel to T in the patterns taken with the x-ray beam parallel to M [Figs. (19-21)b], and along the direction parallel to M in the patterns obtained with the x-ray beam parallel to T [Figs. (19-21)c], are consistent with the conclusion that the dominant preferred orientations in films I, III and B1 are the Transcrystalline and Row(ac) orientations.

A summary of the various deductions discussed above concerning the preferred orientation characteristics of films I, III and B1 will be given at the end of this section, where they will be compared with the orientation characteristics of film F1 to which we turn to at this juncture.

An initial indication that the orientation characteristics of film F1 might differ substantially from those of the other three films was that it is positively birefringent [Appendix B(f)] whereas films I, III and B1 are negatively birefringent (Appendix B(f) and reference [1]). As indicated briefly earlier in this section (p. 21) and as we shall examine in more detail in what ensues, this is borne out by the pole figure as well as the SAXD results.

The (200), (020) and {110} pole intensity distributions exhibited by film F1 (Fig. 15) and the SAXD pattern taken with the x-ray beam parallel to N (Fig. 22a, Fig. 23) exhibit none of the various interrelated characteristics associated with the Transcrystalline type of preferred orientation. While, as will be pointed out in more detail below, it may be readily concluded from the pole figures, coupled with the SAXD data, that Row(ac) is the dominant preferred orientation, with Row(a) an apparent minor component, the (020) and {110} pole intensity distributions (Figs. 15b,c) exhibit deviations from the rotational symmetry about M expected of the Row(ac) and Row(a) preferred orientations. These deviations will be pointed out in due course.

As can be seen in Fig. 15a, the (200) pole intensity in film F1 is highest in and close to the M direction and the pole intensity distribution is close to being rotationally symmetric about the M direction. Both of these features are consistent with the Row(ac) and Row(a) preferred orientations. Referring in this connection to the SAXD patterns in Fig. 22, it can be seen

that the pattern obtained with the x-ray beam parallel to N (Fig. 22a) exhibits diffuse diffraction spots which lie in the M direction. This latter feature indicates that the dominant preferred orientation is Row(ac). The spacing corresponding to the spots is approximately 18 nm. The SAXD pattern taken with the x-ray beam parallel to T (Fig. 22b), which exhibits spots which also lie along M, is consistent with Row(ac) being the dominant preferred orientation.

The (020) and {110} pole intensity distributions in film F1 (Figs. 15b, c) are consistent, in their broad outlines, with Row(ac) being the dominant preferred orientation and Row(a) a minor constituent. However, the observed distributions differ from the expected rotationally symmetric ones (about the M direction) characteristic of both the Row(ac) and Row(a) orientations. In the case of the (020) pole intensity - which is highest in the NT plane than elsewhere as would be expected of both types of orientation - the observed intensity, instead of being uniform in all directions in that plane, is actually slightly higher in and around the T direction (intensity$\geq$Imin+7ΔI/9) than in the N direction (intensity in the range Imin+5ΔI/9 to Imin+6ΔI/9). The trace of contour line #7 may be noted in this connection, as well as the dispositions relative to the N and T directions of the three regions of highest intensity which are circumscribed by contour line #8. An apparently related deviation from the expected rotationally symmetric intensity distribution about M is manifested in the {110} pole figure shown in Fig. 15, as evidenced by the disposition of the broad arced regions of higher intensity circumscribed by contour lines #7 and #8 which straddle the χ=30° latitude.

It may be reasonably concluded from a consideration of the 'deviational' features of the (020) and {110} pole figures pointed out in the previous paragraph, coupled with the (200) pole figure and the small angle x-ray diffraction characteristics described earlier, that while the dominant orientation in film F1 is of the Row(ac) type (with some Row(a) orientation), there exists in the film a slight surfeit of lamellae which are oriented with their a-axis preferentially parallel to M, and with their b-axis preferentially in the NT plane but at angles of up to about 50° to T. It would follow that the c-axis in these lamellae lies in the NT plane.

In summary, the orientation characteristics exhibited by the (200), (020) and {110} pole figures and SAXD patterns of films I, III and B1 can be interpreted in terms of an idealized composite model in which it is envisaged that the films consist mainly of two "populations" of twisted lamellar crystals: namely a Transcrystalline population, and a "row-structured" population of the Keller-Machin type [7] which we refer to as Row(ac).

The Transcrystalline lamellae are oriented with their b-axis preferentially parallel to N, with the a and c axes preferentially parallel to the MT plane and randomly oriented in that plane (See Appendix A). An important feature of the Transcrystalline type of preferred orientation which should be borne in mind, and which will be discussed in connection with the mechanical properties of the films (in Section E), is the fact that the distributions of both the a and c axis orientations in the MT plane are isotropic.

In the case of the Row(ac) population in which, averaged over all the constituent lamellae, the b-axis is oriented preferentially parallel to the NT plane and is randomized in that plane, the a and c-axes are, on average, preferentially oriented parallel to the M direction (see Appendix A). The

orientation distribution of the latter axes is cylindrically symmetrical about the M direction, and is clearly anisotropic in the MT plane in contrast with the Transcrystalline population.

Comparison of the pole figures and SAXD patterns exhibited by films I, III and B1 in terms of the Transcrystalline/Row(ac) composite orientation model described above indicates that, on a relative scale, film B1 contains appreciably less Row(ac) material than films I and III, i.e. it is structurally less anisotropic with respect to the M as compared to the T directions than the latter two films in which the pole intensity distributions are closely similar to one another.

Film F1 is structurally the most anisotropic of the four films studied. The pole figure data and small angle diffraction patterns indicate that it consists predominantly of Row(ac) material. Various orientation features which are typical of the Transcrystalline orientation and which were exhibited in the pole figures of films I, III and B1, were not manifested in the pole figures of film F1.

The results of an attempt to simulate numerically the observed (200) and (020) pole intensity distributions exhibited by the four films are described in the next section (D(iii)).

We close this section with some observations derived from a brief examination of surface replicas of film F1 which confirm the row-structured nature of its fine structure. A light micrograph (phase contrast transmission optics) of the actual film is shown in Fig. 33. Micrographs of nitrocellulose replicas of opposite surfaces of the film taken under similar optical conditions but at a higher magnification are shown in Fig. 34. A carbon replica of one of these nitrocellulose replicas was prepared by shadowing the latter with Pt/Pd, followed by evaporation of a film of carbon

onto the shadowed surface. The nitrocellulose was then dissolved away. Transmission electron micrographs of portions of the resulting carbon replica of the film surface are shown in Figs. 35, 36.

As can be seen in Fig. 33 the film F1 exhibits an overall mottled appearance as was the case for films I, III and B1 [1]. However, in contrast with the later films fine striations running parallel to the machine direction (M) could be faintly discerned. Both of these features can be seen more clearly in the higher magnification micrographs of the nitrocellulose replicas shown in Fig. 34 in which the arrows point to regions in the fields of view where finely separated (of the order of 1 μm) striations running parallel to the M direction can be seen most clearly. Examination of the carbon replicas in an electron microscope (Fig. 35) reveals ridges of varying sharpness running parallel to the M direction. They correspond to the striations seen in the light microscope. These ridges are crossed and/or bridged by lamellae whose edges are oriented at right angles to M, as is typical of row structures (e.g. see reference [7]). The lamellar morphology of the surface texture and the orientation of the lamellae with their edges transverse to the machine direction can be seen more clearly in the higher magnification electron micrograph shown in Fig. 36. Similar exploratory experiments on film III indicate that etching techniques may be required to reveal the nature of the surface texture of this film. Such experiments, and a detailed electron microscopical study of the fine structure of the four films would complement the findings reported in this section. They fall however beyond the scope of the present investigation.

(iii) <u>Numerical Simulation of Pole Figure Data</u>

In order to provide quantitative comparisons among the pole figure data obtained from the various films we performed numerical simulations in which we attempted to match the observed pole intensity distributions using a suitable probability density function. We used the Bingham distribution [17, 18], which is of the form:-

$$F(K_1, K_2, \phi, \chi) = C(K_1, K_2)\exp [K_1(L \cdot \mu_1)^2 + K_2(L \cdot \mu_2)^2] \dots\dots\dots\dots\dots\dots 1$$

where $C(K_1 K_2)$ is the normalization constant, μ_1 and μ_2 are two members of an orthogonal triad of unit vectors, and are regarded as parallel to the N and T directions in the films respectively. L is a unit vector representing the direction of an observed pole,

$$L = (\cos\phi\cos\chi, \sin\phi\cos\chi, \sin\chi) \dots\dots\dots\dots\dots\dots\dots\dots\dots\dots 2$$

given the above definitions Equation 1 reduces to:

$$F(K_1, K_2, \phi, \chi) = C(K_1 K_2)\exp[\cos^2\chi(K_1\cos^2\phi + K_2\sin^2\phi)] \dots\dots\dots\dots\dots 3$$

The form of the intensity distribution in this model is controlled by only K_1 and K_2. Our simulation efforts consisted of adjusting the values of K_1 and K_2 so that the positions of the points at which the intensity was half way between the minimum intensity and maximum intensity along the $\phi=0°$ and $\phi=90°$ meridians (longitudes) of the simulated pole figure matched those in the experimental (200) and (020) pole figure data.

The K_1 and K_2 values obtained for the (200) and (020) poles for films I, III, B1 and F1 are given in Table 12. Fig. 31 and Fig. 32 illustrate respectively the contour plots of the simulated (200) and (020) pole data.

As can be seen from a comparison of the simulated pole figures (Figs. 31, 32) and the experimental pole figures (Figs. 16,17), the sets of parameters given in Table 12 reproduce the main qualitative features of the experimental pole figure plots, but the latter data have more intensity in the wings of the peaks than is implied by Eq. 1. The functional form of Eq. 1 would have to be modified to provide for a less rapid fall-off of intensity from the maxima. The functions needed to model the data become even more complex if one seeks to describe features such as the bifurcated maxima in the (020) pole figure of film F1. Furthermore in future quantitative studies the matter of correcting the experimental data for background and absorption effects will need to be explored. These considerations notwithstanding, the function given in Eq. 1 is capable of representing qualitatively the behavior of a wide range of orientation distributions. This is further illustrated by the inclusion in Table 12 of the values of K_1 and K_2 for the (200) and (020) pole distributions corresponding to the Transcrystalline, Row(ac) and Row(a) preferred orientations. Comparison of these values with those of the films shows that the B1 film is closer to the limiting case of the Transcrystalline orientation than any of the other films. The differences between films I and III are relatively minor with the values of K_1 and K_2 for both films occupying intermediate positions between those for the Transcrystalline and Row type preferred orientations. The values of K_1 and K_2 for film F1 are closer to those for the Row type orientations.

In summary, the results of the numerical simulations described above are qualitatively consistent with the interpretations (discussed in Section Dii) of the nature of orientations in the four films, and the main differences between them, in terms of the Transcrystalline, Row(ac) and Row(a) models.

The main differences in the $\underline{a}$ and $\underline{b}$ axis orientations among the films are clearly, if qualitatively, reflected in the values of the parameters K_1 and K_2 in the Bingham-type probability density function (Eq. 1) used in the simulations.

E. Summary/Discussion/Conclusions

The various aspects of the structure and properties of films I, III, B1 and F1 investigated in the present study are summarized below where the results for the four films are compared and discussed with reference to various features of films I, III, and B1 which have been reported in our previous study [1]. For convenience in this latter connection we have listed in Table 15 the previously obtained data [1] on the methyl group content, molecular weights (M_w, M_n), intrinsic viscosity, peak melting temperature, and elongations-to-break (uniaxial stretching in the M and T directions) of films I, III and B1. The corresponding data for film F1 which were determined in the present study, and are described in detail in Appendix B of this report, are also listed in Table 15, together with the recently acquired data on the shrinkage behavior exhibited by the four films upon melting (see Section C p. 16).

The following similarities and/or differences have been observed among the four films:-

(i)   The methyl group content, and hence the branching in the
        constituent chains in film F1 (0.48 CH_3/100 C atoms) is
        considerably lower than in films I, III and B1 (2.1 CH_3/100 C
        atoms).

(ii) The <u>molecular weight distribution</u> of film F1 is narrower, and its apparent <u>weight average molecular weight</u> (M_W=129,000) is lower, than in films I, III and B1. The values of the <u>apparent</u> molecular weights of films I, III and B1, listed in order of increasing magnitude are as follows: Film B1, M_W=155000; film I (three determinations), M_W=202000-216000; film III (three determinations), M_W=240000-255000.

(iii) Although the weight average molecular weight of film F1 is lower than those of films I, III and B1, its <u>intrinsic viscosity</u> (η=1.59 d/g) is higher. The <u>intrinsic viscosities</u> of the latter three films in order of increasing magnitude, and in accordance with their increasing molecular weights, are: Film B1, η=1.13 dl/g; film I, η=1.23 dl/g; and film III, η=1.27 dl/g. The departure exhibited by film F1 from the expected monotonic increase in viscosity with increase in molecular weight is explicable in terms of the much lower branch content of the constituent chains in that film (see Appendix B(c)).

(iv) <u>The peak melting temperature</u> of film F1 (122°C-123°C) is higher than the peak melting temperatures exhibited by films I (106.8°C), III (106.2°C) and B1 (105.5°C). This substantial difference between film F1 as compared to the other films can be reasonably attributed to the lower degree of branching in the constituent chains in film F1. A critical aspect in the construction of heavy-lift balloons is the <u>thermal fusion of</u> <u>adjoining gores</u>. The presumably regulated thermal conditions

under which this process has traditionally been carried out on lower melting films such as films I, III and B1 may need to be modified in the construction of balloons from film F1.

(v)   The weight % crystallinity of film F1 (50.6%), calculated from density measurements, is slightly higher than in films I (46.6%), III (46.5%), and B1 (48.2%). Crystallinity is governed by the intrinsic stereochemical characteristics of the polymer chains (i.e. branching), the molecular weight, as well as the thermal and other processing parameters (draw ratio, blow ratio) used in film production. The dependence of crystallinity on this multiplicity of variables notwithstanding, it remains somewhat surprising that the crystallinity of film F1 is only slightly higher than that in the other films considering that the chains in film F1 are considerably less branched. This matter has not been pursued any further in view of the lack of specific information on the processing variables used in the production of any of the films.

(vi)   The (200), (020) and {110} pole figures, considered in conjunction with the SAXD data, indicate that the orientation distributions of the a and c axes in all four films, are peaked in the M direction, as would be expected of the Keller-Machin [7] "row structure" model which is referred to as Row(ac) in this report (See Appendix A, and Section D). These anistropic features of the a and c axis orientation distributions in relation to the M and T directions vary however among the films.

(vii)   Comparison of the pole figures and SAXD patterns exhibited by the films indicates that in contrast with film F1 in which the Row(ac) type of preferred orientation is the dominant one, its manifestation is less pronounced in films I and III (which are structurally closely similar to one another), and least pronounced in film B1.

(viii) The orientation distributions in films I, III and B1, a common characteristic of which is that the b-axis distribution is peaked in the N direction (this feature is more pronounced in film B1 than in films I and III), can be reasonably accounted for in terms of an idealized composite orientation model. In this model the crystalline regions in the films are regarded as consisting mainly of two populations of twisted lamellar microcrystals, with the orientation distribution in one population being of the Row(ac) type, and that in the other being Transcrystalline-like (see Appendix A and Section D). The preferred orientation characteristics of the latter population are that the b-axis is preferentially oriented parallel to N. The _a_ and _c_ axis orientations are isotropic in relation to the M and T directions in the films. Film B1 contains a higher proportion of Transcrystalline orientation relative to the Row(ac) orientation as compared to films I and III. Correspondingly, it is structurally less anisotropic with respect to the M and T directions than films I and III. No evidence of the Transcrystalline orientation was detected in film F1 which is structurally the most anistropic among the films in relation to the M and T directions.

(ix)   There is evidence in the pole figures of all four films of the presence of minor component regions having orientations which differ from the Row(ac) and Transcrystalline orientations.

(x)   The morphological characteristics exhibited in electron micrographs of the replica of one of the surfaces of film F1 confirm the "row-structure" nature of the fine texture of that film.

(xi)   The birefringence (n_M-n_T) of film F1 is positive, whereas films I, III and B1 exhibit negative birefringence. Great caution must be exercised in interpreting birefringence measurements in films. Birefringence is a function of several factors namely: (a) the orientation characteristics of the crystalline lamellae, (b) the prevailing molecular organization in the disordered interlamellar regions whose contribution to the overall birefringence is not independently predictable, and (c) the fractional contents of crystalline and disordered regions [24]. The refractive index parallel to the c-axis in orthorhombic polyethylene, $(n_c=1.575)$ is greater than that parallel to the a-axis $(n_a=1.514)$, and to the b-axis $(n_b=1.519)$ [25]. We note that the positive birefringence exhibited by film F1 is qualitatively consistent with the deduction, derived from the pole figures and small angle diffraction patterns, that the orientation distribution of the c-axis in that film is peaked parallel to the M direction, as is characteristic of the Row(ac) orientation. By the same token films I, III and B1 might have been expected to exhibit positive birefringence, but with lower magnitudes than in film F1, since they contain Row(ac) material in relatively smaller proportions.

The fact that films I, III and Bl are negatively birefringent suggests "over-compensating" negative contributions to birefringence from the disordered regions.

(xii) The dimensional changes which the films undergo in the M and T directions upon melting at 140°C have been examined. Films I, III, and Bl shrink in both the M and T directions. Shrinkage in all three films is larger in the M than in the T direction. The values of R_M (shrinkage in the M direction) range from 4 to 5 (Table 8), and those of R_T (shrinkage in the T direction) range from 2.3 to 3.2. The values of the ratio R_M/R_T for the three films fall in the following ranges: Film III (1.45-2.14, Table 8), film I (1.33-1.81), and film Bl (1.26-1.46). The dimensional changes which film Fl undergoes upon melting differ from those of films I, III and Bl in two respects. First, it shrinks by a factor of 2-3 more in the M direction (R_M=9.8-13.3, Table 8). Second, it expands by 25%-42% in the T direction. These various observations are qualitatively consistent with the expectation that shrinkage in the MT plane will tend to be larger in the direction along which the orientation distribution of the chain axes (i.e. the c-axis in the crystalline regions) is peaked. As adduced from the pole figures and the small angle x-ray diffraction patterns, the c-axis is preferentially oriented parallel to M in all four films. This feature is a characteristic of Row(ac) material which is the dominant constituent of film Fl (R_M=9.8 to 13.3, R_M/R_T=13.8 to 19.3), and occurs in smaller proportion in the three other films, for which R_M(4 to 5) and R_M/R_T (1.33 to 2.14) are expectedly much

lower. The average values of R_M/R_T for films Bl, I and III are 1.36, 1.51 and 1.71 respectively. The lower value of R_M/R_T for film Bl is consistent with the pole figure and SAXD data which indicate that its orientation characteristics in the MT plane are the least anisotropic of the four films. We can only note the difference in the averages of R_M/R_T between films I and III. The possibility that this difference reflects relatively subtle differences in orientation between these films remains an open question.

(xiii) The four films were subjected to equal biaxial deformation under inflation at 23°C and -73°C. At 23°C films I and Bl deformed by almost equal amounts in the M and T directions near the pole of the bubble. There was no evidence of necking. In contrast both films III and Fl exhibited necking in the transverse direction, and as a result deformed significantly more in the transverse direction than in the machine direction. Film III exhibited several necks over the surface of the bubble, whereas film Fl exhibited only one neck. For each of the four films the same pattern of behavior was found to occur at -73°C.

(xiv) Comparison of all the mechanical measurements made on the four films at 23°C indicates that there is a rather good correlation between the results of the equibiaxial inflation experiments, and those from the elongation to break experiments in uniaxial extension (Table 15). In both sets of experiments films Bl and I exhibit balanced (isotropic) deformation in the M and T directions, whereas films III and Fl exhibit preferential deformation parallel to T at large strains.

(xv)   The following observations emerge from a consideration of the extension to break data exhibited by the films in uniaxial extension (data in Table 15) in relation to the results of the orientation studies. The ratios E_M/E_T (E_M=extension to break in the M direction/extension to break in the T direction) for films films B1, III and F1 at 23°C are 1.04, 0.71, 0.56 respectively. There is an apparent correlation between these ratios and the fact that the orientation of the crystalline regions with respect to M and T is correspondingly least anistropic in film B1 and, in increasing order, more so in films III and F1. It is evident however that film I (E_M/E_T=1.02), which is structurally more closely similar to film III but mechanically akin to film B1 at 23°C, does not fit into this scheme. There are no evident orientation-related trends among the E_M/E_T ratios of the films at -73°C.

(xvi)   Constant rate of clamp separation, and creep to failure experiments indicate that the differences in molecular weight and/or molecular weight distributions of the polymer in films I, III and B1, are reflected to some extent in the tensile properties at 23°C of unoriented samples prepared by melting the films and allowing them to cool and crystallize under ambiant conditions. Samples made from the polymer with highest molecular weight (film III) had the highest tensile strength (18.6 MPa) and the lowest strain to break (5.4 in creep). Samples made from the lowest molecular weight material (from film B1) had the lowest tensile strength (15.3 MPa) and the largest strain to break (6.6 in creep).

Appendix A

Orientation Models

The interpretations of the results of the (200), (020), and {110} pole figure determinations and the small angle x-ray diffraction experiments reported in Section D, are based on three idealized models of preferred orientations (and combinations thereof). These models are referred to as the Transcrystalline, the Row(ac) and the Row(a) models respectively. They are described below following a synopsis of some fundamental features of the crystallography and morphology (fine structure) of melt crystallized polyethylene.

(i) Some Crystallographic and Morphological Characteristics of Melt Crystallized Polyethylene

The unit cell of polyethylene (Fig. 24) is orthorhombic. Its parameters are a=0.74 nm, b=0.493 nm, c=0.2534 nm, $\alpha=\beta=\gamma=90°$. The chains are oriented parallel to the c-axis. The (200), (020) and (002) poles lie along directions parallel to the $\underline{a}$, $\underline{b}$, and $\underline{c}$ axes respectively.

Under quiescent conditions (i.e. in the absence of flow) branched and linear polyethylenes crystallize from the molten state in the form of spherulitic aggregates (Fig. 25a) whose radial spans usually vary from circa 1 μm to 100 μm depending on the conditions of crystallization. The average spherulite size diminishes the lower the crystallization temperature due to the higher spherulite nucleation density (nuclei/unit volume). At sufficiently low crystallization temperatures the dimensions attained by spherulites before they impinge can fall below the level (circa 1 μm) at which they can be distinctly resolved under the optical microscope. Detailed descriptions and discussions of the optical and fine structural characteristics of polyethylene (and other polymer) spherulites can be found

in references [14] and [15] which include ample bibliographies. We limit ourselves here to a listing of some main characteristics of the morphology and associated crystallographic details of polyethylene spherulites which have a bearing on the various distinguishing features of the preferred orientation models which will be described below.

Polyethylene spherulites consist of a spherically symmetric radiating array of long and narrow crystals (Fig. 25b) which are twisted about the radial direction and which are on the order of 1 μm wide or less depending on the crystallization temperature. These crystals are lamellar in character (Fig. 25c), their thickness being typically on the order of 10 nm. They are oriented with their b-axis parallel to the radial direction. The c-axis in the lamellae is oriented normal, or closely so, to the plane of the lamellae within which the chain molecules are folded back and forth between opposite surfaces of the lamellae (Fig. 25c). Both the c-axis and the a-axis in the crystals are oriented normal to the radial direction about which the lamellae are twisted, as indicated above. The twist period is the same along every radial path. Correspondingly, upon proceeding along the lamellae from the center to the outer regions of the spherulite along any radial path there is a periodic rotation of the a and c axes about the radius (Fig. 25b). The disordered regions in the spherulites are sandwiched between neighboring lamellae (Fig. 25c). Included in these disordered regions are the chain folds at the surfaces of the lamellae, chain ends, and interlamellar tie molecules. The thickness and width of the lamellae decrease the lower the crystallization temperature as does the twist period.

The morphological and crystallographic characteristics of the preferred orientation models described below derive from the structure of spherulites. The main features to bear in mind in this connection is that the b-axis in the twisted lamellae is oriented parallel to the radial direction with the a and c axes normal to the radius about which they rotate periodically.

(ii) <u>Transcrystalline Orientation Model</u>

In this model twisted lamellae similar to the constituent radially oriented lamellae in spherulites are regarded as being oriented with their b-axis parallel to N (i.e. normal to the MT plane) (see Fig. 26) in the film. Correspondingly, the a and c axes which are perpendicular to b are oriented parallel to the MT plane. Furthermore due to the twisting of the lamellae about b, the a and c axes are randomized in the MT plane. These features are summarized in Table 11. The idealized (200), (020), (002) and {110} pole figures corresponding to these preferred orientation characteristics are also shown in Fig. 26. Note that the (200) and (002) pole figures are identical. The two arcs in the {110} pole figure pass through the points whose coordinates are (ϕ=-124°,χ=0°), (ϕ=-90°, χ=34°), (ϕ=-56°, χ=0) and (ϕ=56°, χ=0°), (ϕ=90°, χ=34°), (ϕ=124°, χ=0°) respectively.

The transcrystalline orientation is most frequently encountered near the surface of molded specimens which have been rapidly cooled from the molten state. Due to the more rapid cooling at the specimen surface the spherulite nucleation density is much higher than in the interior. With so many nuclei in close proximity to one another the growth of spherulites can only proceed into the interior of the sample along the direction perpendicular to the surface. This results in a surface layer in which the twisted lamellae are oriented with their b-axis preferentially parallel to the direction of growth, i.e. normal to the surface of the specimen. <u>Whether extensive</u>

regions having the transcrystalline orientation exist near the outer surface of the blown films, or whether this type of preferred orientation of lamellae arises in some different manner remains an open question which has not been pursued in the present study.

(iii) Row(ac) Orientation

This is the well established Keller-Machin "Row Structure" [7], see Fig. 27(i). Under the influence of extensional flow, there form in a molten extrudate fibrous (diameter of the order of 10 nm) nuclei in which the chain molecules are oriented parallel to the extrusion direction. As the extrudate cools, spherulites are nucleated along the length of these fibrils. The developing spherulites which are centered on and lie along the same fibril are however in such close promixity to one another that they can only develop radially along directions perpendicular to the fibril axis, i.e. perpendicular to the extrusion (machine) direction. The successive disclike growths ("cylindrites") which are thus formed along each fibril correspond to diametric cross-sections of spherulites. As in spherulites, the radiating twisted lamellae are oriented with their b-axis parallel to the radial direction in the cylindrites, with the a and c axes normal to and rotated about the radial direction.

A schematic representation of such row structures as they would be oriented in a film (and as viewed along the M direction) is depicted in Fig. 28 together with the corresponding idealized (200), (020), (002) and {110} pole figures. As summarized in Table 11, and as can be seen from the (020) pole figure, the b-axis is oriented preferentially parallel to the NT plane, and is randomized in that plane. The distributions of the a and c axis orientations are similar to one another. They are both broadly peaked in the M direction ($\chi=90°$) and are cylindrically symmetrical about that

direction [7]. The (200) and (002) pole intensities decrease progressively along all meridians (longitudes) with decreasing χ. The {110} poles are distributed along all meridians between latitudes χ=0° and χ=34°.

(iv) Row(a) Orientation

This model has been discussed by Keller and Machin (Ref. [7], p. 68). While, in common with the Row(ac) model, the lamellae in the cylindrites are oriented with their b-axis parallel to the radial direction, and the a and c axes are normal to that direction, this model differs from the Row(ac) model in the following respects. The lamellae are not twisted, but are oriented with the a-axis parallel to the extrusion (machine) direction, and the c-axis perpendicular to that direction [Fig. 27ii]. It has been suggested that this type of row structure is formed under conditions of higher stress than attain the Row(ac) structure [7].

A schematic representation of such Row(a) structures as they would be oriented in a film (and as viewed along the M direction) is depicted in Fig. 29 together with the corresponding idealized (200), (020), (002) and {110} pole figures. As summarized in Table 11, the a axis is oriented parallel to M, and the b and c axes are oriented parallel to the NT plane and are randomized in that plane. The {110} poles are uniformly distributed around the χ=34° latitude.

The pole figures corresponding to the Transcrystalline, Row(ac), and Row(a) orientations are shown collectively in Fig. 30.

It should be noted that the preferred orientation characteristics of the a, b, and c axes relative to M, T, and N in the Transcrystalline and Row(a) models correspond respectively to the hypothetical orientations depicted in Fig. 25a and Fig. 25b in our previous report [1].

Appendix B

Film F1: Branching, Molecular Weight Distribution (from Size Exclusion
Chromatography), Intrinsic Viscosity, Melting/Crystallization (from
Differential Scanning Calorimetry), Density/Crystallinity, Birefringence,
Tensile Properties at 23°C (Uniaxial Extension in the M and T Directions)

As additional background for comparing the structural characteristics
and physical properties of film F1 with those of films I, III and B1, the
features listed above, which had been previously examined for the latter
three films [1], were also determined for the "newer" film F1.

(a) Branching: Methyl Group Content

The FTIR method of analysis was similar to that used for the other
polyethylene films [1]. The sample was prepared by hot pressing six layers
of film at 130° C. The thickness of the sample was 4.6 ± 0.2 mils as
determined with a micrometer caliper. The IR spectrum in the frequency
region between 1330 and 1400 cm-1 differed significantly from those obtained
from the other films indicating a lower methyl group content. By resolving
the complex band profile shown in Fig. 37 according to the method of Rueda,
Balta Calleja and Hidalgo [19] the peak absorption of the methyl band at
1378 cm^{-1} was determined. From this quantity and the film thickness the
methyl group content per 100 carbon atoms was calculated using the expression

$$\varepsilon \ (CH_3/100C) = 0.085 \ k - .09$$

where k is the peak absorption divided by the thickness in cm. The methyl
group content was determined to be 0.48 per 100 carbon atoms, or
approximately 1/4 the value reported for films I, III and B1 [1].

(b) <u>Size Exclusion Chromatography (SEC)</u>

With the same apparatus and bank of columns used previously to examine the Category I, III, Bl and other films [1] SEC runs were carried out at 130°C in 1,2,4 trichlorobenzene on the Fl film, as well as on the Category I and III films as a crosscheck with the previous work. A recalibration, necessary because the columns had not been used for some time, indicated that no change had taken place. As before, the chromatograms extended to the exclusion limit for these columns which is about 4 million for linear polyethylene.

A method for calculating molecular weights of branched whole polymers, requiring several assumptions, has been given in the literature [20]. It is assumed that the extent of branching is independent of the molecular weight of the species making up the distribution, an assumption which would not be expected to be generally true and which has been shown to be incorrect for low density polyethylene [21]. In addition the relationships used to derive the dependence of the number of branch points on the radius of gyration [22] apply to a specific type of branching which does not necessarily occur in low density polyethylene. For this reason, no attempt was made to use this method to calculate molecular weights.

The calculations of molecular weight were carried out for the polymers within the calibration range, and <u>assuming the polyethylene is linear.</u> Because of this latter assumption the calculated molecular weights obtained in the present series of measurements (Series C) and those obtained earlier for films I, III, and Bl (Series A, Series B, see Table 2, reference [1]), all of which are listed in Table 13, are referred to as <u>apparent molecular weights.</u> The correct molecular weights <u>are likely to be higher</u> because of the effect of branching and because extremely high molecular

weight material was excluded from fractionation by the columns; some of this extremely high molecular weight material might include microgels, known to occur in branched polyethylenes.

The apparent molecular weight values obtained for films I and III at different times fall within the expected error range of the experiments. An overlay of chromatograms of films I, III, and F1 (Fig. 38) shows that the F1 film has a narrower molecular weight distribution than the other two. For example, at an elution volume of 33 ml, which according to the column calibration corresponds to a molecular weight of 420,000, the peak height, which is proportional to the amount of component of that molecular weight present in the film, is only one half as high in the F1 film as in the film I. This lower content of high molecular weight component results in the F1 film having a weight average molecular weight of 129,000 compared to 200,000 and 255,000 for films I and III respectively and 154600 for the B1 film. The number average molecular weights of the films are not too far different from each other, ranging from 21,000 to 30,000.

(c) Intrinsic Viscosity

The relative flow times of several dilute solutions of the F1 film of different concentrations at 130°C in 1,2,4 trichlorobenzene were measured with a capillary viscometer in the manner described in the previous report [1]. The data were extrapolated to zero concentration to give a limiting viscosity number or intrinsic viscosity, [n].

The observed values previously measured [1] for films I, III and B1 are given along with that of F1 in Table 13. In the case of the F1 film it was found necessary to increase the dissolution temperature from the more customary 135-140 C range, used previously for the other films, to about 160°C for one hour to effect complete solution.

The value of $[\eta]=1.59$ for film Fl is substantially higher than the values found for the other three films which were 1.23 (film I), 1.27 (film III) and 1.13 (film Bl).

According to the Mark-Houwink relation,

$$[\eta] = KM^{\alpha} ,$$

(where K and α are empirical constants which depend on the polymer, the solvent, and the temperature) the viscosity increases monotonically with molecular weight. Hence on the basis of the dilute solution viscosity measurements alone one would be led to conclude that Fl has a higher molecular weight than films I, III, and Bl films. This is in apparent contradiction to the molecular weights obtained by SEC shown in Table 13, but can be explained in the light of the considerably lower methyl group content (and hence branching) in the chains of film Fl as compared to those in films I, III and Bl (see Appendix B(a) above).

It is well known that solutions of polymers with long chain branching have a lower viscosity than linear polymers of the same molecular weight. This is because the branched chain molecule is more compact and consequently has a smaller hydrodynamic volume than an unbranched chain random coil, which in a good solvent is more extended and occupies a larger volume. Since viscosity is a measure of hydrodynamic volume the viscosity will be smaller for a branched polymer than for a linear one of the same molecular weight. By the same token, polymer having fewer branches may exhibit a higher intrinsic viscosity than a highly branched one even though the molecular weight of the latter is greater, which appears to be the case for the Fl film compared to the other three films.

(d) Melting/Crystallization: Differential Scanning Calorimetry (DSC)

As was the case in our earlier screening of films I, III, B1 as well as others [1], the melting and crystallization behavior of samples of film F1 were probed with a differential scanning calorimeter using heating and cooling rates of 20°C/min. Each sample was subjected to two consecutive heating and cooling cycles as follows: The film specimen, initially cooled to -40°C was heated at 20°C/min to a temperature (140°C) above the specimen melting range. It was then cooled at 20°C/min to -40°C and then was subjected to a second (similar) heating and cooling cycle. DSC curves exhibited by a film specimen upon heating and cooling through two consecutive cycles are shown in Fig. 39. The peak melting temperatures exhibited by two specimens in the first heating cycle were 122.4°C and 122.6°C. In both specimens a pronounced shoulder was observed on the low temperature side of the melting isotherm (Fig. 39a) at circa 115°C. The exothermic peak observed in the first cooling cycle occurred at 104.6°C and 104.7°C respectively (Fig. 39b). In the second heating cycle (Fig. 39c) the melting endotherm was narrower than that in the first cycle, i.e. there was no evidence of a pronounced shoulder below the peak melting temperature which occurred at 122.6°C in one sample and 121.8 in the other. Upon cooling for the second time the samples exhibited an exothermic peak at 104.7°C and 104.6°C (Fig. 39d). No attempt was made to investigate the origins of the shoulder in the melting endotherm exhibited by the specimens in the first heating cycle. Melting and partial recrystallization and/or changes in contact between the specimen and the pan containing it as a result of the pronounced shrinkage which film F1 undergoes upon melting (see Section C of this report) may be among the possible causes of the shoulder.

The main aspect of the results summarized above is that the peaks of the melting endotherm and the crystallization exotherm exhibited by the F1 film both occur at higher temperatures than the main polymer melting and crystallization peaks exhibited by films I, B1 and III which occurred (see table 5, reference [1]) in the range of 105.5°C-106.8°C (melting) and 91.9°C-94.4°C (crystallization). These substantial differences between the F1 film and the other three films are consistent with the considerably lower degree of branching [see Appendix B(a) above] in the constituent chains of film F1.

(e) Density: Crystallinity

The density of two specimens of the F1 film was determined at 23±0.1°C using a water/ethanol density gradient column. Appropriate precautions were taken to deaerate the specimens prior to immersion in the columns. Within experimental error (±0.0005g/cc) the density of both specimens was found to be the same, namely 0.9225g/cc. The corresponding weight % crystallinity was calculated to be 50.6% assuming, as was done previously [1] for the other films, that the densities of purely crystalline polyethylene (i.e. the unit cell density) and the density of entirely amorphous polyethylene are 1.000g/cc [13b] and 0.8547g/cc [23] respectively. In comparison, the densities of films I, III and B1 were in the range 46.2%-48.2%.

(f) Birefringence

Assuming, on the basis of measurements provided by NASA, that the thickness of film F1 is 16.5 μm (0.65 mil), its birefringence in the MT plane was measured in six randomly chosen regions in an area of about 20cmx20cm. The birefringence, $\Delta n = (n_M - n_T)$, where n_M and n_T are the refractive indices parallel to the M and T directions respectively was found to be +0.0016 in

each case, i.e, $n_M > n_T$ in contrast with films I, III and B1. In the latter three films Δn was negative, i.e, $n_M < n_T$, and was in the range (-0.0009) to (-0.0019).

(g) Tensile Tests on Film F1 at 23°C

Tensile tests were conducted at 23°C on four specimens of the film F1, two cut parallel to the machine direction and two cut parallel to the transverse direction. The procedures used were those described in Section H(i) in reference [1]. The results are summarized in Table 14. A comparison between the results for the film F1 and those for films I, III, and B1 (Table 21 (Reference [1]) reveals the following differences in behavior:

(i)   The yield stress is somewhat higher in both the M and T directions for the film F1 than for the films I, III, or B1.

(ii)   The stress at break is significantly higher for the film F1 in the M direction than for any of the other three films.

(iii)   The strain at break is much greater for the film F1 in the T direction than for any of the other three films.

An additional set of experiments was done to examine the creep to failure behavior of the film F1 under constant load conditions at 23°C. Two creep tests were done, one using a tensile specimen cut parallel to the machine direction, and a second one cut parallel to the transverse direction. The experiment was performed as follows. Initially the specimen was subjected to a small constant load and the creep strain measured as a function of time until the creep curve reached a plateau (creep strain nearly constant with time). The applied load was then increased by a small increment and the creep strain was again determined until a plateau value was reached. This procedure was repeated until failure occurred. The results

were the following. The specimen cut parallel to the machine direction
failed at a strain of about 3.5 under an applied stress of 30 MPa. On the
other hand, the specimen cut along the transverse direction failed at a
strain of 5.75 under an applied stress of 12.5 MPa. When compared to the
results for the specimens stretched at a constant rate of clamp separation
(Table 14), the large differences observed between the two sets of results
would, as was the case for the remolded unoriented material (Section B(4)),
indicate that considerable material was pulled out of the clamps during the
constant rate of clamp separation experiment.

References

1. Khoury, F., Crissman, J. M., Fanconi, B. M., Wagner, H. L., Bolz, L. H., Harding, C. A., NBSIR 84-2989 (NASA), Issued 1985.

2. Volungis, R. J., and Stein, R. S., J. Polymer Sci. 20, 199 (1956).

3. Holmes, D. R., and Palmer, R. P., J. Polymer Sci. 31, 345 (1958).

4. Aggarwal, S. L., Tilley, G. P., and Sweeting, O. J., J. Appl. Polymer Sci, 1, 91 (1959, J. Polymer Sci. 51, 551 (1961).

5. Krigbaum, W. R. and Roe, R.-J., J. Chem. Phys. 41, 737 (1964).

6. Lindenmeyer, P. H. and Lustig, S., J. Appl. Polymer Sci., 9, 227 (1965).

7. Keller, A. and Machin, M. J., J. Macromol. Sci. B1, 41 (1967).

8. Desper, C. R., J. Appl. Polymer Sci. 13, 169 (1969).

9. Maddams, W. F. and Preedy, J. E., J. Appl. Polymer Sci. 22, 2721 (1978); idem 22, 2739 (1978); idem 22, 2761 (1978).

10. White, J. L. and Spruiell, J. E., Polymer Eng. Sci. 21, 859 (1981).

11. Choi, K.-J., Spruiell, J. E., and White, J. L., J. Polymer Sci. Polymer Phys. Ed. 20, 27 (1982).

12. Among the difficulties mentioned by Lindenyer and Lustig, as well as Keller and Machin is that, due to the intrinsically very low intensity of the (002) reflections, it is often not possible to obtain well resolved (002) pole figures. This problem was also encountered in the early stages of the present study and was not explored any further.

13. Bunn, C. W., (a) Chemical Crystallography, p. 233, Oxford University Press (1949) and (b) Trans. Faraday Soc. 39, 482 (1939).

14. Khoury, F. and Passaglia, E., in "Treatise on Solid State Chemistry," Vol. 3, (Hannay, B. N. Editor), Chapter 6, Plenum Press N.Y. (1976).

15. Bassett, D. C., "Principles of Polymer Morphology", Cambridge University Press, N.Y. (1981).

16. Vonk, C. G., in "Small Angle X-ray Scattering", (Gleiter, O. and Kratky, O., Editors), Chapt. 13, p. 436, Academic Press, N.Y. (1982).

17. Bingham, C., "Distributions on the Sphere and the Projective Plane", PhD Thesis, Yale University (1964).

18. Hardia, K. V., Statistics of Directional Data, Academic Press, N.Y., pp. 212-247 (1972).

19. Rueda, D. R., Balta'-Calleja, F. H., and Hidalgo, A., Spectrochemica Acta 35A, 847 (1979).

20. Drott, E. E., and Mendelson, R. A., J. Polymer Sci., Part A-2, 8, 559 (1973).

21. Wagner, H. L. and McCrackin, F. L., J. Appl. Polymer Sci., 21, 2833 (1977).

22. Zimm, B. H., and Stockmayer, W. H., J. Chem. Phys. 17, 1301 (1949).

23. Davis, G. T., Eby, R. K., J. Appl. Phys. 44, 4274 (1973).

24. Stein, R. S. and Wilkes, G. L., in "Structure and Properties of Oriented Polymers", Chap. 3, (I. M. Ward, Editor), Wiley, N.Y. (1975).

25. It is commonly assumed, to a good approximation, that the refractive indices of an ideal orthorombic polyethylene crystal are the same as in single crystals of normal paraffins, and that $n_a=1.514$, $n_b=1.519$, and $n_c=1.575$, Bunn, C. W. and Danbeny, R. De P., Trans. Faraday Soc. 50, 1173 (1954).

26. Hoffman, J. D., Davis, G. T., and Lauritzen Jr., J. I. in "Treatise on Solid State Chemistry", Vol. 3, (Hannay, B. N., Editor), Chapter 7 (see Fig. 14), Plenum Press, N.Y. (1976).

TABLE 1

Comparison between Biaxial Deformation under Inflation Experiments
and Elongation at Break in Uniaxial Extension Experiments at 23°C.
R is the Ratio of the Strain in the Transverse Direction to that
in the Machine Direction.

Film	R_B	R_u
I	0.94	0.98
B1	1.06	0.96
III	1.54	1.40
F1	2.20	1.80

R_B - From equibiaxial inflation of film to a condition just prior to
failure

R_u - From elongation at break in uniaxial extension experiments

TABLE 2

Range of Values of True Stress[a] During Inflation of Films
at Three Levels of Applied Pressure at 23°C

Applied Pressure (Pa)	Film I Roll 315477	Film II Roll 112877	Film B1 Roll 367006
5000	9.3-9.9[b]	9.3-9.6	9.0-9.6
7000	12.2-12.6	12.1-12.5	11.9-12.2
9000	15.9-18.5	16.0-19.2	17.2-20.4

[a] True Stress given in MPa.
[b] The number on the left represents the minimum value of true stress and the number on the right the maximum value measured during the inflation experiment.

TABLE 3

Range of Values of True Stress[a] for Each Film at
Five Levels of Applied Pressure at -73°C

Applied Pressure (kPa)	Film I Roll 315477 Sample 1	Film III Roll 112877 Sample 1	Film B1 Roll 367006 Sample 1
24	42.3-42.9[b]	42.5-42.7	42.5-42.9
27	46.7-46.8	46.9-46.9	46.9-47.1
30	52.9-53.0	52.6-52.6	52.0-52.0
33	60.6-84.4	58.9-60.0	57.9-59.2
34	(c)	(c)	>80

(a) True stress given in MPa.

(b) The number on the left represents the minimum value of true stress
and the number on the right the maximum value measured during the
inflation experiment.

(c) Specimen failed before 2 minutes.

TABLE 4

Summary of Tensile Tests at 23°C on
Unoriented Specimens Remolded From Balloon Film
(Constant Rate of Clamp Separation)[a]

Film	Roll Number	Specimen Number	Yield Stress (MPa)	Strain at Yield	Tensile Strength (MPa)	Strain at Break[b]
I	315477	1	12.0	0.13	–	–
I	315477	2	11.8	0.14	–	–
I	315477	3	11.6	0.14	–	–
I	315477	4	–	–	17.8	13.6
I	315477	5	–	–	14.7	10.5
I	315477	6	–	–	17.9	14.1
I	315477	7	–	–	18.2	14.1
III	112877	8	11.4	0.14	–	–
III	112877	9	11.3	0.12	–	–
III	112877	10	11.0	0.14	–	–
III	112877	11	–	–	20.2	15.8
III	112877	12	–	–	15.6	14.7
III	112877	13	–	–	18.8	10.5
III	112877	14	–	–	19.2	14.5
III	112877	15	–	–	19.4	14.3
B1	367006	16	12.0	0.12	–	–
B1	367006	17	12.2	0.13	–	–
B1	367006	18	11.8	0.13	–	–
B1	367006	19	12.0	–	13.7	9.25
B1	367006	20	11.7	–	14.2	10.9
B1	367006	21	11.7	–	16.6	14.0
B1	367006	22	11.7	–	14.7	11.2
B1	367006	23	11.6	–	17.4	15.1

(a) Strain rate 991% per minute.

(b) The values shown in this column are based on the clamp separation at
     failure. They are, therefore, an over estimate of the true elongation
     at break since a considerable amount of material is pulled out of the
     clamps (see text).

TABLE 5

Average Values of Tensile Properties of
Remolded Balloon Film at 23°C, as
Determined from Constant Rate of Clamp
Separation Experiments

Film	Roll Number	Average Yield Stress (MPa)	Average Strain at Yield	Average Tensile Strength (MPa)	Average Strain at Break[a]
I	315477	11.8	0.14	17.2	13.1
III	112877	11.2	0.13	18.6	14.0
Bl	367006	11.8	0.13	15.3	12.1

(a) The values shown in this column are based on the clamp separation at failure. They are, therefore, an over estimate of the true elongation at break since a considerable amount of material is pulled out of the clamps (see text).

TABLE 6

Time to Failure under Creep for Specimens
of Remolded Balloon Film at 23°C

Applied Stress (MPa)	Time to Failure (minutes)		
	Film I	Film III	Film B1
12.5	1.6×10^4	6.5×10^2	2.0×10^3
15.0	1.0×10^3	2.4×10^2	2.0×10^2

TABLE 7

Maximum Strain Under Creep for
Specimens of Remolded Balloon Film
at 23°C

Applied Stress (MPa)	Film III	Maximum Strain Film I	Film Bl
10.0	3.83[a]	4.10[a]	4.94[a]
12.5	4.71	5.16	5.85
15.0	5.39	5.75[b]	6.55

[a] Failure did not occur. The value shown represents the creep strain after 10^4 minutes.

[b] Three specimens of film I tested at 15 MPa failed prior to one minute under load.

TABLE 8

Film Shrinkage at 140°C[*]

Film	Roll Number	Gore Number	R_M	R_T	Film Thickness (mil)
III	111958	121	3.97	2.71	0.8
III	111958	121	4.11	2.60	
III	112578	101	4.16	2.61	0.8
III	112578	101	4.07	2.56	
III	112618	130	4.51	2.79	0.8
III	112618	130	4.62	2.79	
III	112673	--	4.10	2.35	1.0
III	112673	--	4.29	2.35	Cap
III	112674	--	4.00	2.31	1.0
III	112674	--	4.14	2.33	Cap
III	112861	173	4.32	2.82	. 0.8
III	112861	173	4.00	2.83	
III	112877	--	4.45	2.19	0.8
III	112877	--	5.00	2.33	
III	112877	--	4.65	2.65	0.8
III	112877	--	4.62	2.67	end of roll
III	112880	142	4.80	2.87	0.8
III	112880	142	5.00	2.99	
III	112881	--	4.38	2.42	0.8
III	112881	--	4.48	2.40	
III	112882	--	4.76	2.32	0.8
III	112882	--	4.80	2.27	
III	112884	--	4.65	2.33	1.0
III	112884	--	4.74	2.42	
IV	311071	--	4.22	2.45	0.8
IV	311071	--	4.12	2.39	
IV	311597	--	4.69	2.21	0.7
IV	311597	--	4.96	2.35	
IV	311926	--	4.30	2.50	0.8
IV	311926	--	4.72	2.40	

Table 8 (cont'd)

Film	Roll Number	Gore Number	R_M	R_T	Film Thickness (mil)
IV	312445	-	5.21	2.29	0.7
IV	312445	-	4.76	2.59	
II	313865	53	5.00	2.11	0.8
II	313865	53	4.80	2.50	
II	313865	53	4.72	2.59	
II	313890	137	5.26	2.49	0.8
II	313890	137	5.17	2.53	
II	313915	22	4.44	2.38	0.8
II	313915	22	4.80	2.47	
I	315420	-	4.72	2.67	0.7
I	315420	-	4.80	2.65	
I	315441	-	4.00	3.00	0.7
I	315441	-	4.27	3.04	
I	315441	-	4.32	2.95	
I	315453	-	4.15	2.64	0.7
I	315453	-	4.12	2.70	
I	315453	-	4.29	2.69	
I	315477	-	4.15	2.95	0.7
I	315477	-	4.07	3.06	
B1	367006	-	4.00	3.16	0.8
B1	367006	-	4.29	3.16	
B1	367006	-	4.38	3.00	
F1	-	-	10.8	0.75	0.7
F1	-	-	9.8	0.71	
F1	-	-	12.2	0.79	
F1	-	-	13.2	0.69	
F1	-	-	12.0	0.70	
F1	-	-	13.3	0.80	

* Film floated on hot silicon oil at 140°C for ten minutes.
R_m = Ratio of the initial to final dimensions in the machine direction.
R_T = Ratio of the initial to final dimensions in the transverse direction.

TABLE 9

Summary of Shrinkage Measurements[*]

Film	$\langle R_M \rangle$[**]	$\langle R_T \rangle$[**]	$\langle R_M \rangle / \langle R_T \rangle$
III	4.46	2.61	1.71
IV	4.69	2.40	1.95
II	4.88	2.44	2.00
I	4.29	2.84	1.51
B1	4.22	3.11	1.36
F1	11.9	0.74	16.1

[*] Cap material excluded

[**] Average values

TABLE 10

Ratio I(max)/I(min)* for the various Pole Figures

Film	(200)	(020)	(110)
I	6.8	3.9	4.5
III	5.4	3.9	3.9
B1	4.9	4.4	3.2
F1	7.7	4.5	8.3

* I(max) and I(min) are respectively the highest and lowest pole
intensities in the data recorded for each pole figure.

TABLE 11

Preferred Orientation Characteristics of the a,b and c
Crystallopraphic Axes Relative to the M, T and N Directions.

Trancrystalline Orientation: b-axis parallel to N, a and c axes lie in
the MT plane and are randomly oriented in that plane.

Row(ac) Orientation: a and c axes preferentially parallel to M, b-axis
lies in the NT plane and is randomly oriented in that plane.

Row(a) Orientation: a-axis parallel to M, b and c axes lie in the NT
plane and are randomly oriented in that plane.

TABLE 12

Bingham Distribution Parameters (K_1, K_2)

Film	(200) pole K_1	k_2	(020) pole K_1	K_2
B1	-0.5	-4.0	5.5	10.6
III	-1.7	-4.7	7.3	9.5
I	-1.8	-4.1	9.1	11.9
F1	-3.2	-3.8	12.9	12.4
Transcrystalline model	0	$-\lvert K\rvert$	0	$\lvert K'\rvert$
Row(ac) and Row(a)	$-\lvert K\rvert$	$-\lvert K\rvert$	$\lvert K'\rvert$	$\lvert K'\rvert$

TABLE 13

Apparent Molecular Weights and Intrinsic Viscosity Measurements

| | Apparent Molecular Weights | | Intrinsic Viscosity |
	M_w	M_n	$d\ell/g$
Film I			
Series A	216,000	22,300	1.23
Series B	202,000	23,100	
Series C	208,000	21,600	
Film III			
Series A	253,000	20,900	1.27
Series B	255,000	30,100	
Series C	240,000	25,000	
Film B1			
Series B	154,600	22,400	1.13
Film F1			
Series C	129,000	26,000	1.59

Series A and Series B data are from reference [1].

TABLE 14

Tensile Properties of the F1 Balloon Film at 23°C

| Property | Direction | | M/T |
	Machine	Transverse	
Yield Stress	16.6	14.5	1.12
(MPa)	16.6	15.1	
Strain at Yield	0.23	0.15	1.37
	0.18	0.15	
Stress at Break	59.0	26.8	1.82
(MPa)	35.6	25.2	
Strain at Break	6.70	10.52	0.55
	4.95	10.52	

TABLE 15[*]

Summary of Some of the Characteristics of Films I, III, B1 and F1

	I	III	B1	F1
Mol.Wt. Mw	202K-216K	240K-255K	148K-155K	129K
Mn	21.6K-23.1K	25K-30.1K	21.5K-22.4K	26K
CH_3/100C	2.1	2.1	2.1	0.48
Intr.Visc. (dℓ/g	1.23	1.27	1.13	1.59
Density(g/cc)	0.916(5)	0.916(3)	0.919(0)	0.922(5)
	0.917(0)	0.917(0)	0.919(0)	0.922(5)
Crystallinity Wt.(%)	46.6%	46.5%	48.2%	50.6%
Melt Peak °C DSC heating rate 20°C/min.	106.8	106.2	105.5	122.5
Shrink.Ratio M/T	1.51	1.87	1.36	16.1
Strain at M	4.62	4.45	4.91	5.85
Break(23°C) T	4.54	6.24	4.70	10.50
Strain at M	3.19	3.27	2.63	4.55[**]
Break(-70°C) T	2.59	4.34	3.82	2.01
Birefringence $(M_M - N_T)$	-0.0018	-0.0011	-0.0017	+0.0017

[*] Most of the data on films I, II and B1 were reported in reference [1]
[**] NSBF data
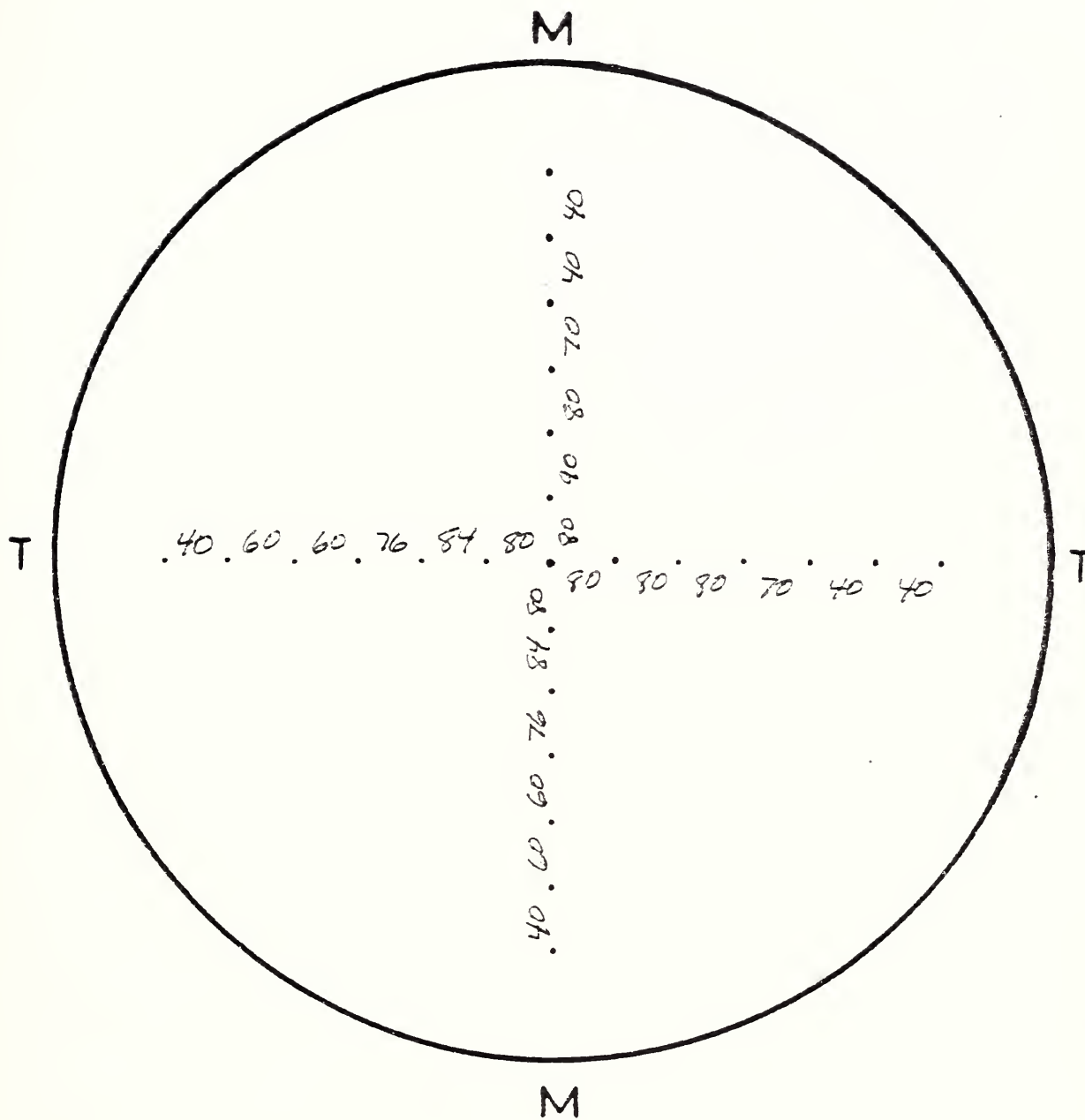
Dentaldam Rubber

Fig. 1. Deformation under inflation at 23°C of a thin sheet of dentaldam rubber. The numbers indicate the percent strain between each set of marks.

CAT. I ROLL 315-77
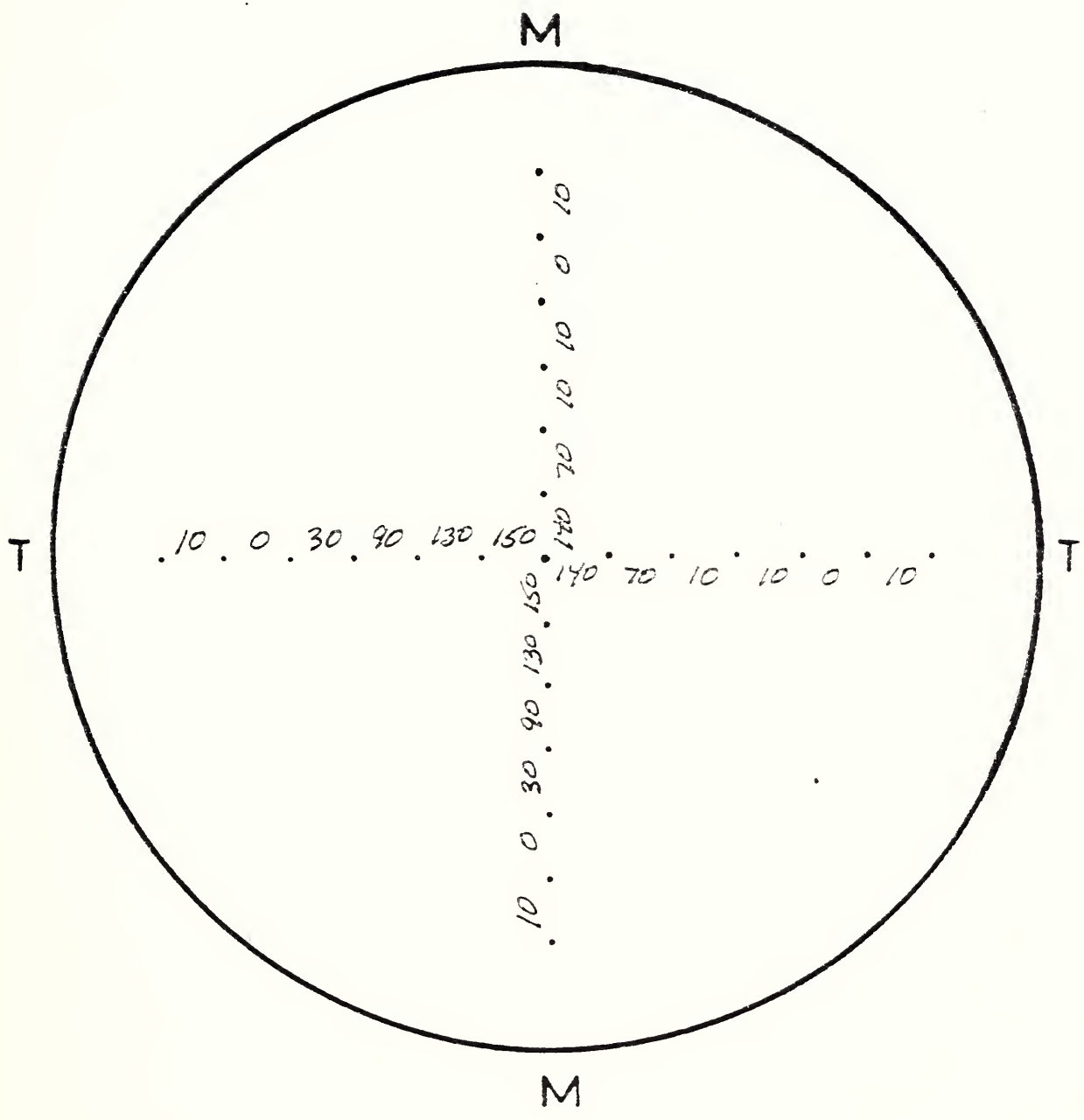
Fig. 2. Deformation under inflation at 23°C of the Cat. I film inflated to a condition just short of failure. The numbers indicate the percent strain between each set of marks.

CAT. B1 ROLL 367006
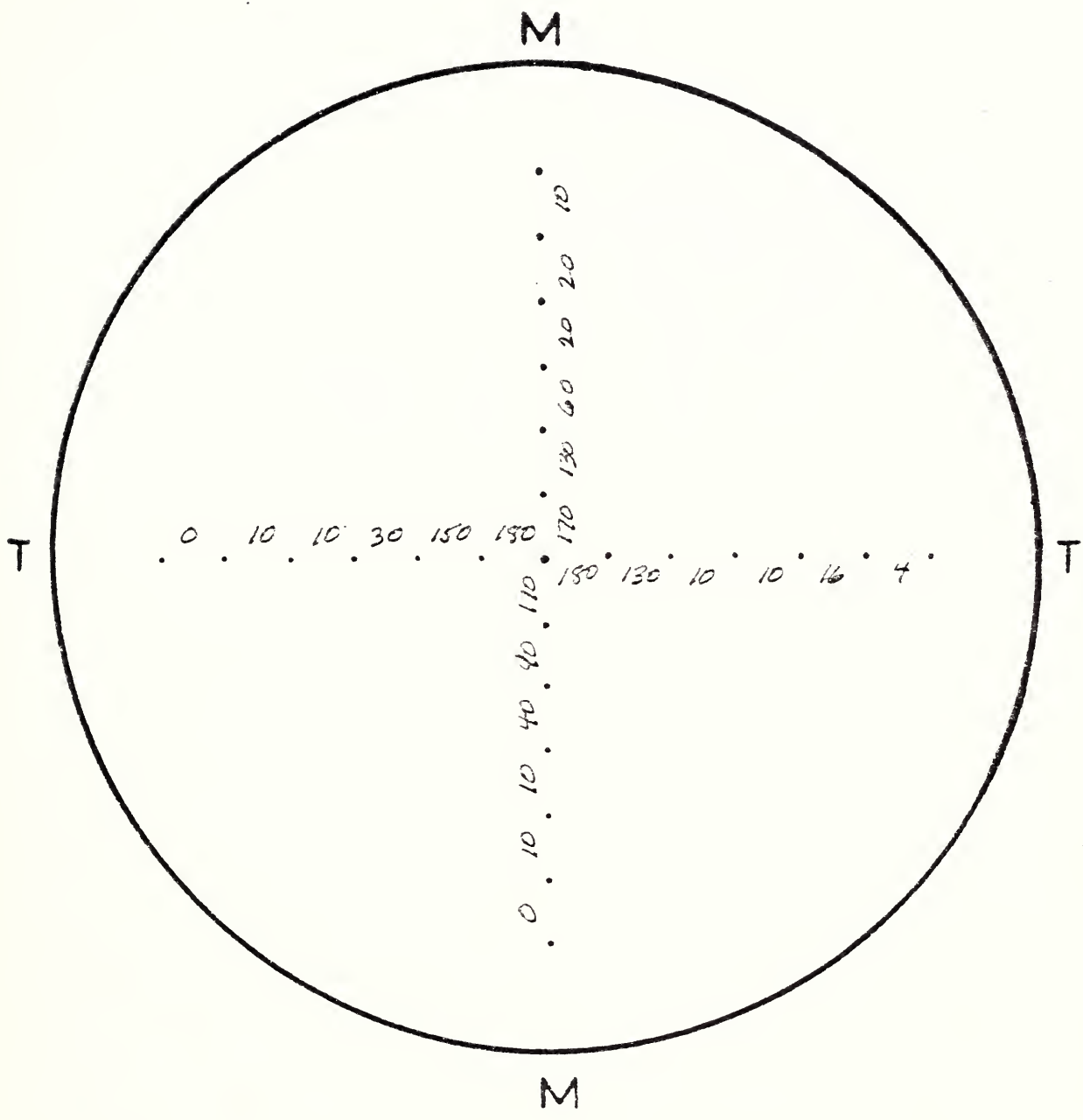
Fig. 3. Deformation under inflation at 23°C of the Cat. B1 film inflated to a condition just short of failure. The numbers indicate the percent strain between each set of marks.
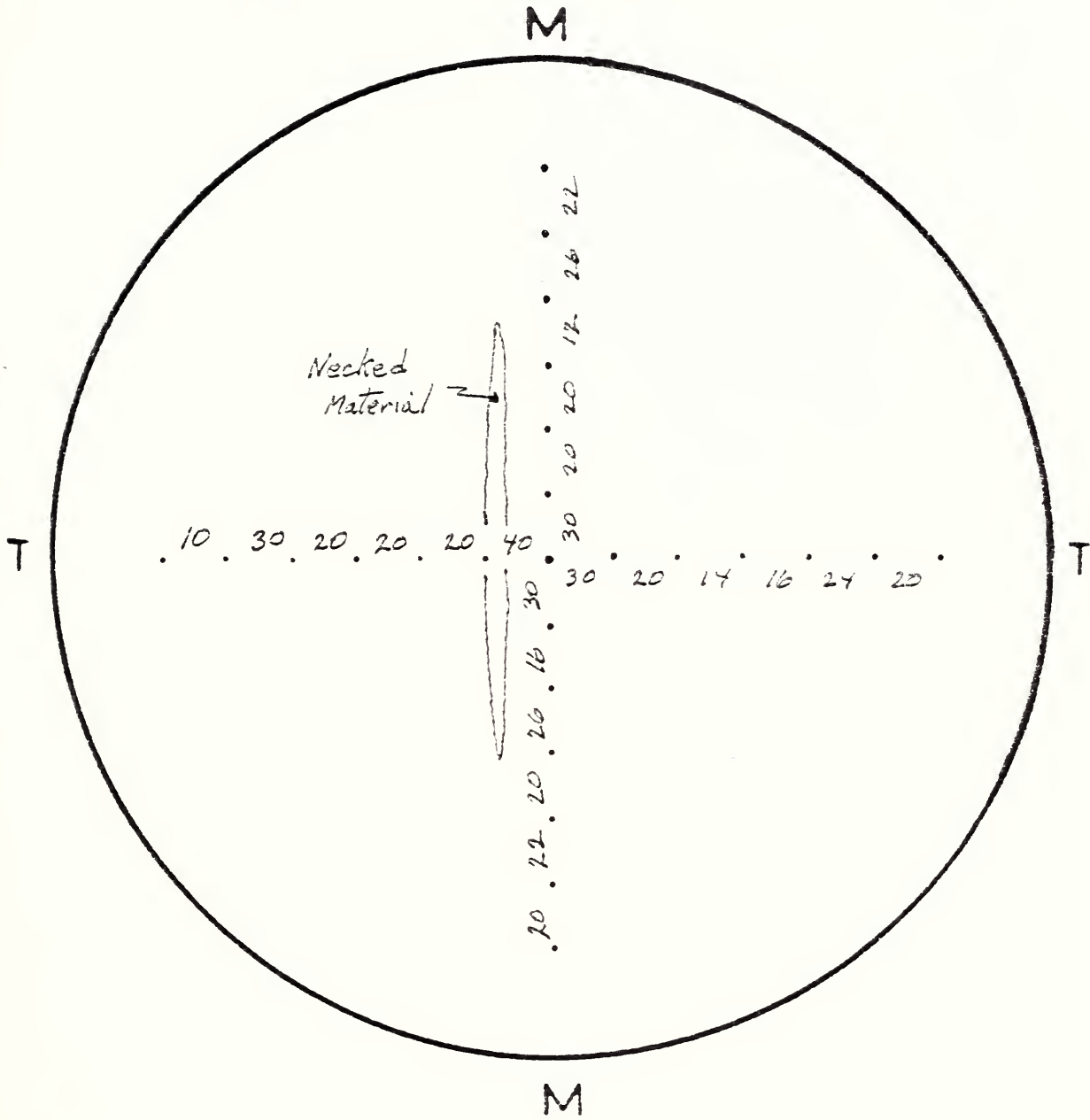
CAT. III ROLL 112ETT

Fig. 4a. Deformation under inflation at 23°C of the Cat. III film. The film
was inflated to the point where necking first occurred.

CAT. III ROLL 112E77
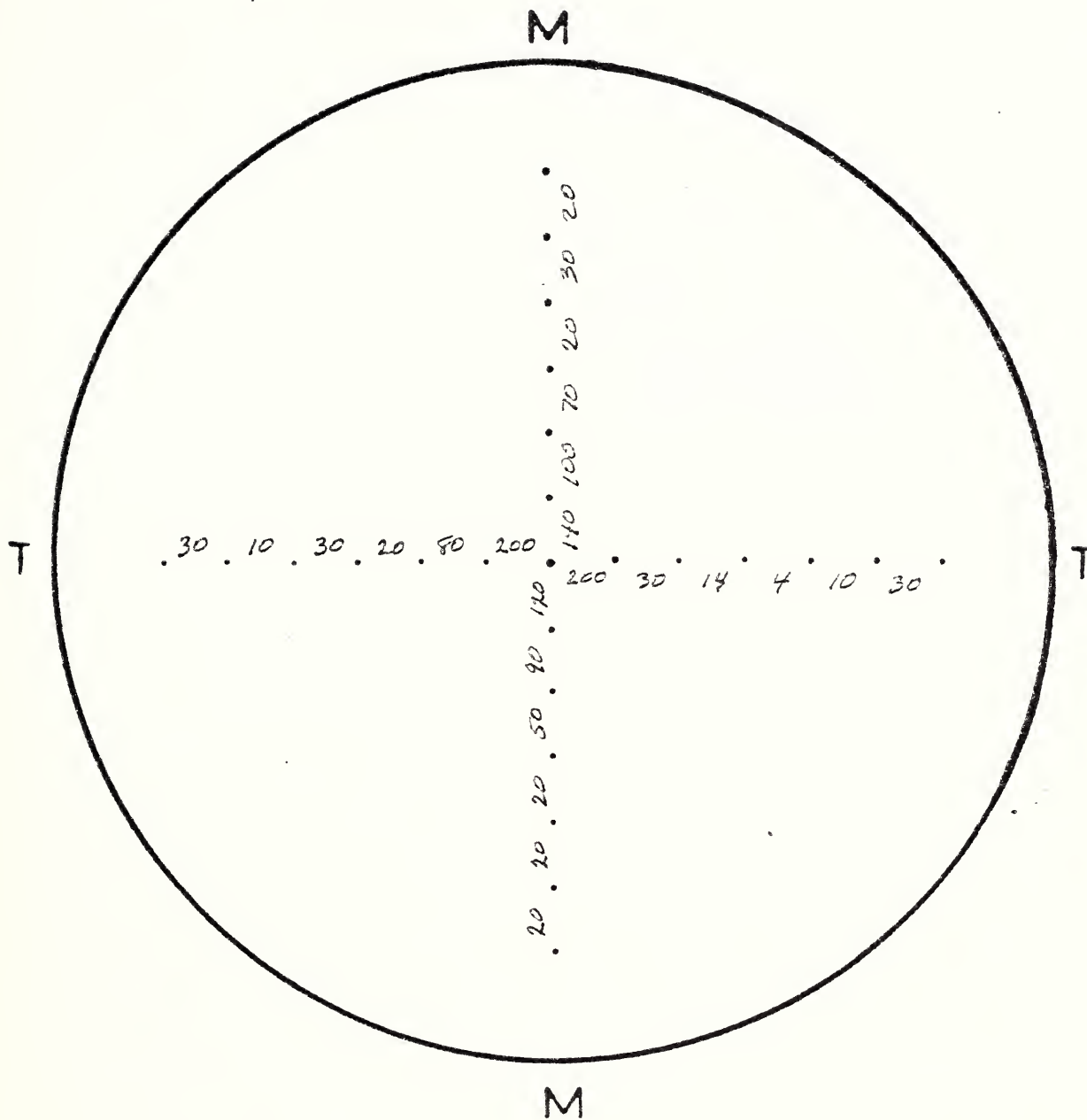
Fig. 4b. Deformation under inflation at 23°C of the Cat. III film inflated to a condition just short of failure. At this stage of inflation several necks were visible in the region nearest the pole.
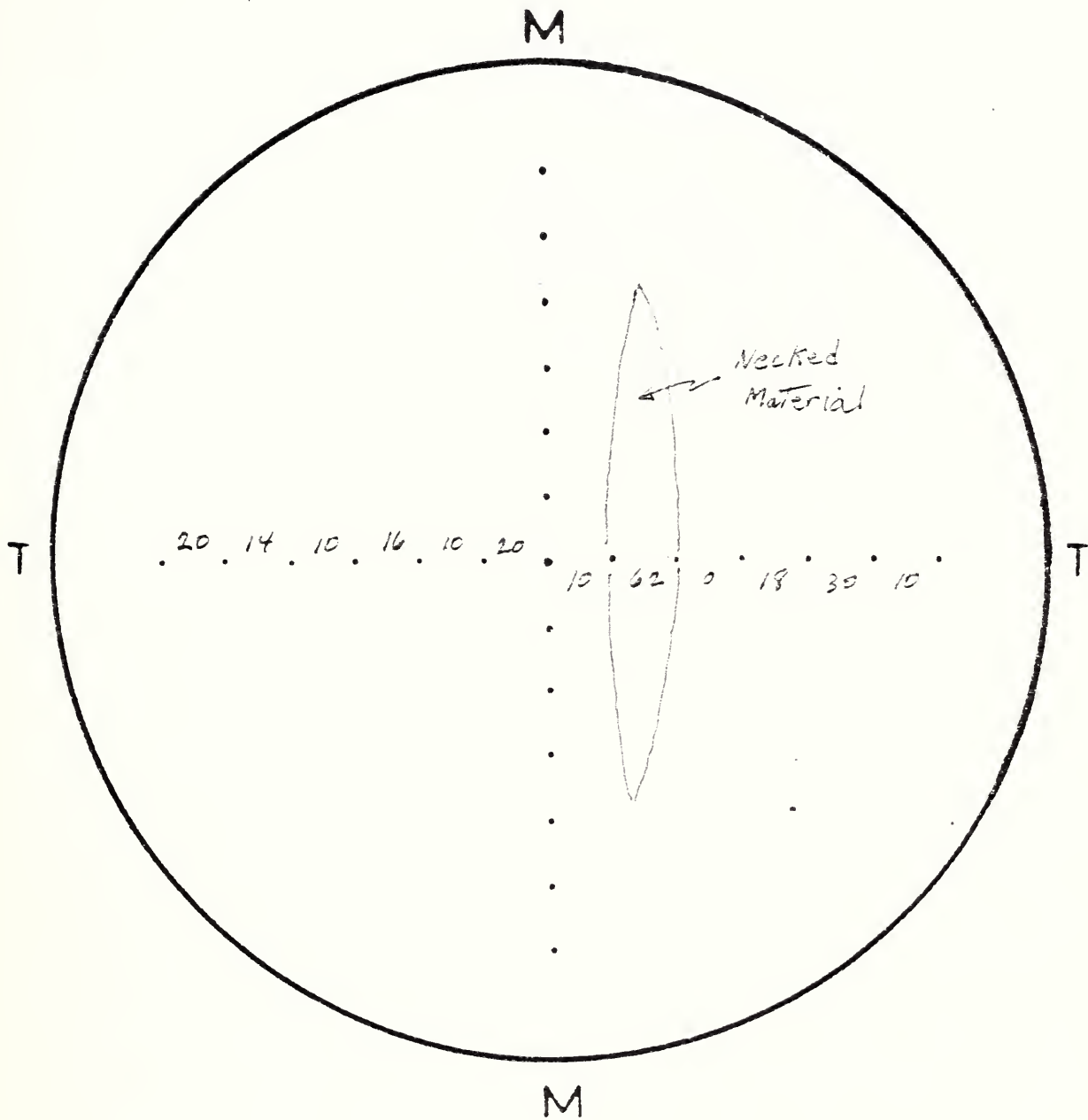
CAT. *F1* ROLL —

Fig. 5a. Deformation under inflation at 23°C of Cat. F1 film. The film was
inflated to the point where necking first occurred. Note that the
neck did not occur in the region nearest the pole.

CAT. *F1* ROLL ——
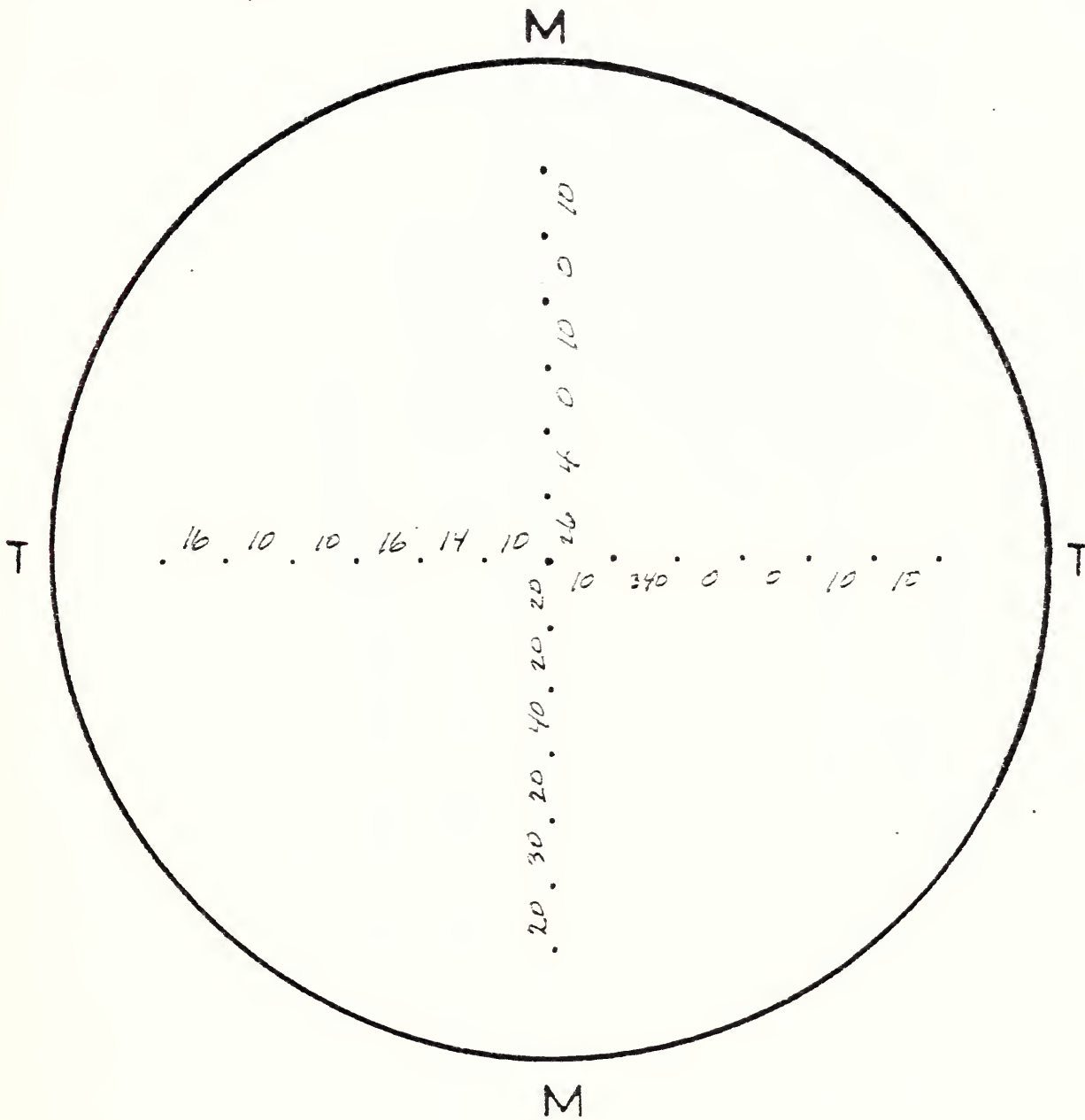
Fig. 5b. Deformation under inflation at 23°C of Cat. F1 film inflated to a condition just short of failure. Note that only one neck has appeared and nearly all the deformation in the transverse direction has occurred in the region between the second and third mark on the right hand branch.
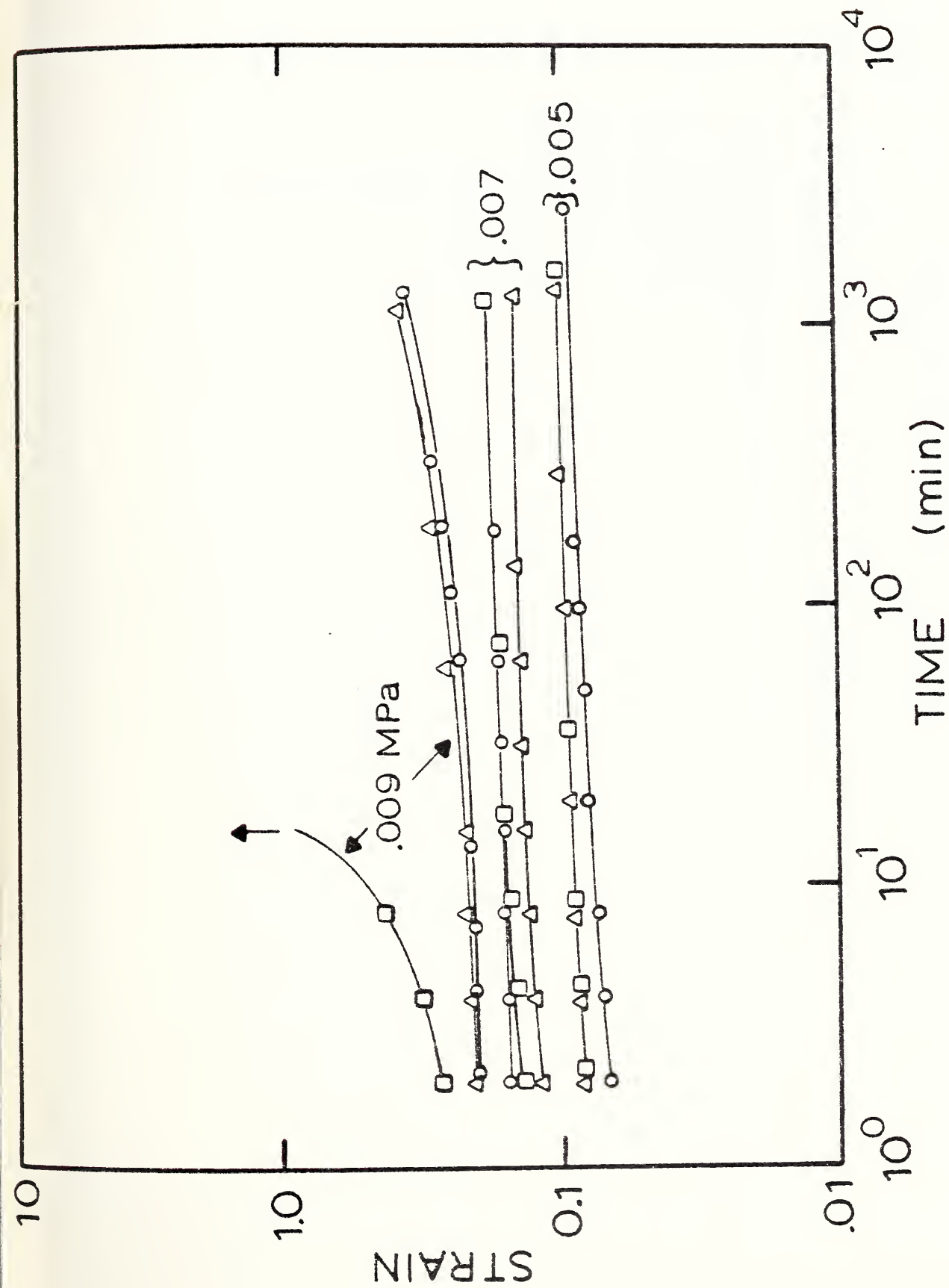
Fig. 6. Log creep strain versus log time for films inflated at three different levels of applied pressure at 23°C. Circles – Cat. I, triangles –Cat. III, and squares – Cat. Bl.
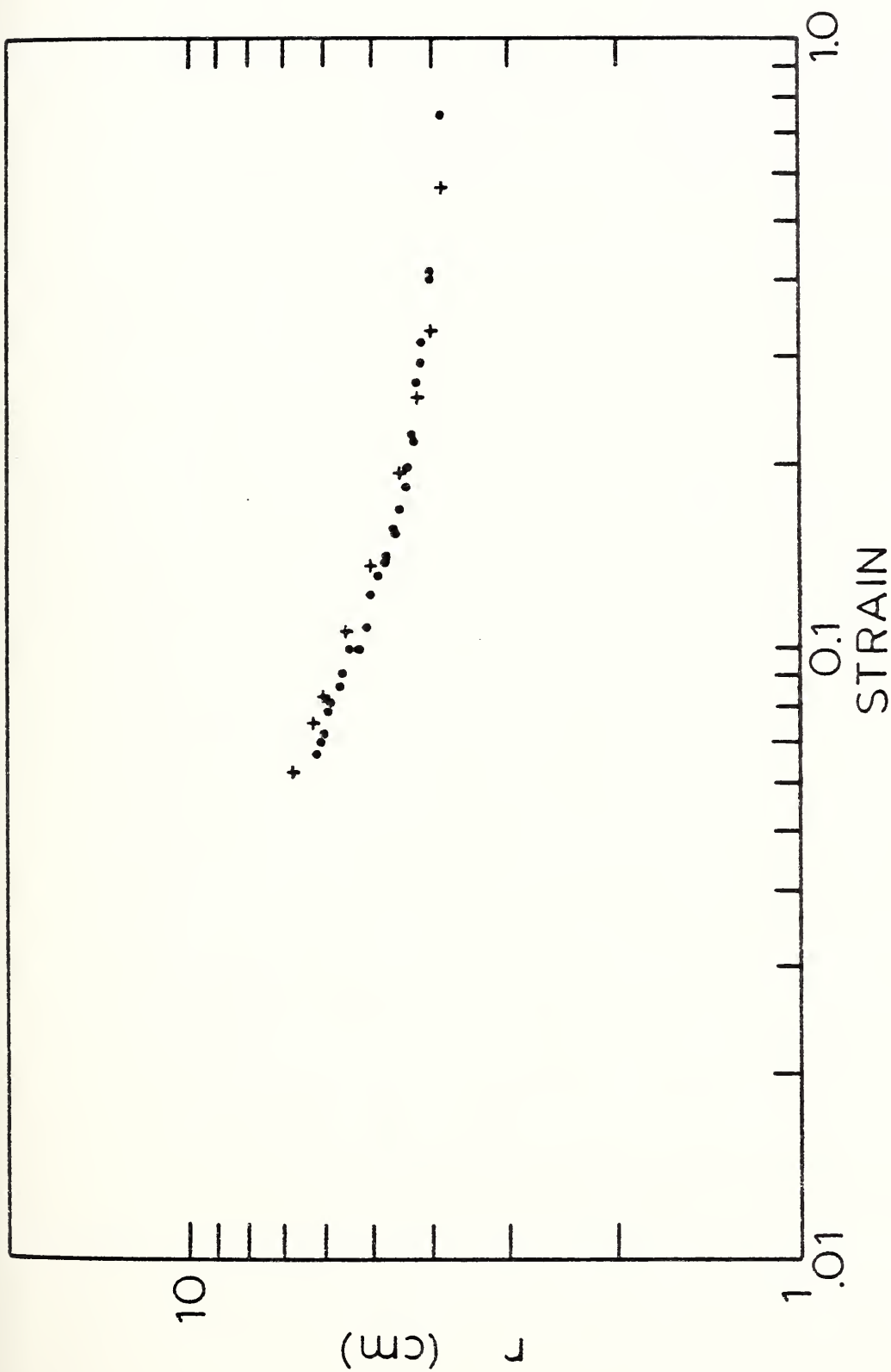
Fig. 7.   Log radius of curvature versus log strain for balloon film under
bubble inflation at 23°C. The filled circles represent data
obtained by direct measurement of the strain between marks placed
1.5 cm on either side of the pole. The crosses represent an
estimate of the strain calculated using the radius of curvature
(see text for details).
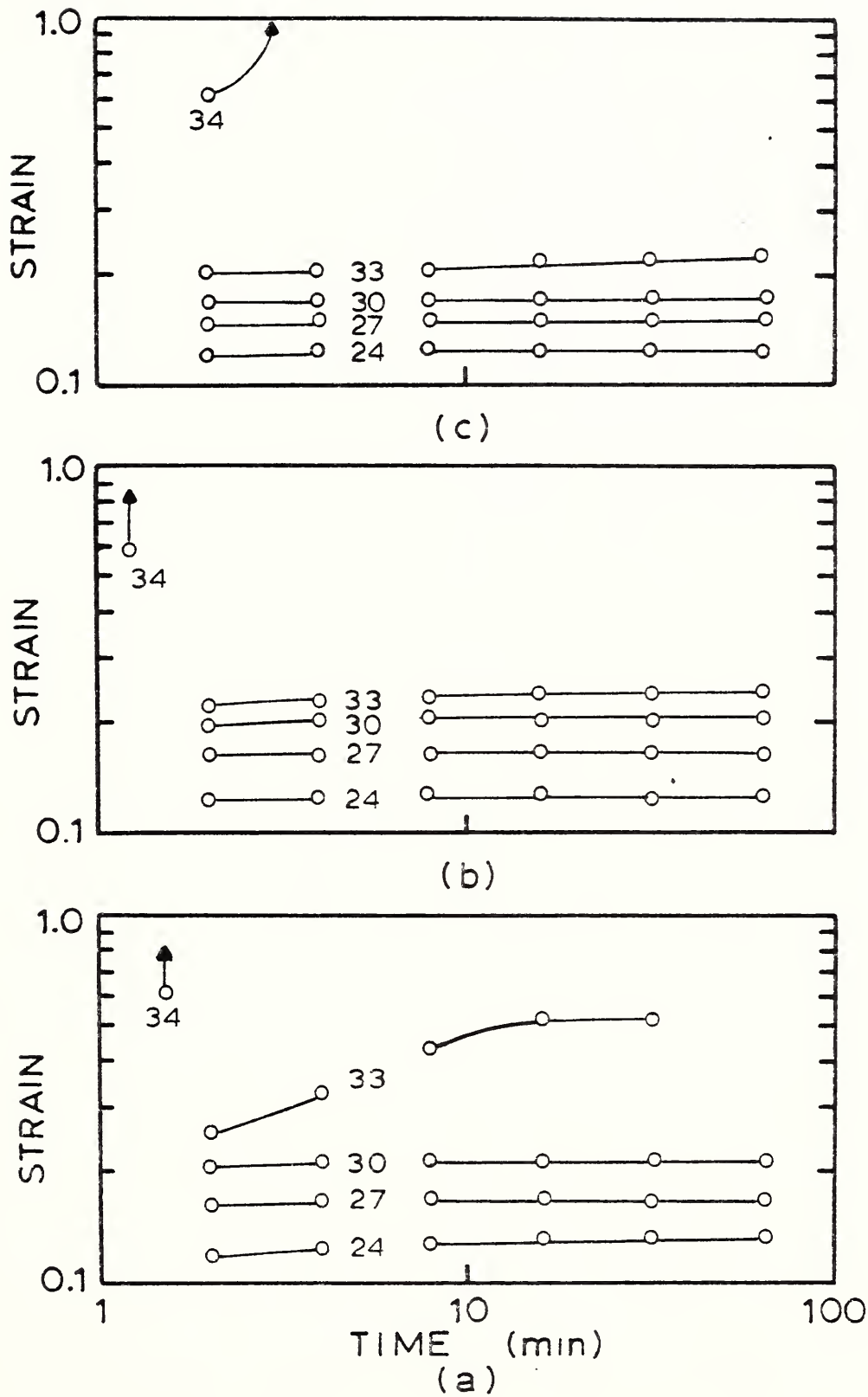
Fig. 8. Log creep strain versus log time for films under bubble inflation at different levels of constants applied pressure (kPa) at -73°C. (a) Cat. I, Roll 315477, (b) Cat. III, Roll 112877, and (c) Cat. B1, Roll 367006.
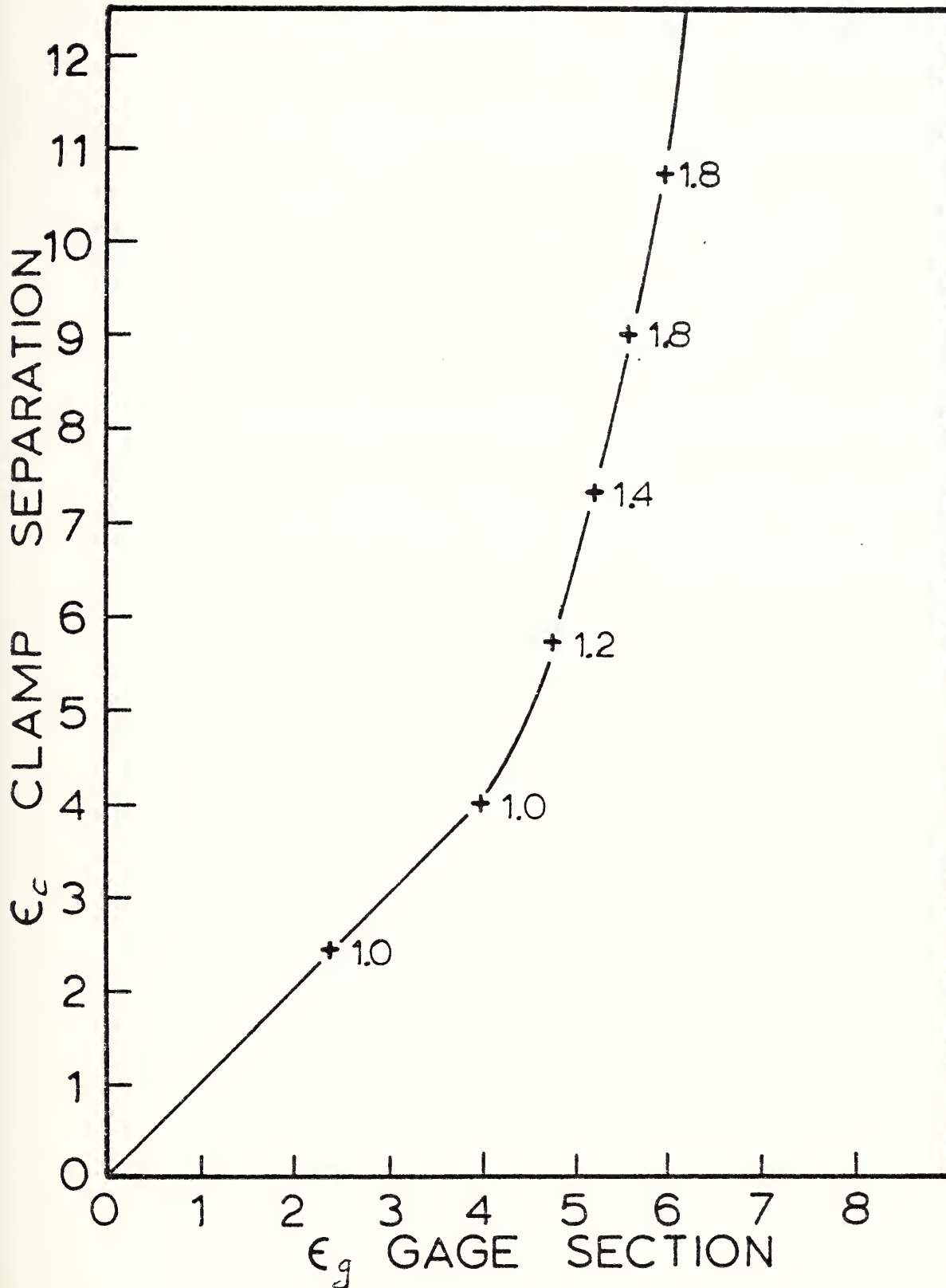
Fig. 9. Strain as determined from the clamp separation (ε_c) versus strain as determined from the gage section (ε_g) from a constant rate of clamp separation experiment. The polymer is remolded balloon film. The numbers next to the crosses indicate the ratio $\varepsilon_c/\varepsilon_g$.
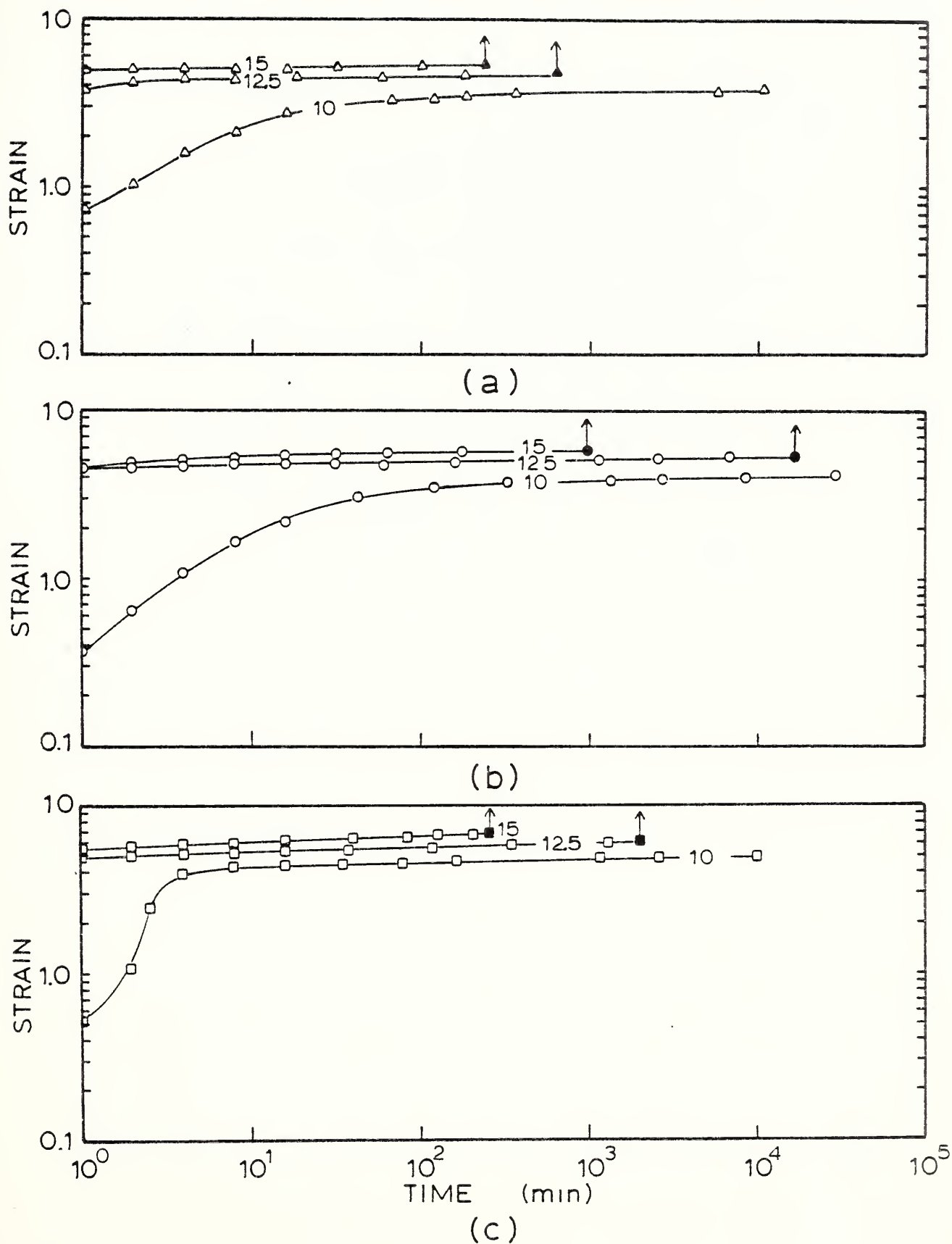
Fig. 10. Log creep strain versus log time for specimens of unoriented remolded balloon film. The numbers shown indicate the applied engineering stress (MPa) for experiments done in uniaxial extension. (a) Cat. III, (b) Cat. I, and (c) Cat. Bl. The arrows indicate failure.
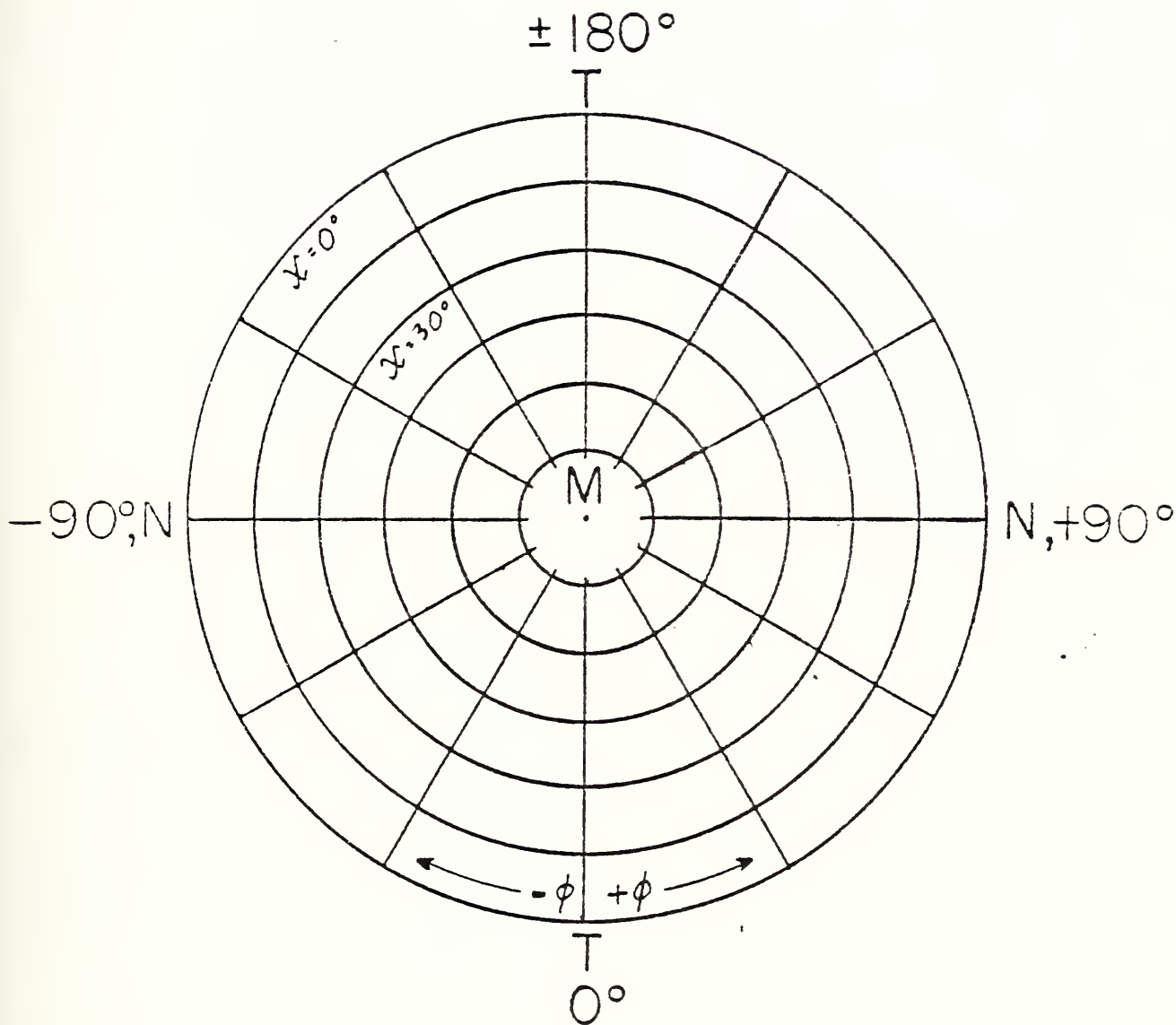
Fig. 11. Azimuthal equidistant projection of the reference hemisphere (see text) in relation to the M, T, and N directions in the film. The radial lines and concentric circles are respectively the projections of the longitudes, φ, and latitudes χ of the hemisphere. M is normal to the plane of projection.
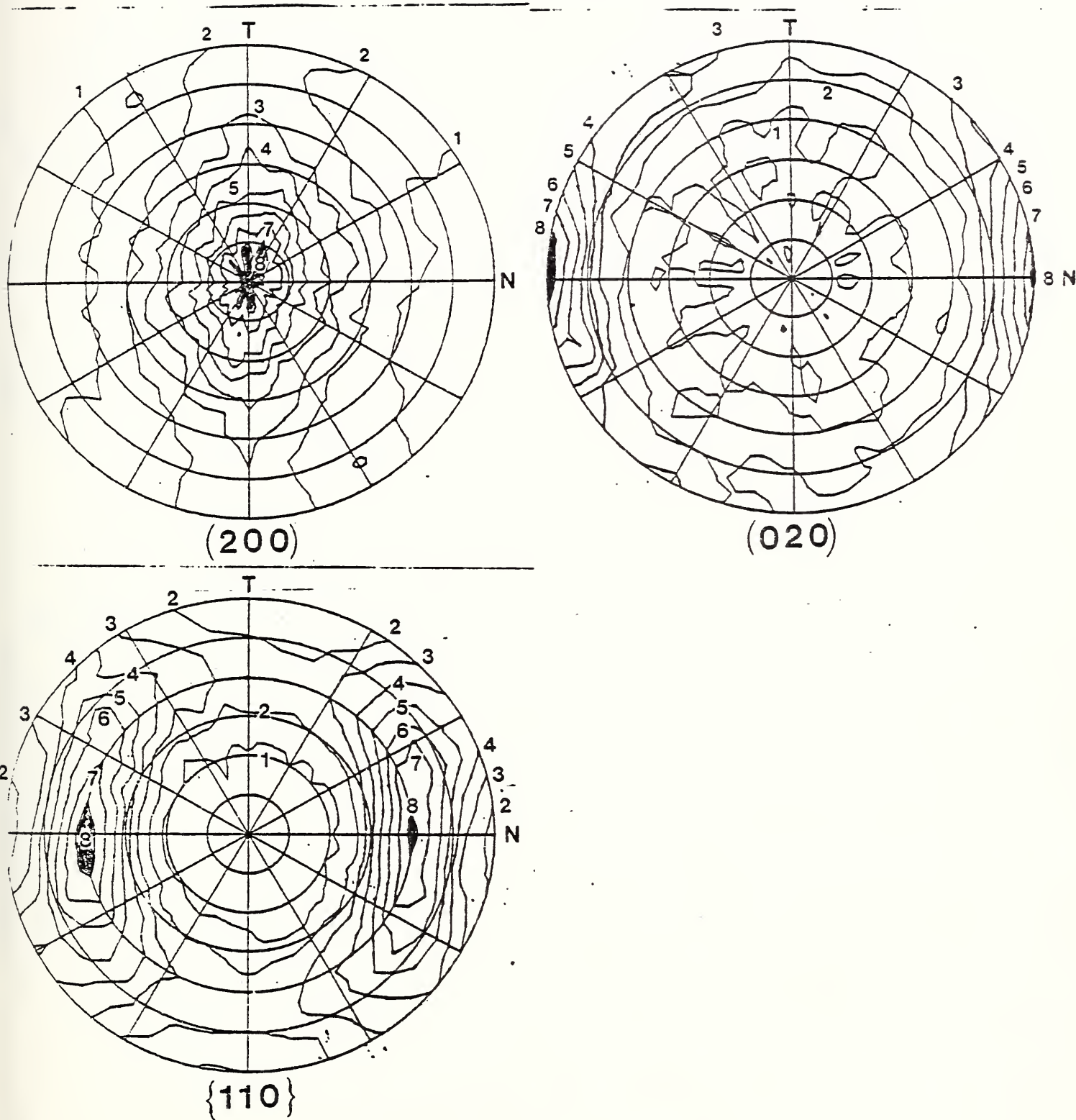
Fig. 12. (200), (020) and {110} pole figures of Cat.I film.
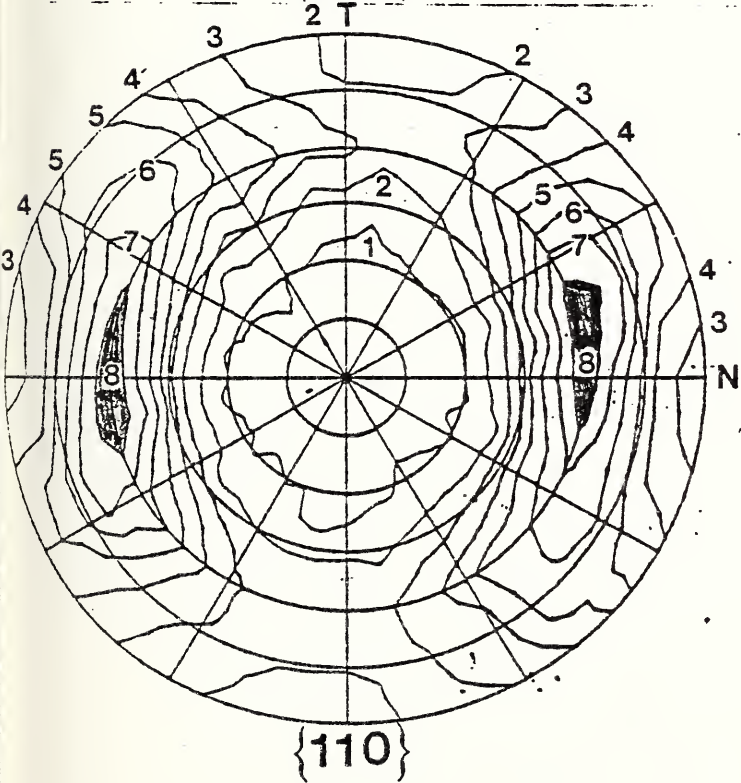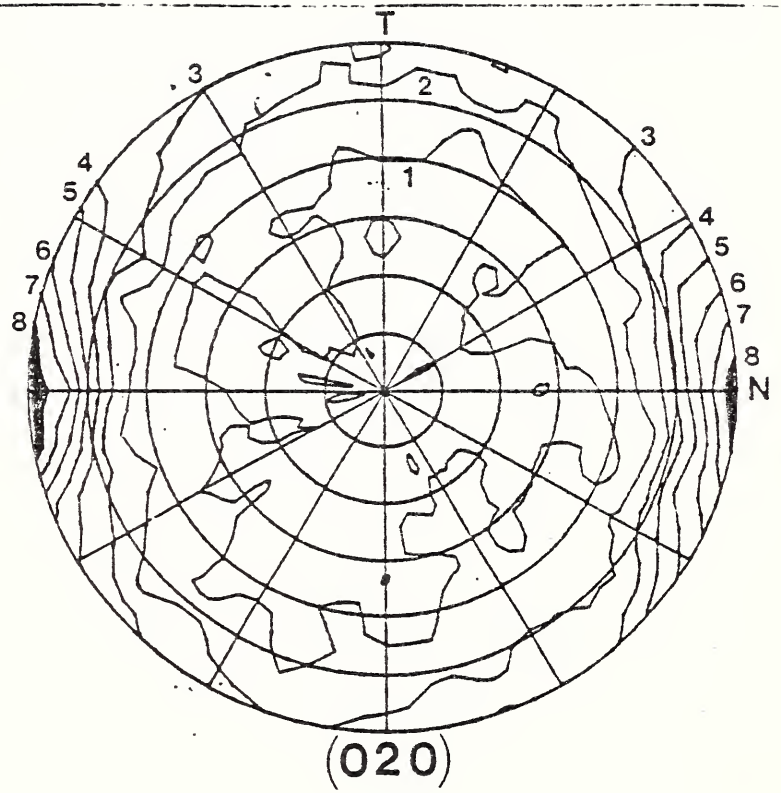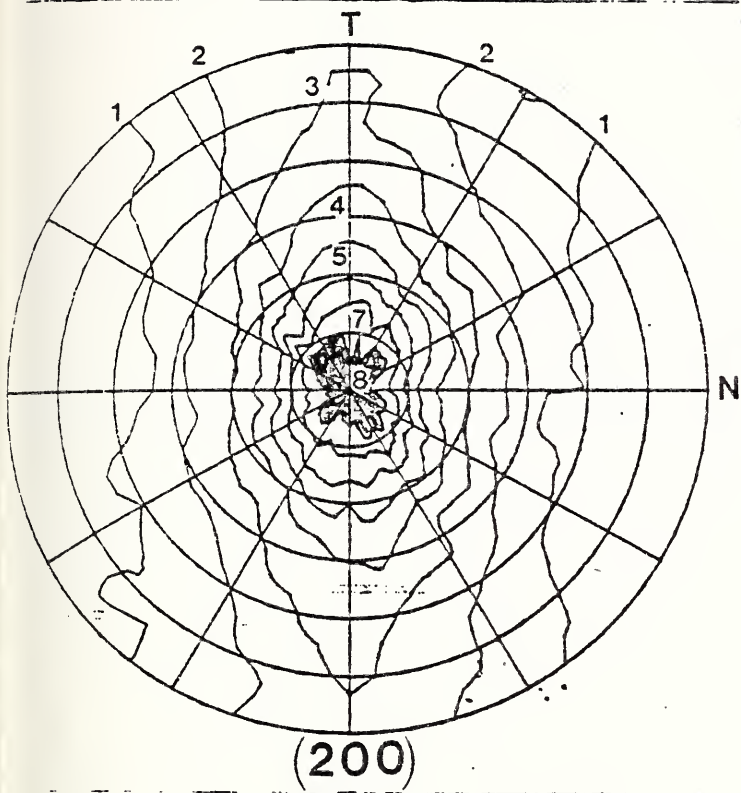
Fig. 13. (200), (020) and {110} pole figures of Cat. III film.
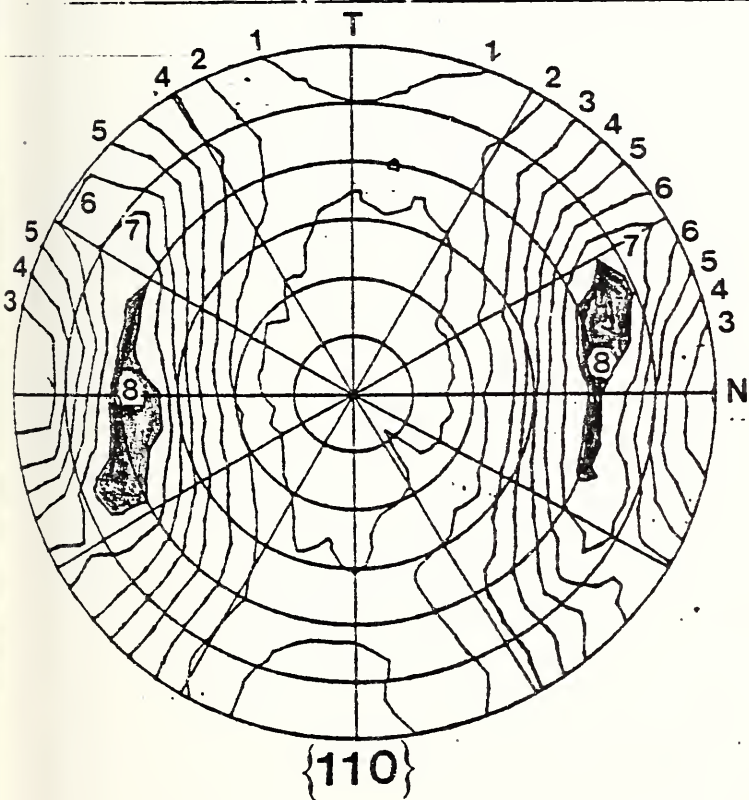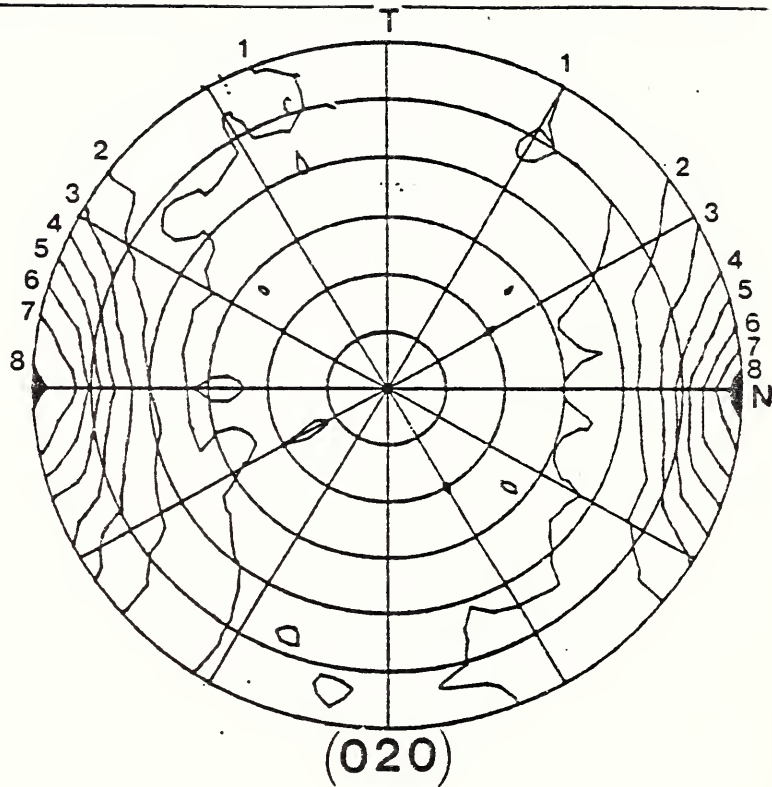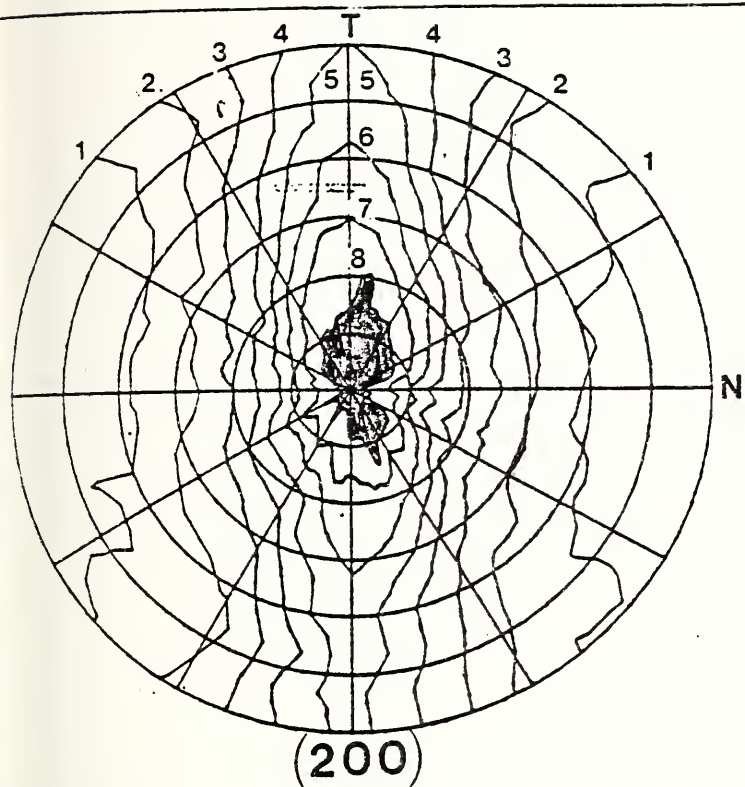
Fig. 14. (200), (020) and {110} pole figures of <u>film Bl.</u>
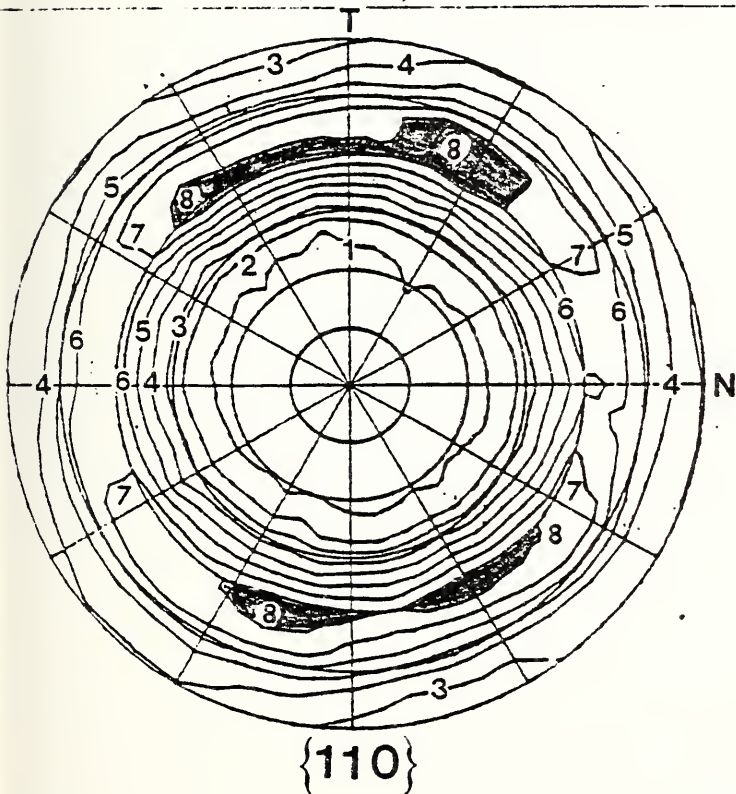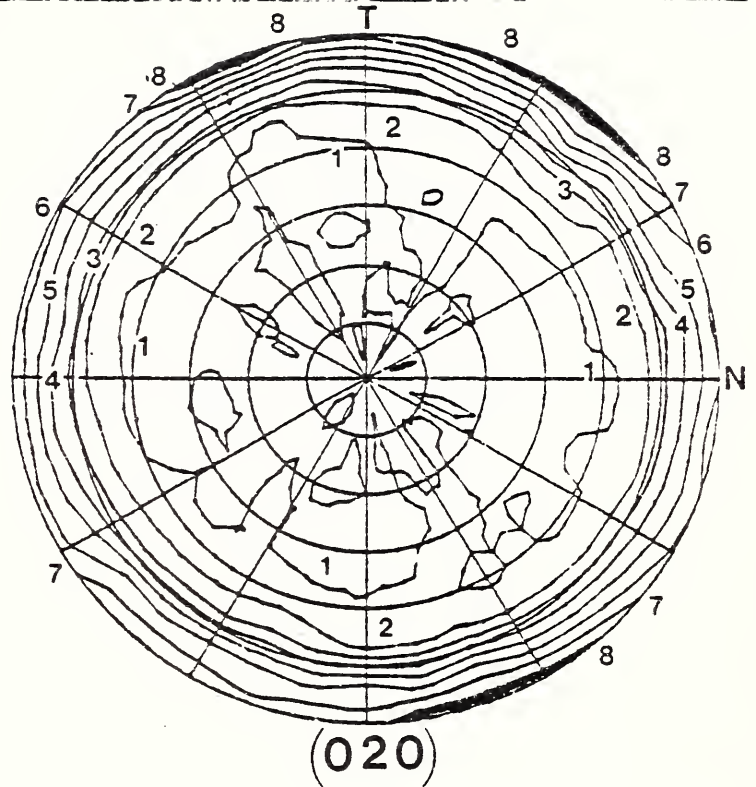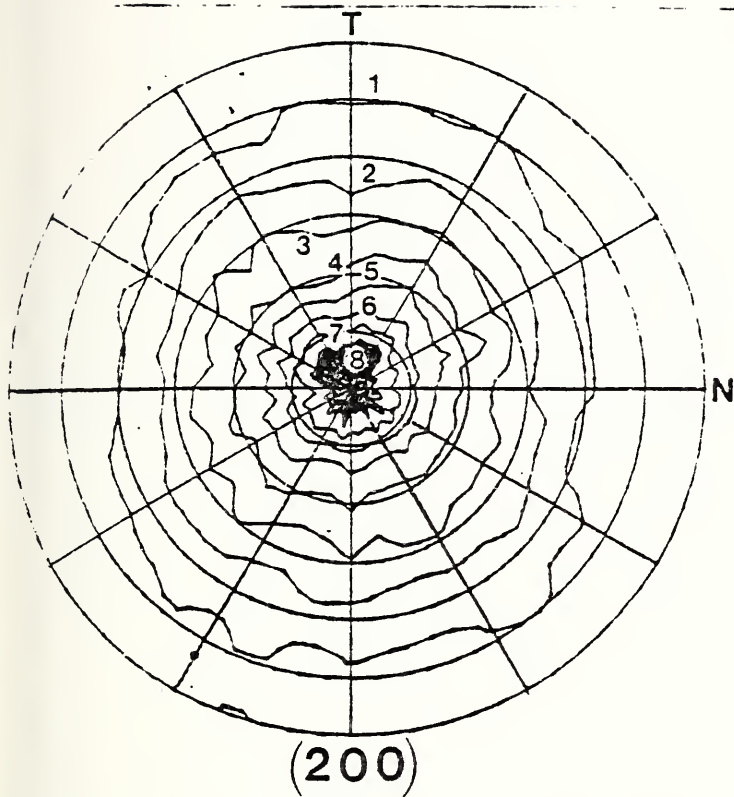
Fig. 15. (200), (020) and {110} pole figures of film F1.
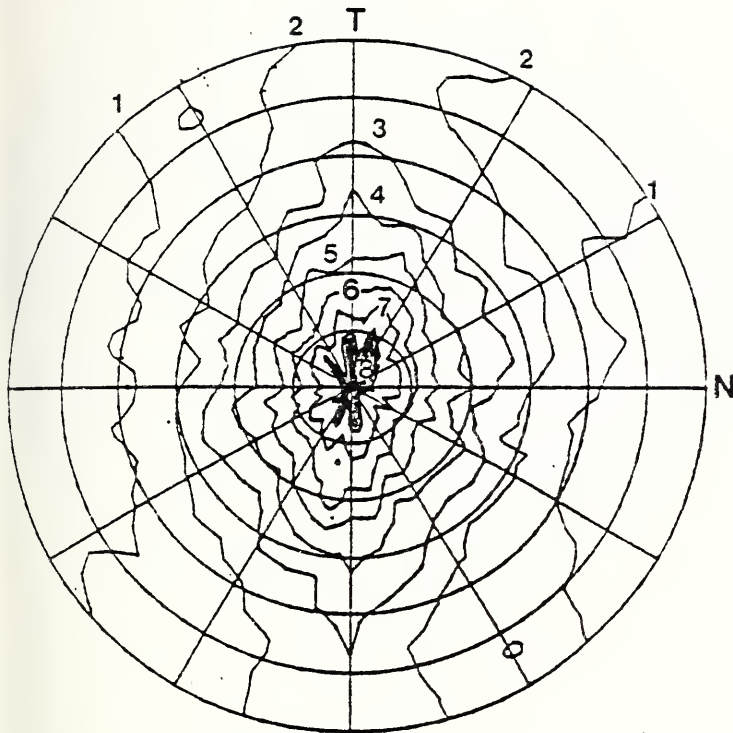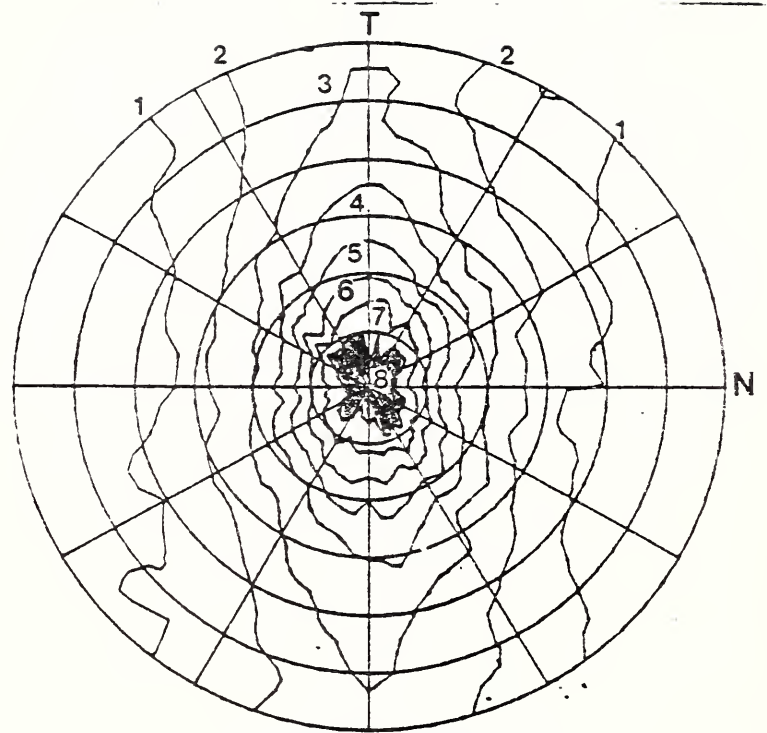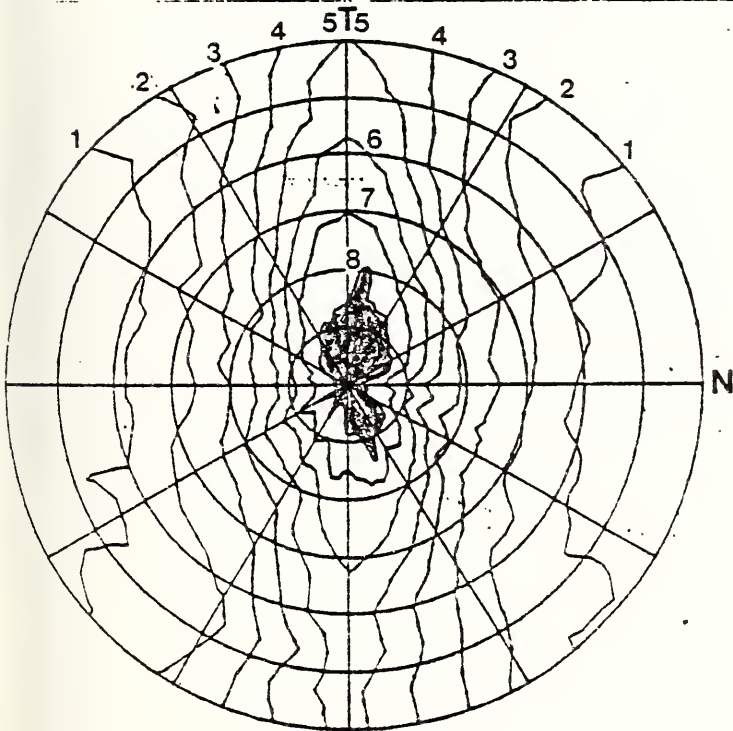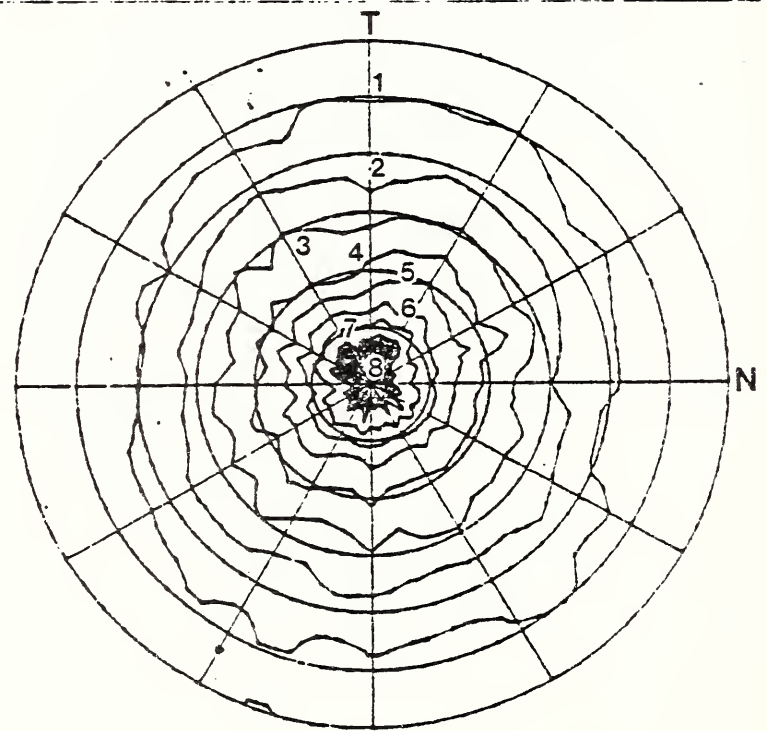
Fig. 16. (200) pole figures of films I, III, Bl and Fl.
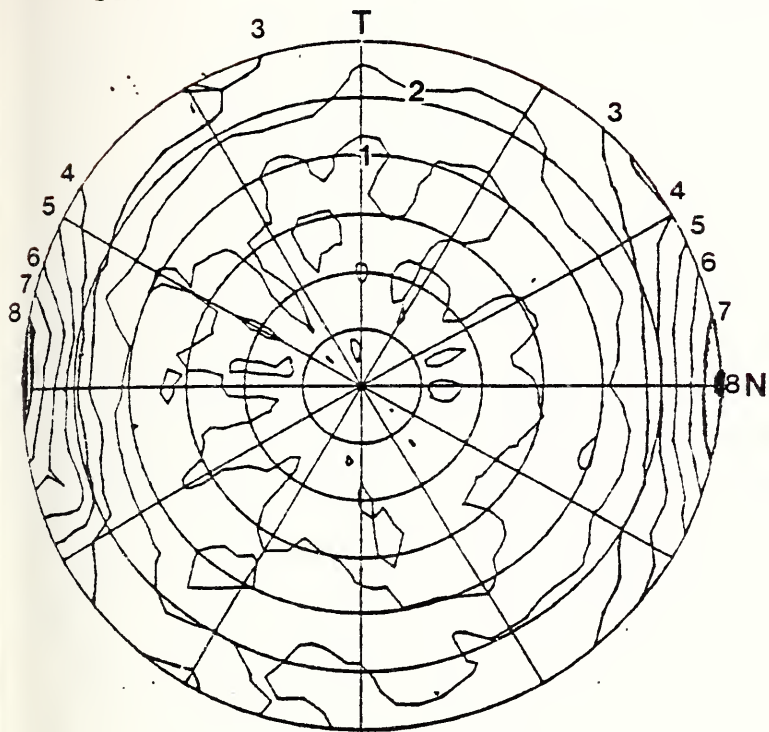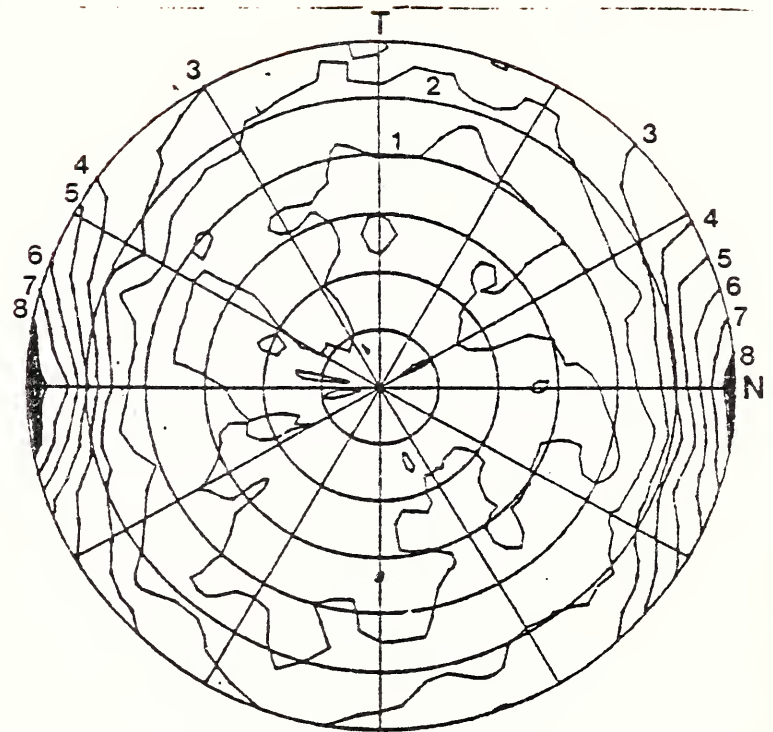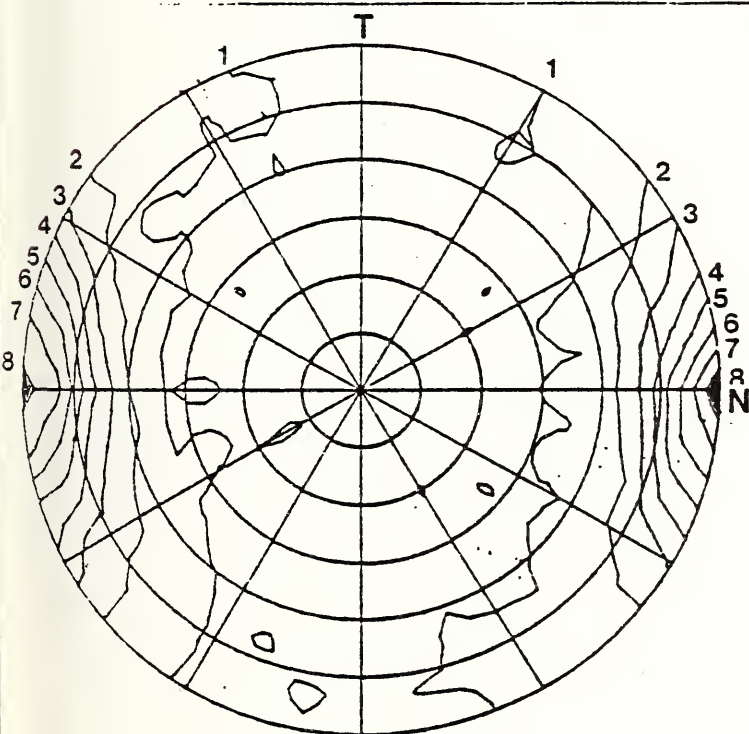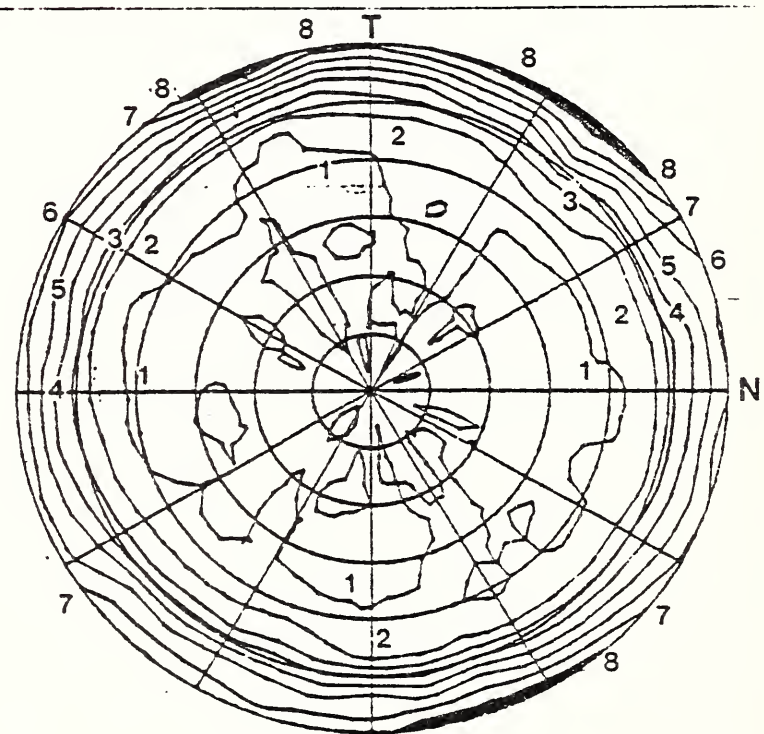
Fig. 17. (020) pole figures of films I, III, Bl, and Fl.
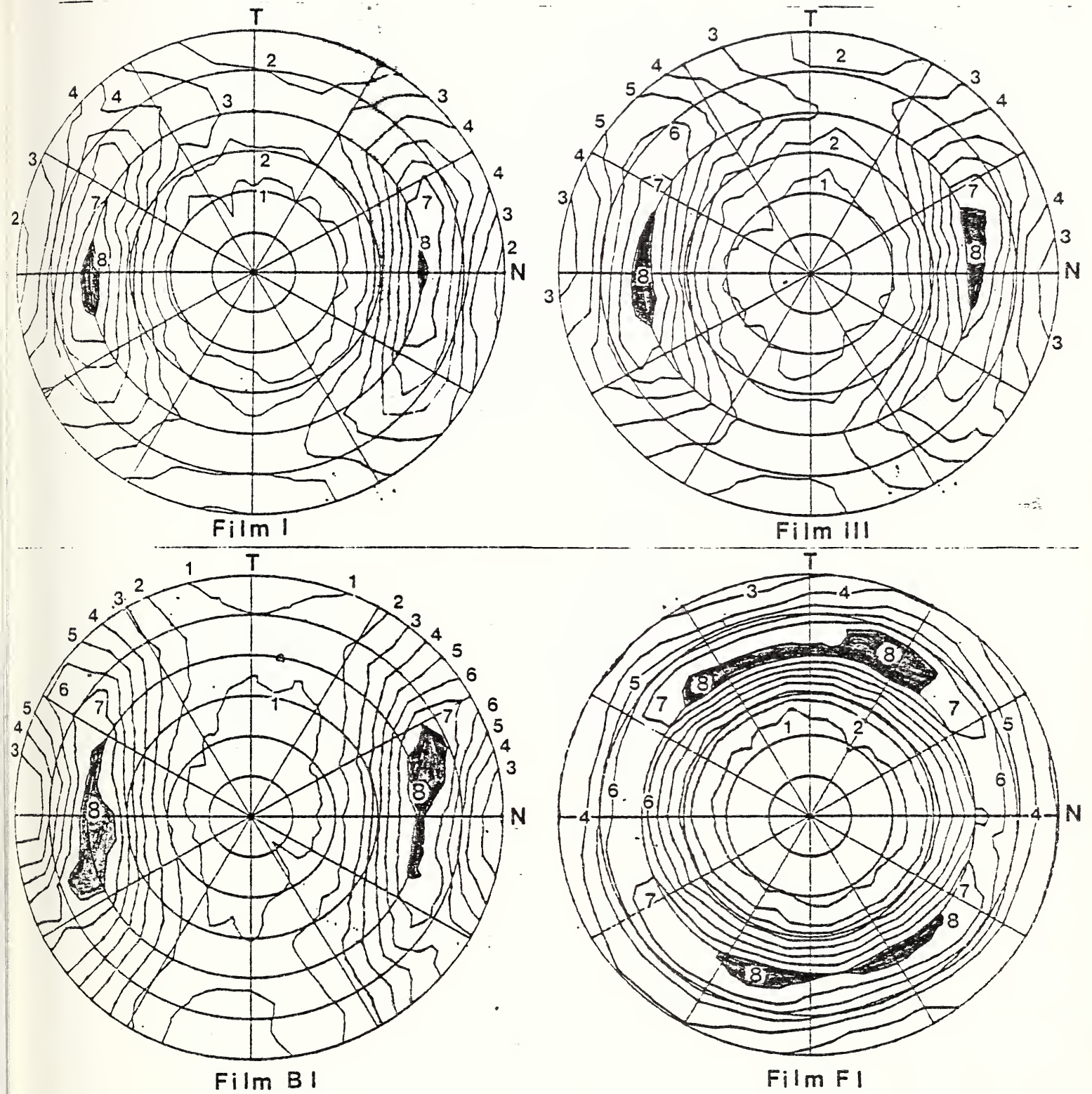
Fig. 18. {110} pole figures of films I, III, Bl and Fl.
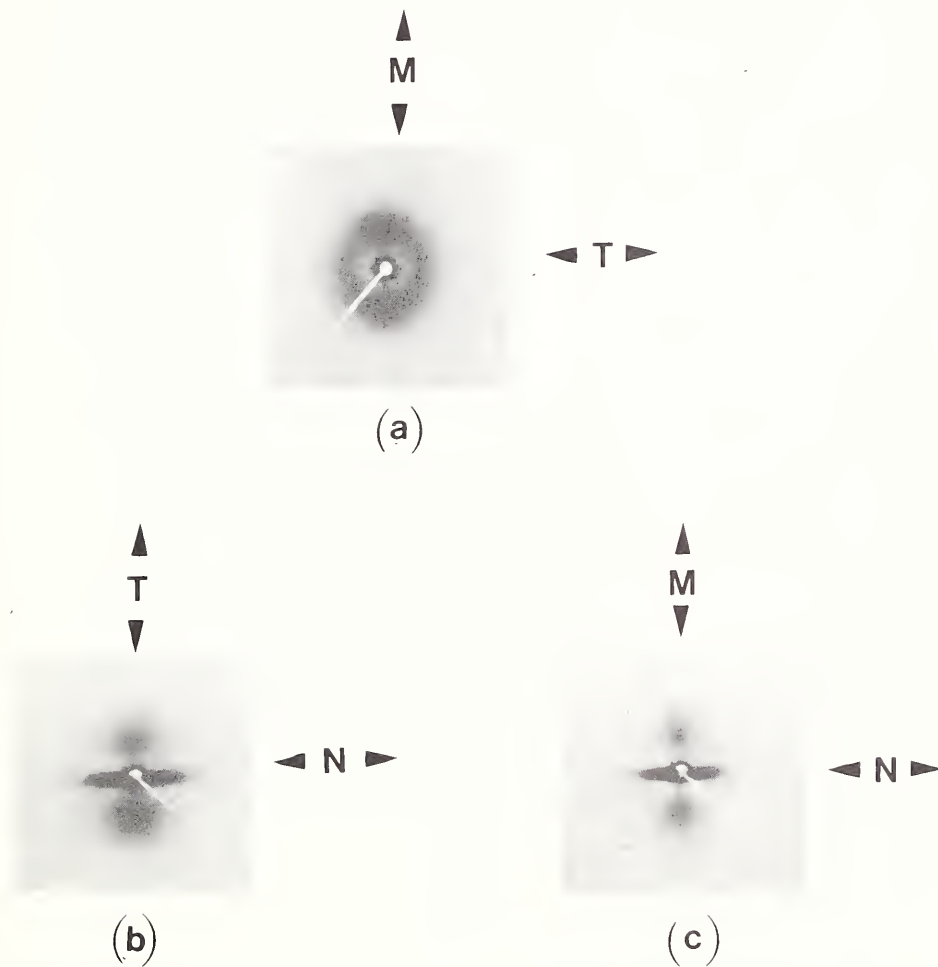
Fig. 19. Small angle x-ray diffraction patterns of Cat. I film. (a) X-ray beam parallel to N, (b) X-ray beam parallel to M, (c) X-ray beam parallel to T.
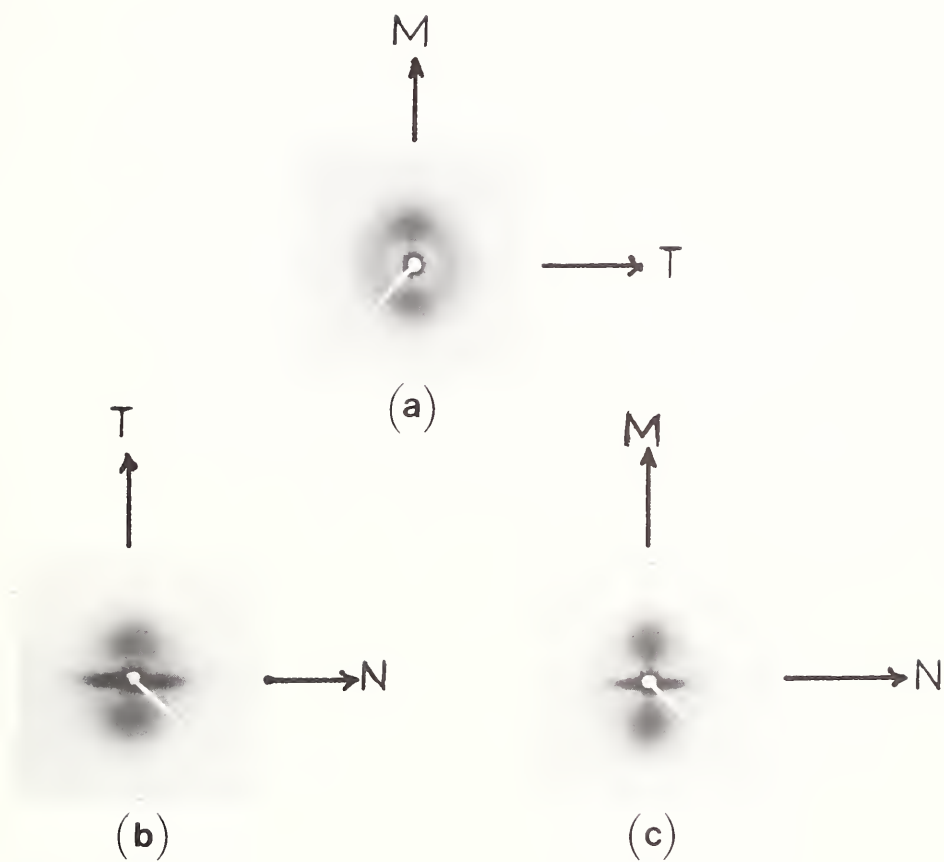
Fig. 20. Small angle x-ray scattering patterns exhibited by Cat. III film. (a) incident beam parallel to N. (b) X-ray beam parallel to M. (c) X-ray beam parallel to T.
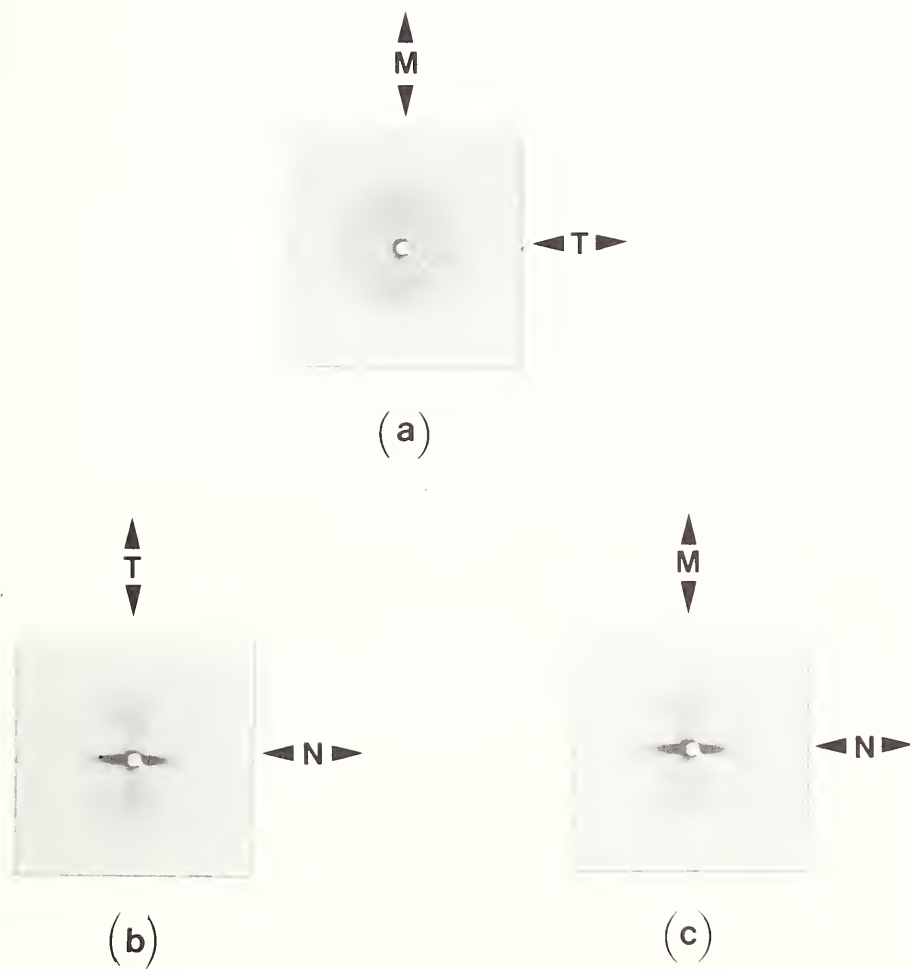
Fig. 21.   Small angle x-ray scattering patterns exhibited by the B1 film.
(a) Incident x-ray beam parallel to N. (b) X-ray beam parallel
to M. (c) X-ray beam parallel to T.

Fig. 22.   Small angle x-ray diffraction patterns from film Fl. Incident beam
in (a) parallel to N direction, (b) parallel to T direction.
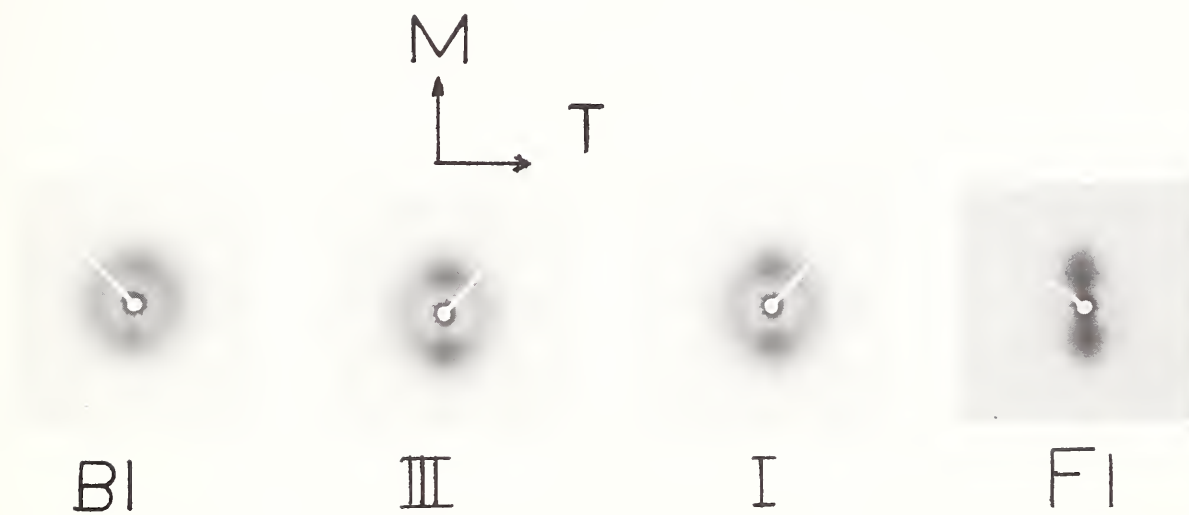
Fig. 23. Small angle x-ray diffraction patterns of films Bl, III, I
and Fl x-ray beam parallel to N.
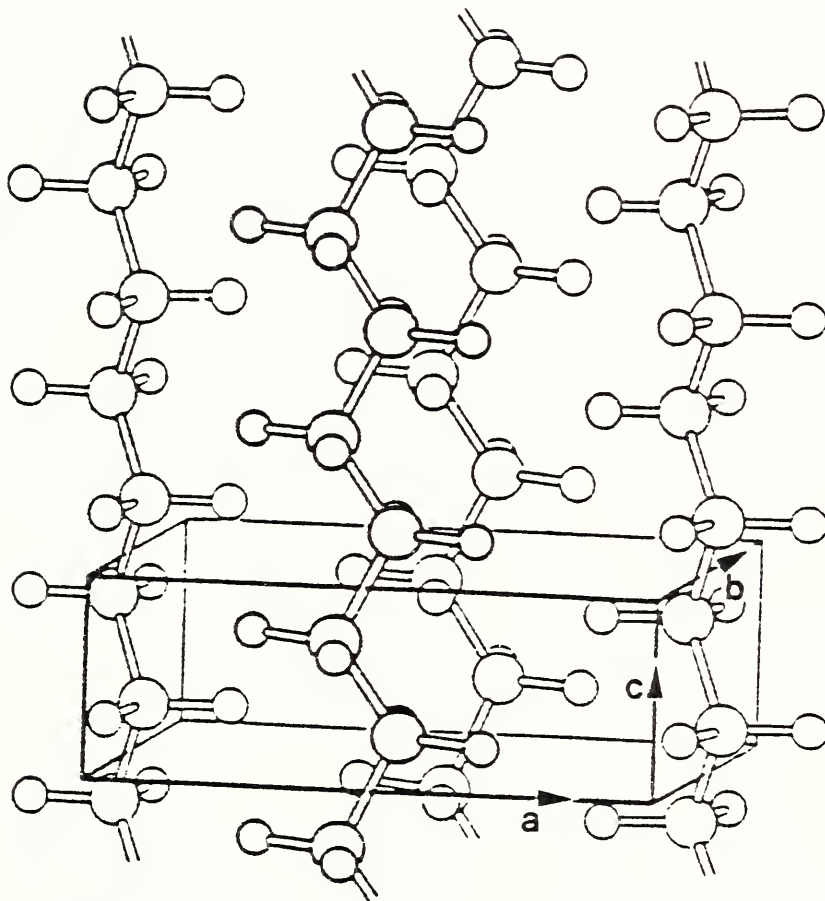
Fig. 24.   Orthorhombic unit cell of Polyethylene, after Bunn [13].

Fig. 25a. Spherulites in a sample of linear polyethylene as seen with a polarizing microscope (crossed polarizer and analyzer).
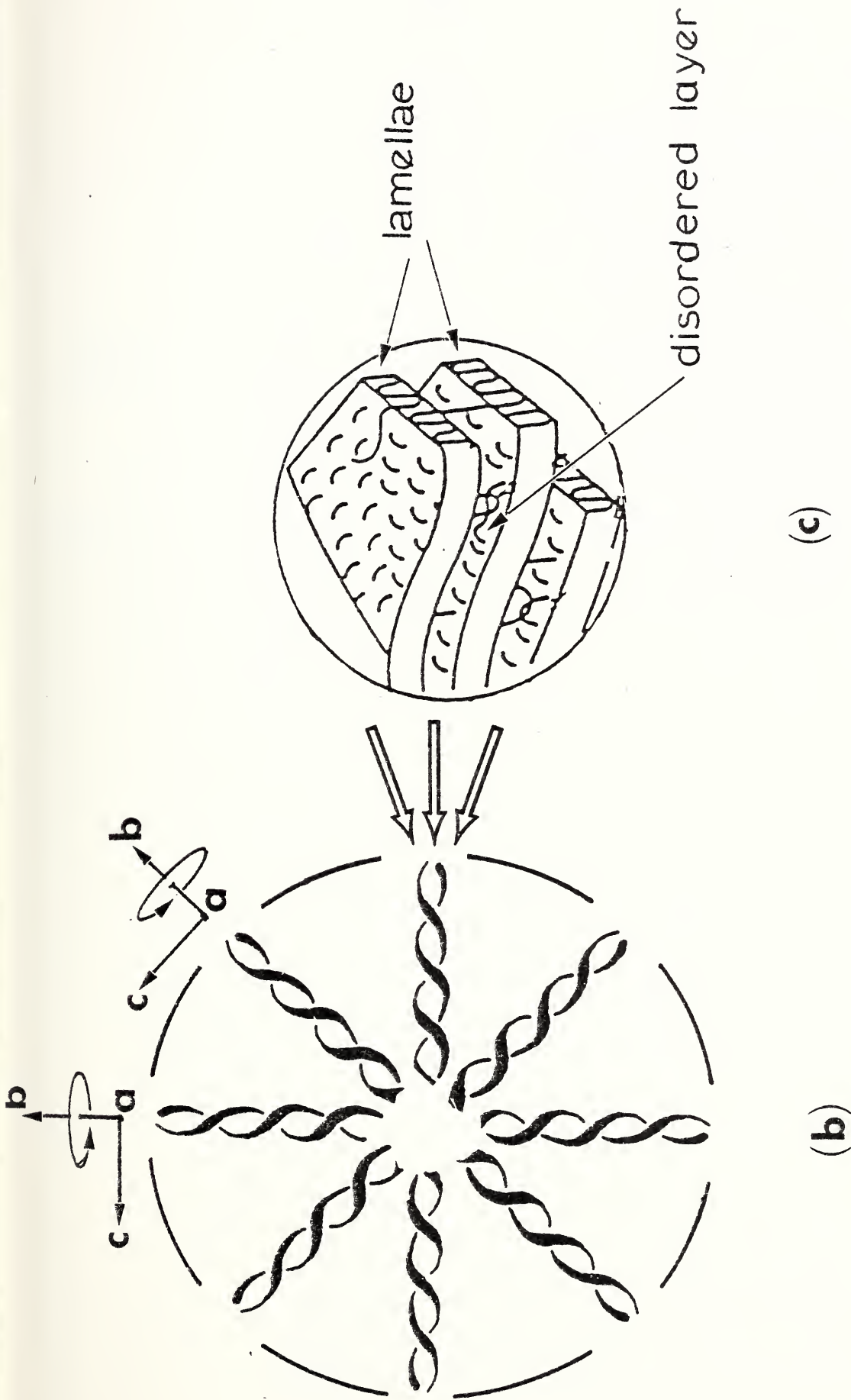
Fig. 25(b,c) A schematic representation of a diametric cross-section of a spherulite illustrating its radiating fine texture is shown in (b). The radiating crystals which are oriented with the b-axis parallel to the radial direction are twisted lamellae. A magnified rendition (after Hoffman et al [26]) of the lamellar character of the crystals in which the chains are folded is shown in (c) which also illustrates the occurrence of disordered layers sandwiched between neighboring lamellae (see text). Note that the c-axis in each lamella is oriented at right angles to the lamellar surfaces between which the chains are folded back and forth. Both the c-axis and the a-axis in the lamellae are oriented at right angles to the radial direction. Due to the twisted nature of the lamellae there is a periodic rotation of the a and c axis orientations about each radial path from the center to the outer regions of the spherulite.
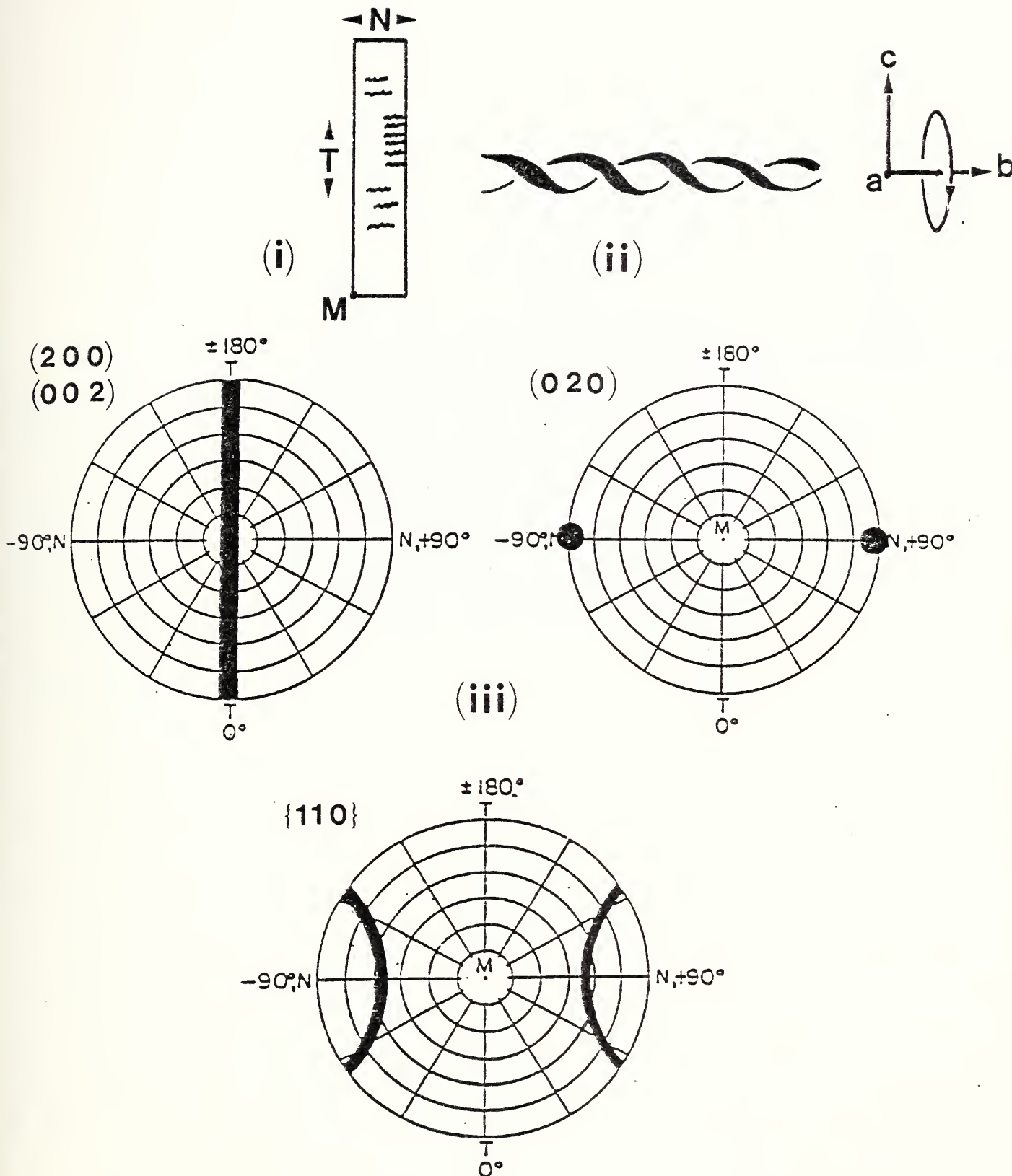
Fig. 26 (i) Schematic representation of Transcrystalline twisted lamellae as seen from the machine (M) direction. (ii) Magnified illustration of twisted lamellae which are oriented with their b-axis parallel to the N direction. Note the periodic rotation of the a and c axis orientations along the length of the twisted lamellae, i.e. about the N direction. Whether extensive regions having the transcrystalline orientation exist near the outer surface of the blown film, or whether regions where this orientation prevails are dispersed in the film remains an open question (see text). (iii) The (200), (020), (002) and {110} pole figures corresponding to the Transcrystalline orientation relative to the M, T and N directions in the film.
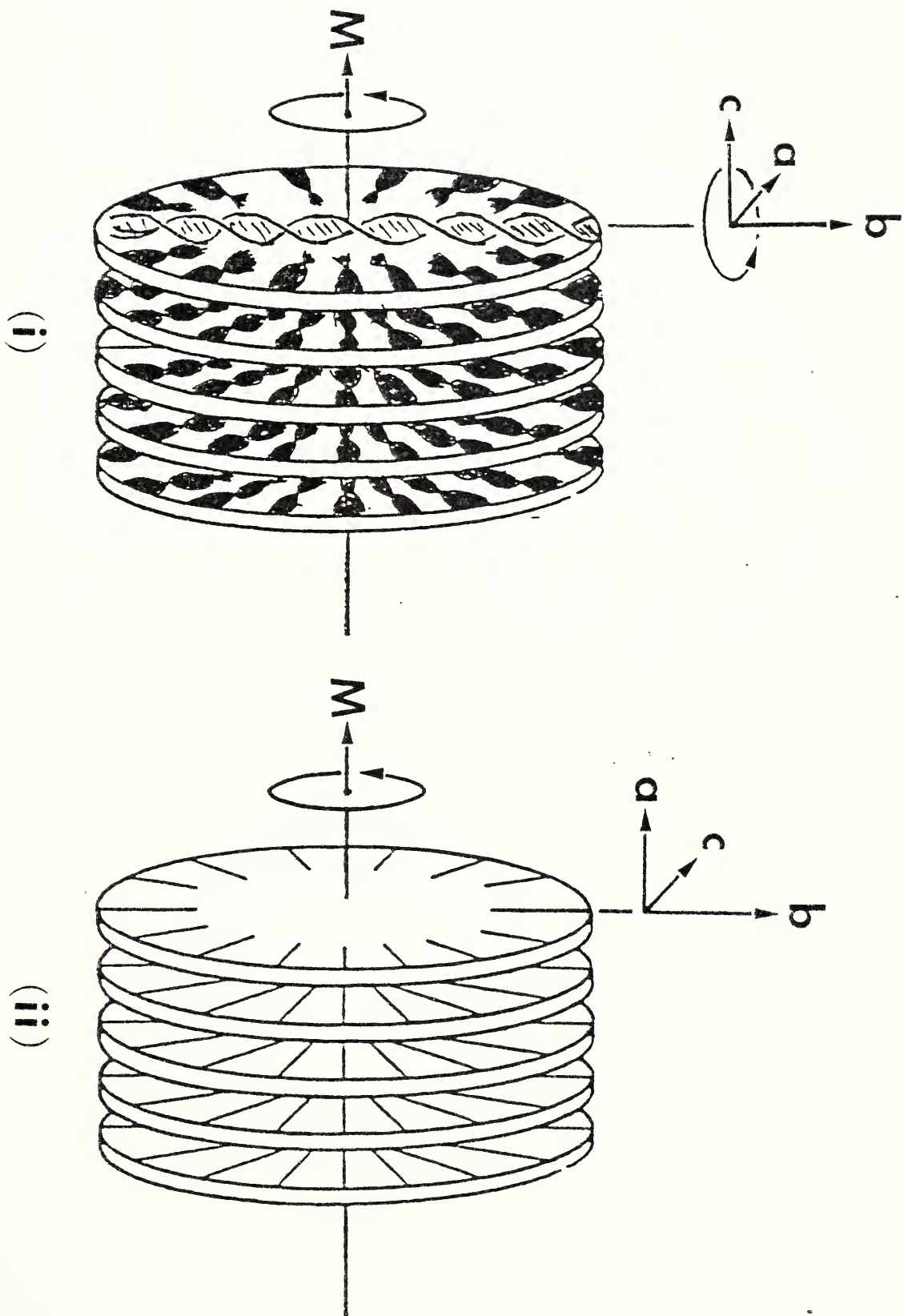
Fig. 27 Schematic representations of (i) the Row(ac) and (ii) the Row(a)
type of row structures in films (after Keller and Machin [7])
showing the orientations of the a, b, and c axes in the radiating
lamellae which constitute the cylindrites (see text). M is the
machine direction. Note that in both models the lamellae are
oriented with the b-axis parallel to the cylindrite radius. In the
Row(ac) structure the lamellae are twisted and, correspondingly,
there is a periodic rotation of the a and c axis orientations along
the length of the lamellae.

(i)

(ii)
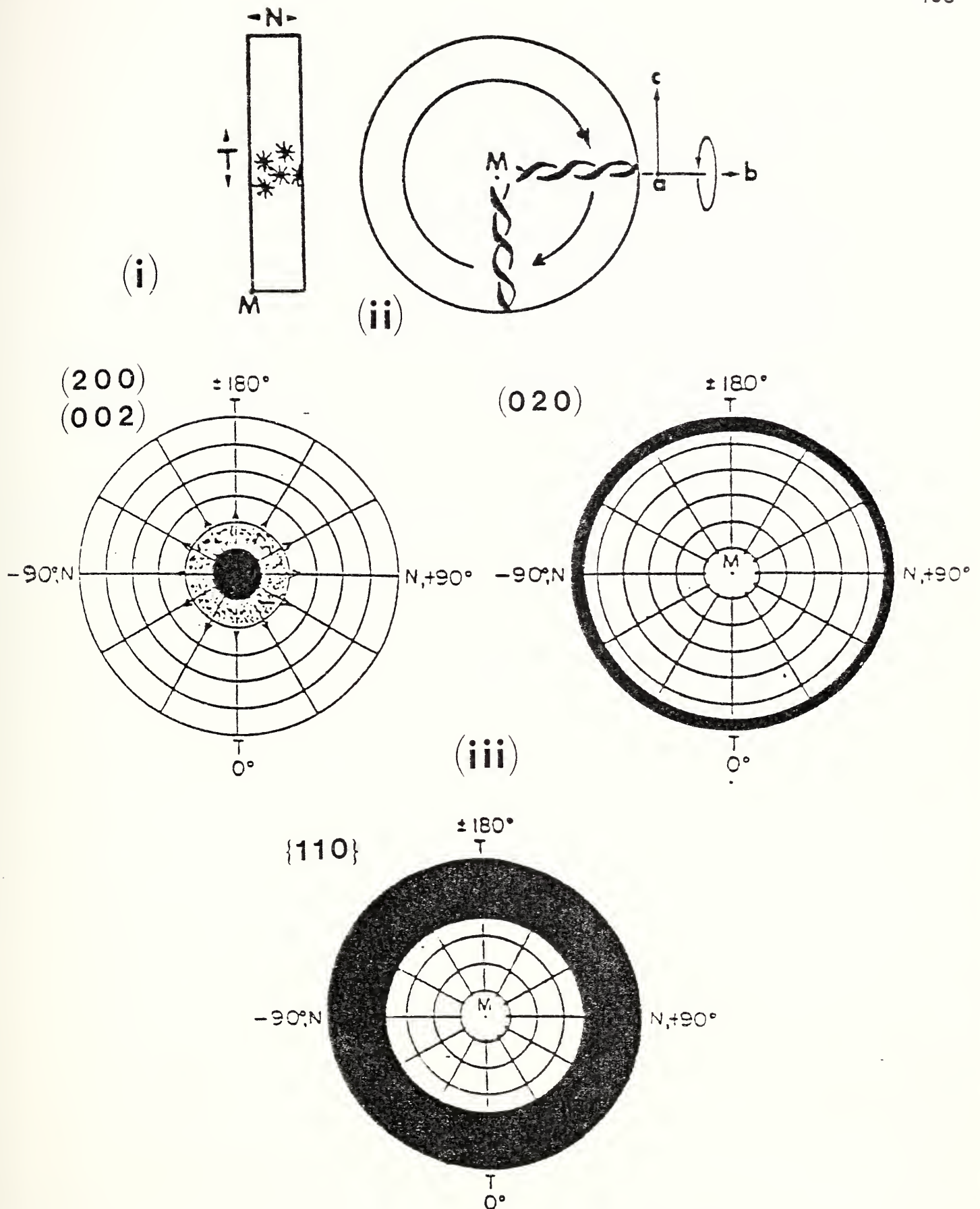
Fig. 28 (i) Schematic representation of the Row(ac) type of structure as
seen from the machine (M) direction. (ii) Orientation
characteristics of the constituent _twisted_ lamellae in the
cylindrites (see Fig. 27) relative to the radial direction.
(iii) The (200), (020), (002) and {110} pole figures
corresponding to preferred orientation characteristics of the
Row(ac) structure relative to the M, T, and N directions in the
film (see text).
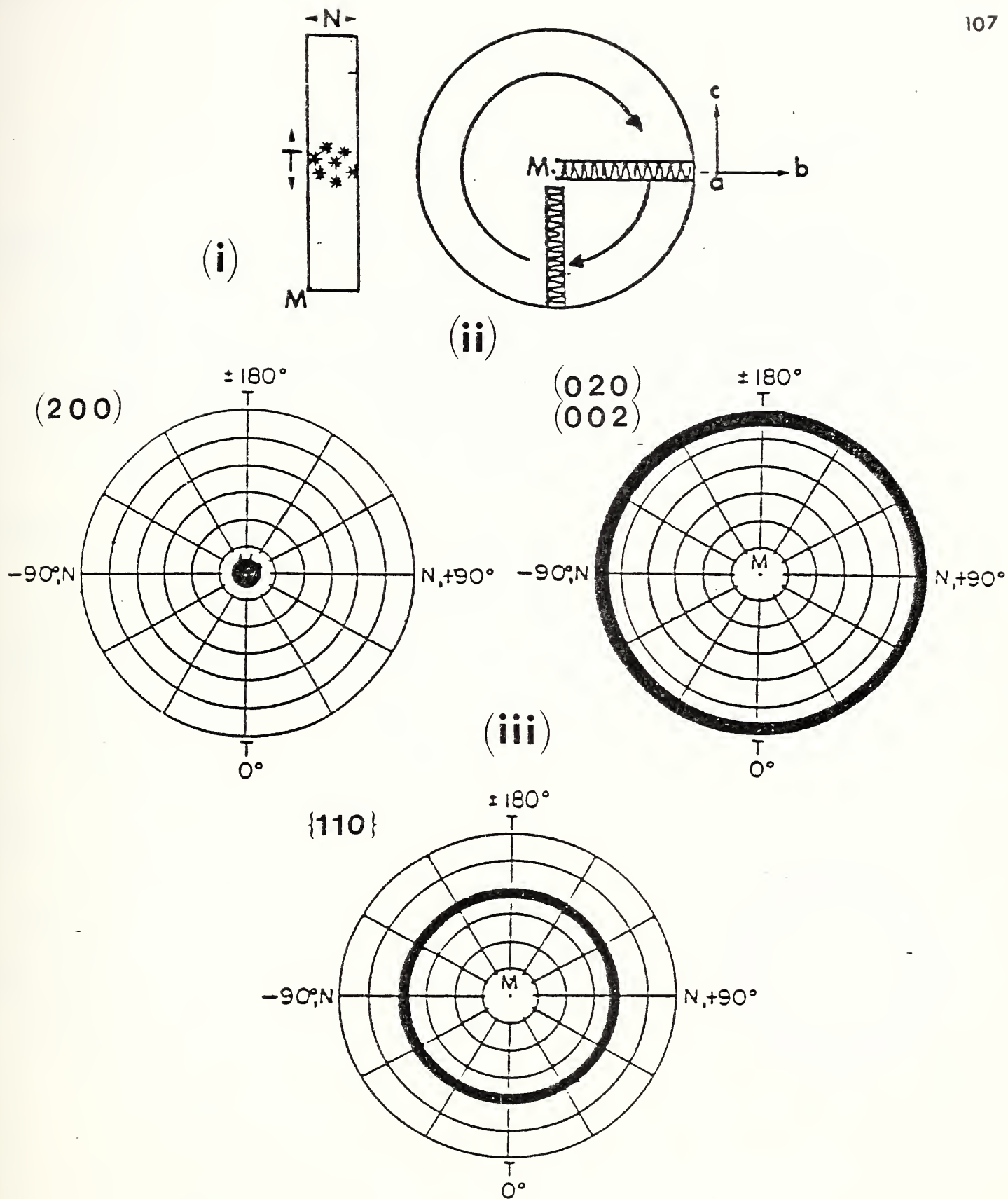
Fig. 29 (i) Schematic representation of the Row(a) type of structure as seen from the machine (M) direction. (ii) Orientation characteristics of the constituent lamellae in the cylindrites (see Fig. 27b) relative to the radial direction. (iii) The (200), (020), (002) AND {110} pole figures corresponding to the preferred orientation characteristics of the Row(a) structure relative to the M, T, and N directions in the film (see text).
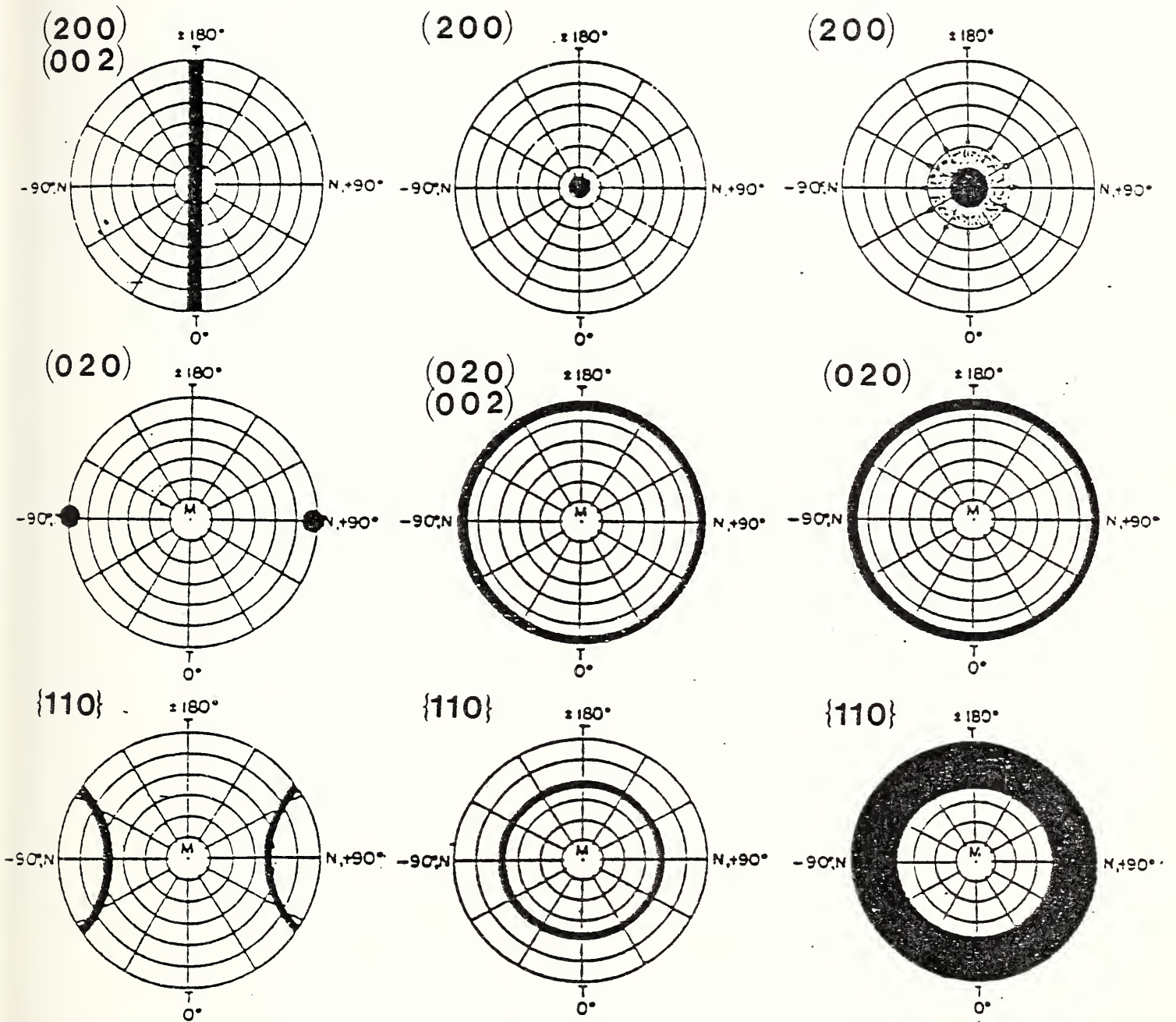
Fig. 30   The (200), (020), (002) and {110} pole figures corresponding to the
Transcrystalline, Row(a), and Row(ac) model orientations in the
films.
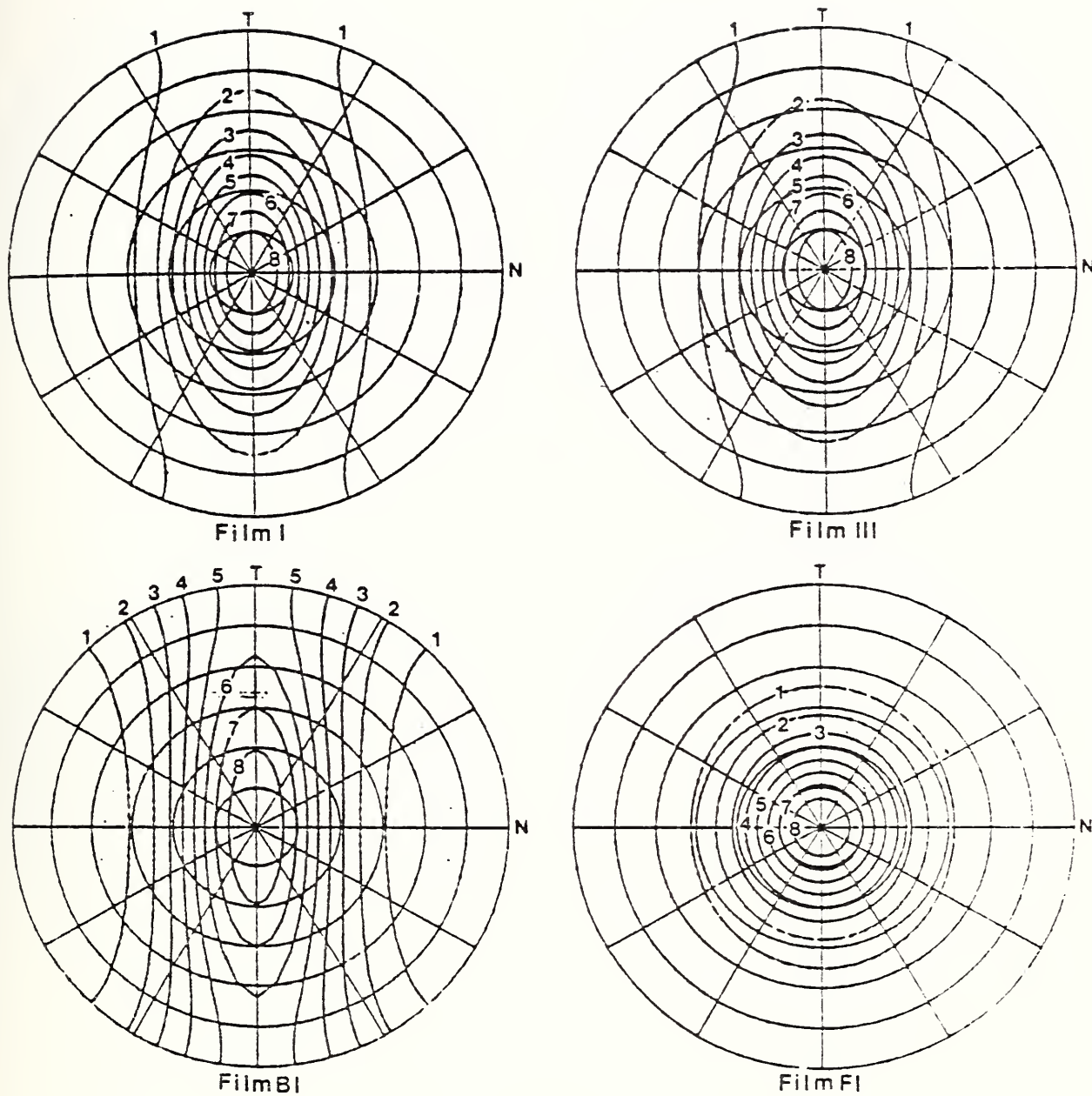
Fig. 31. Pole figures representing the results of the numerical simulations of the (200) pole intensity distributions in the Cat. I, Cat. III, Bl and Fl films.

Fig. 32. Pole figures representing the results of the numerical simulations of the (020) pole intensity distributions in the Cat. I, Cat. III, B1, and F1 films.
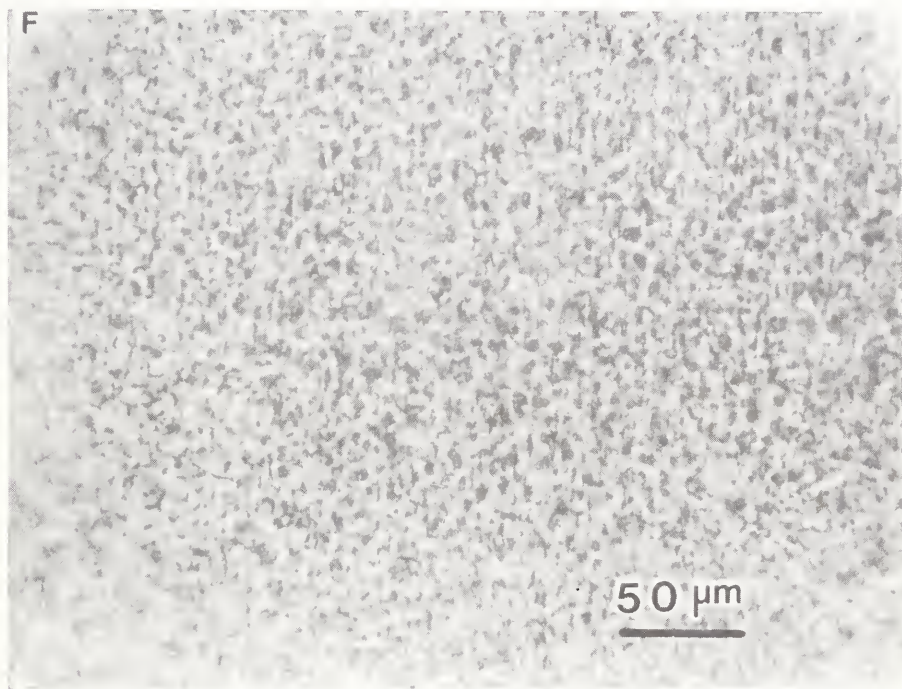
Fig. 33. Phase contrast light optical micrograph of film F1. Machine direction (M) is vertical. Note overall mottled appearance and faintly discernible fine striations running parallel to machine direction.
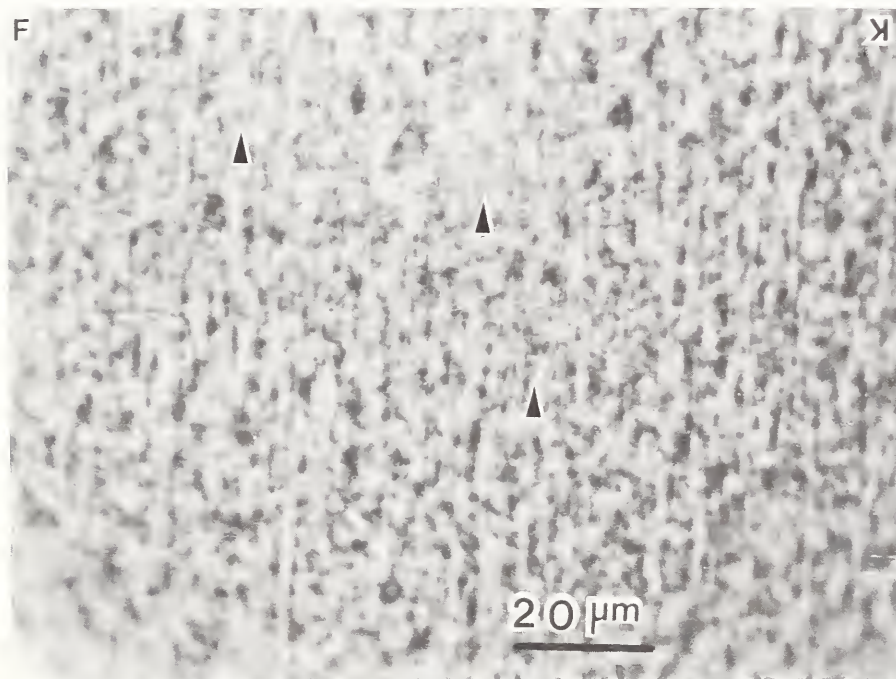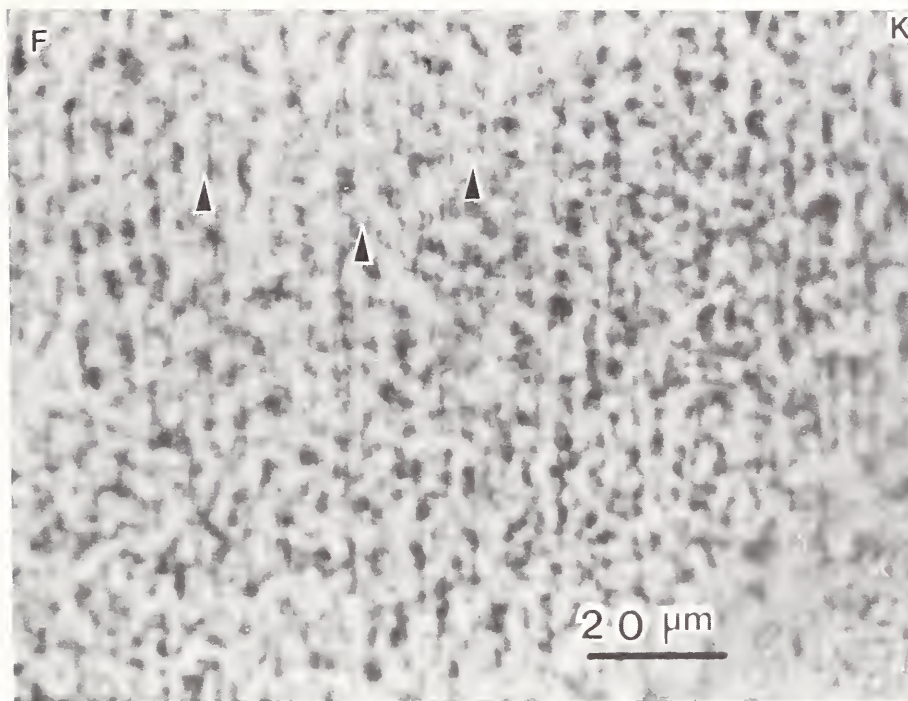
Fig. 34. Phase contrast light optical micrographs of replicas of opposite surfaces of film F1. Machine direction vertical. Arrows point to regions where finely separated striations running parallel to the machine direction can be seen. (Note magnification is higher than in Fig. 33).
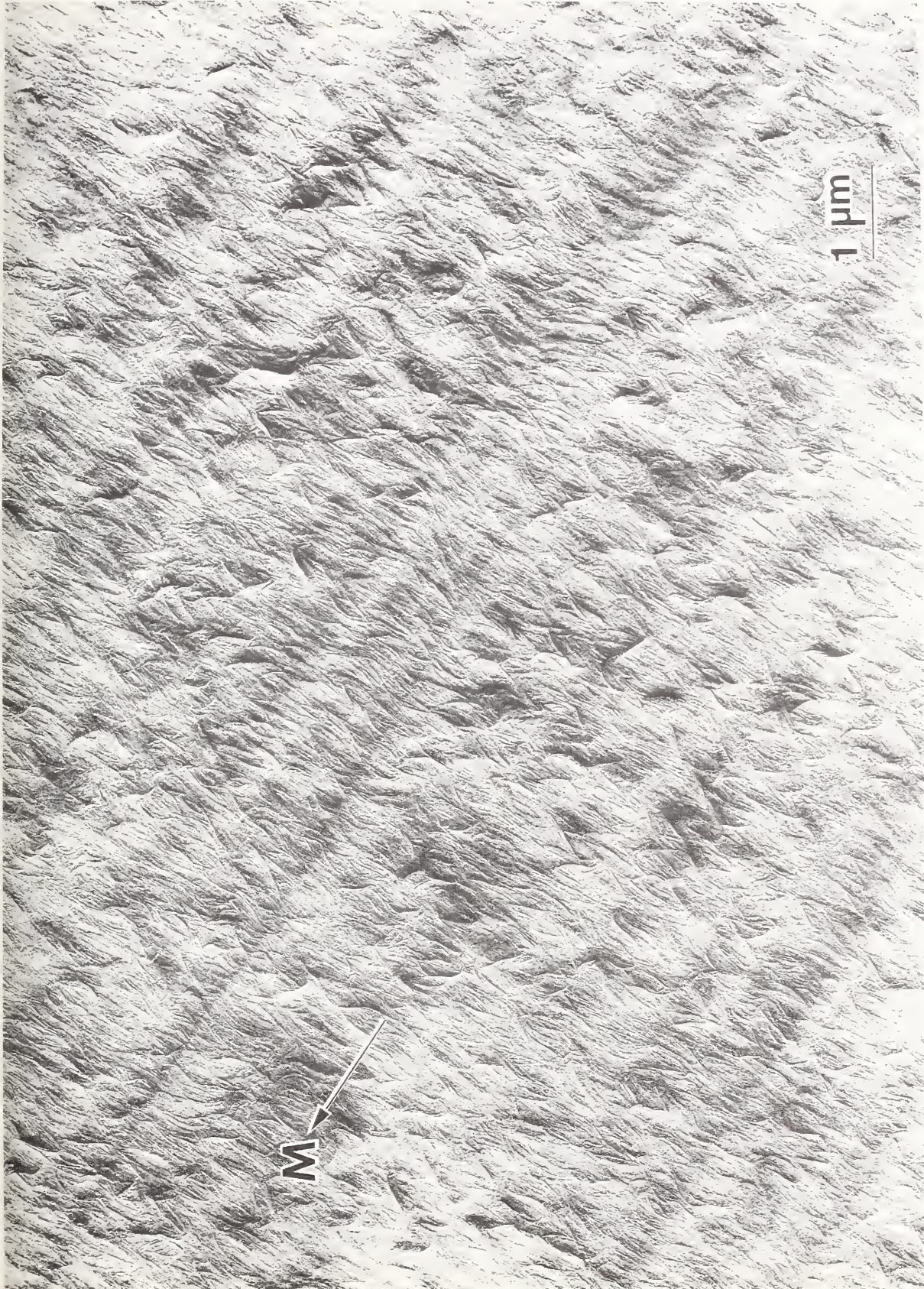
Fig. 35. Electron micrograph of a replica of one of the surfaces of film Fl. Machine (M) direction is parallel to arrow. Note ridges running parallel to M, and the orientation of the lamellar edges at right angles to M.

Fig. 36. Higher magnification electron micrograph of another region of the same surface of film Fl as that replicated in Fig. 35. Machine direction M is parallel to arrow.
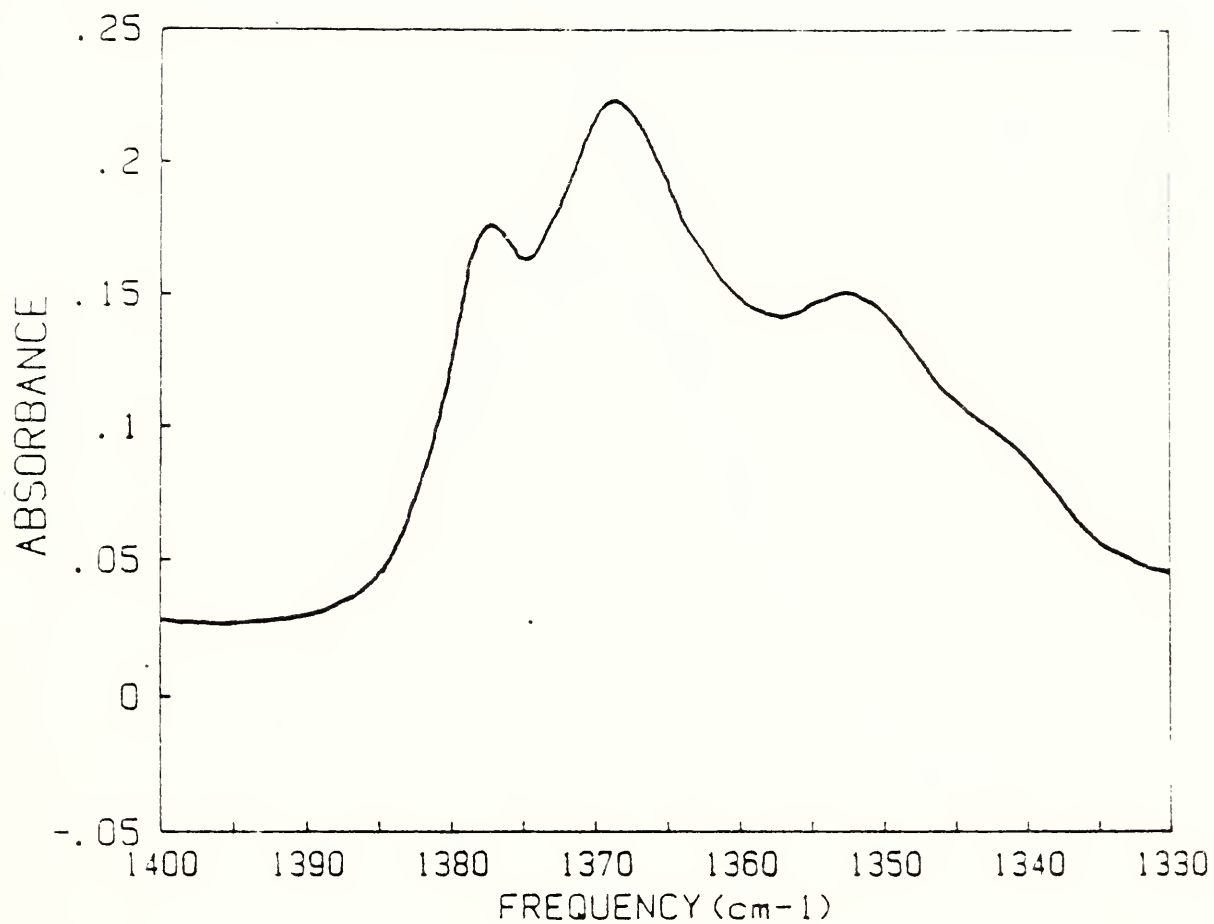
Fig. 37. - Room temperature Infrared Spectrum in the frequency range 1330 cm^{-1} to 1400 cm^{-1} obtained from the F1 film after it had been melted and cooled to room temperature.
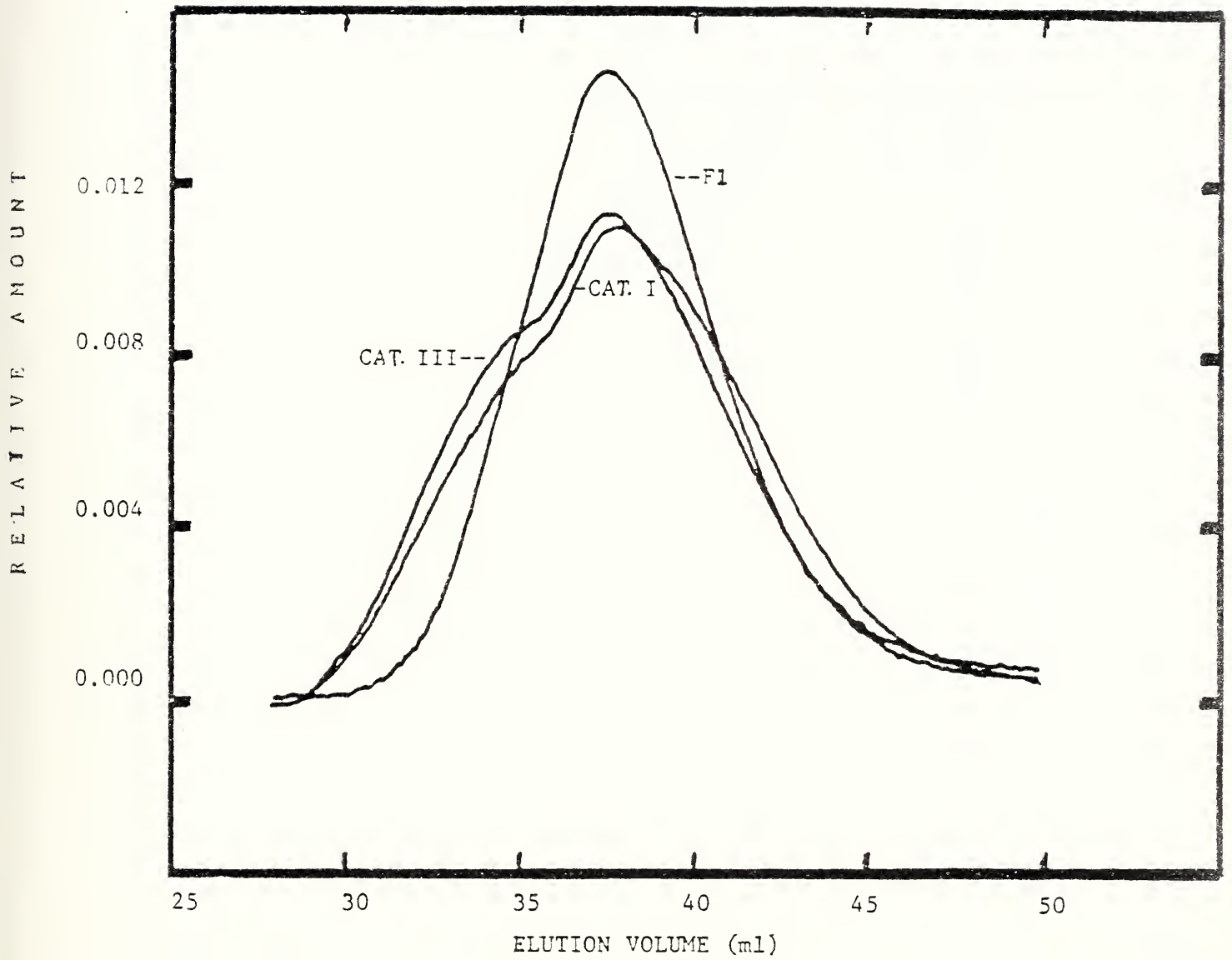
Fig. 38. Normalized Size Exclusion Chromatographs of the Cat. I, Cat. III and Fl films (Series C measurements, Table 13).
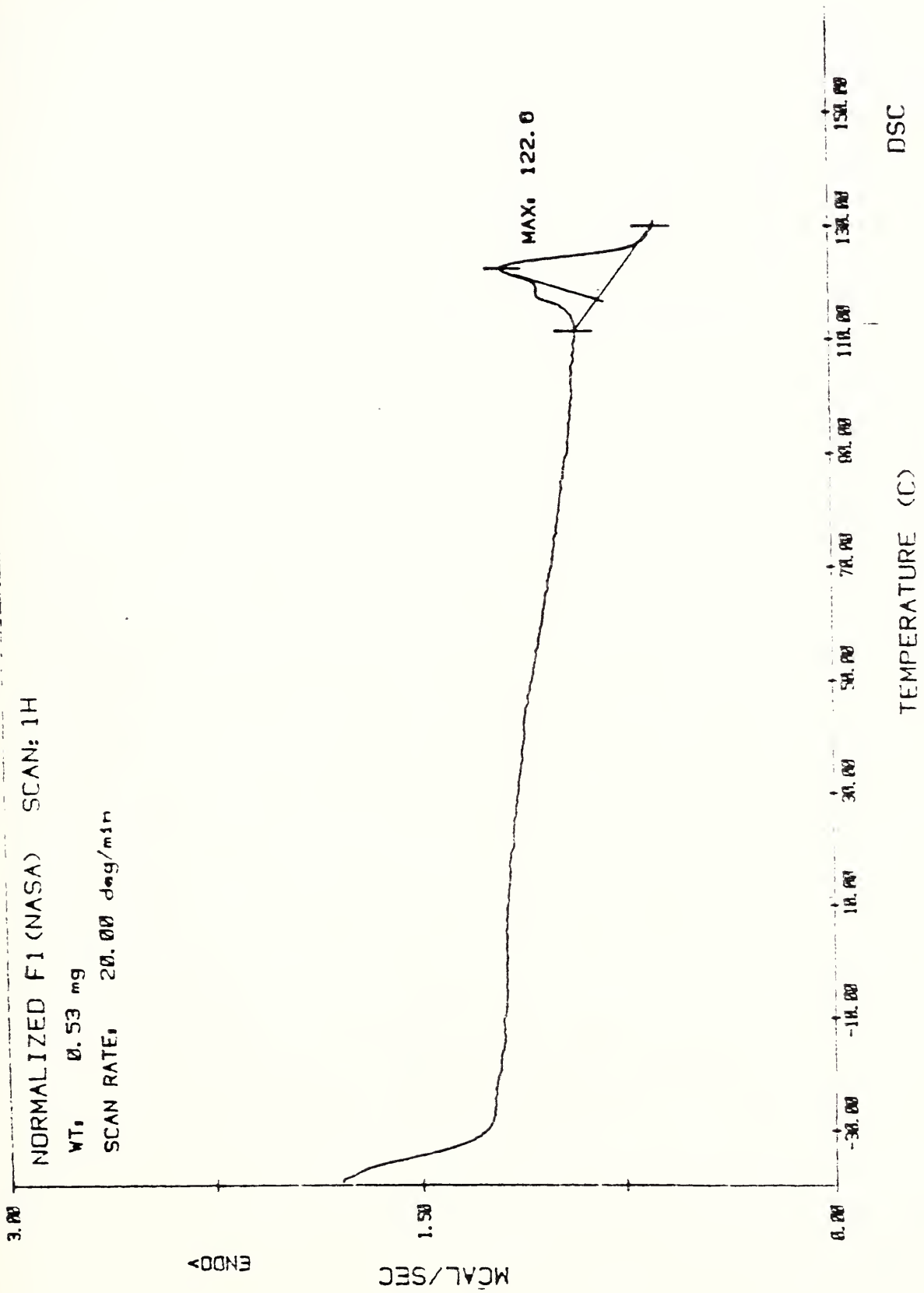
Fig. 39a. DSC scan of Film F1: First heating cycle
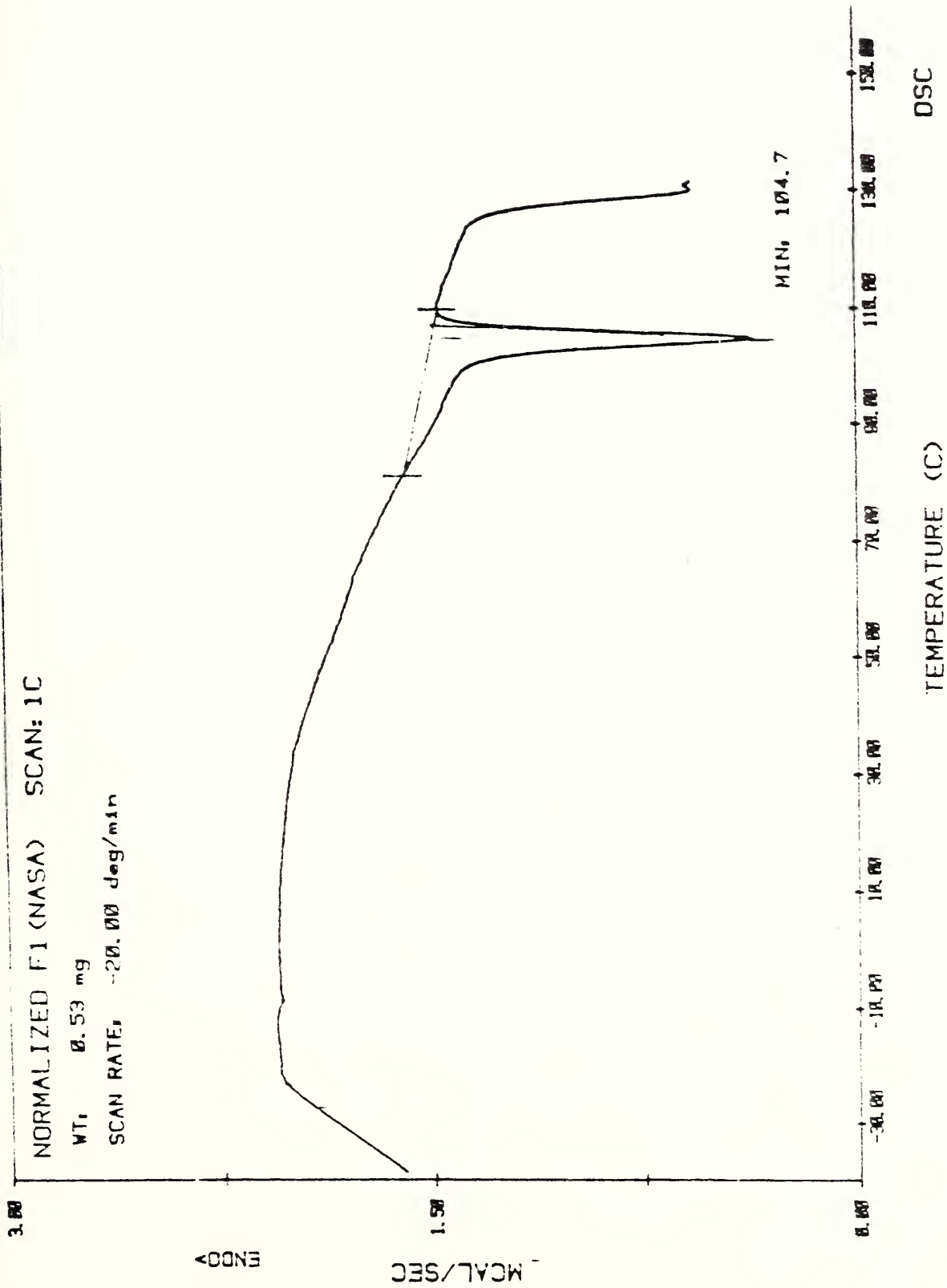
Fig. 39b. DSC scan of Film F1: First cooling cycle
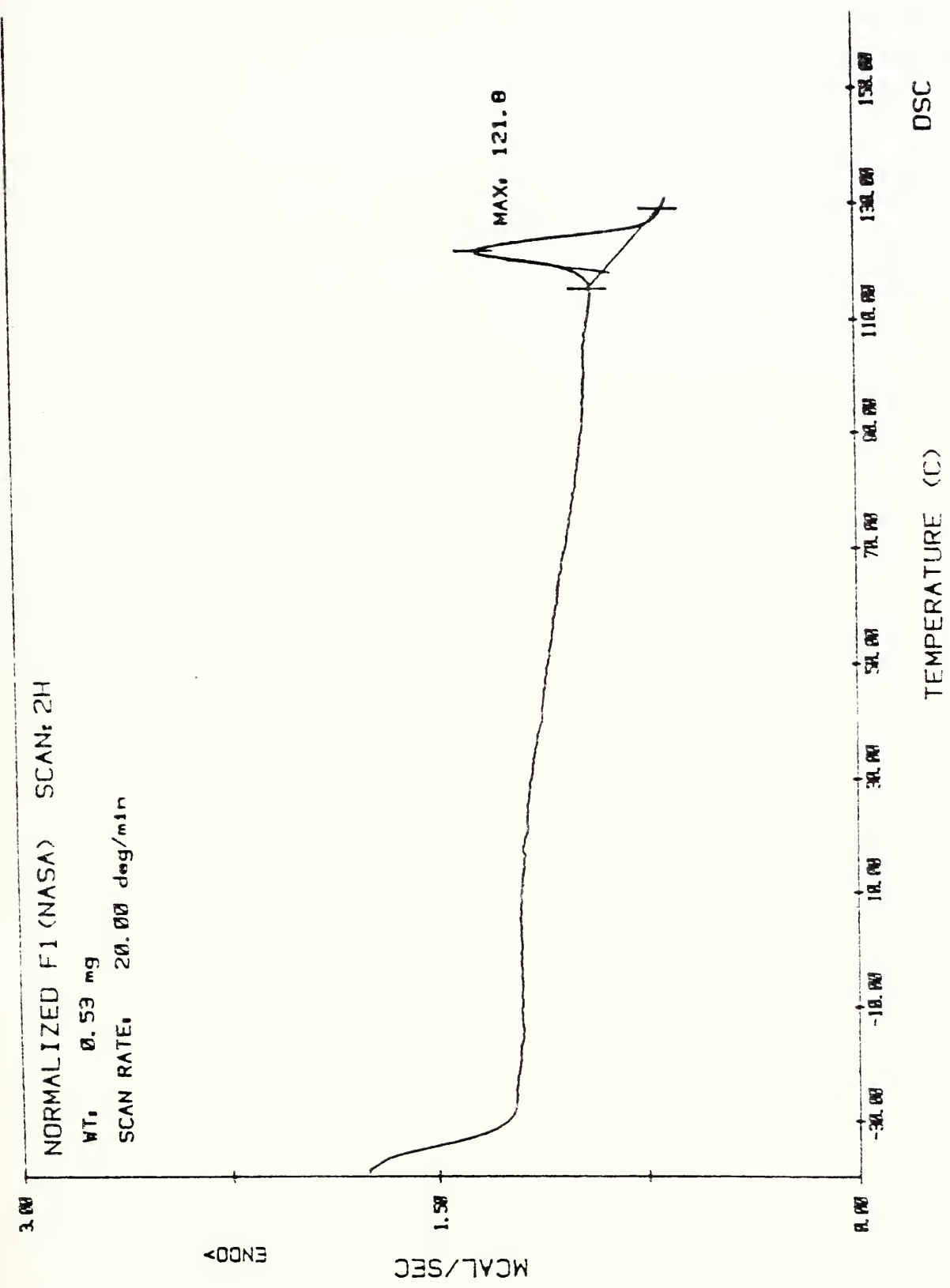
Fig. 39c. DSC scan of Film F1: Second heating cycle
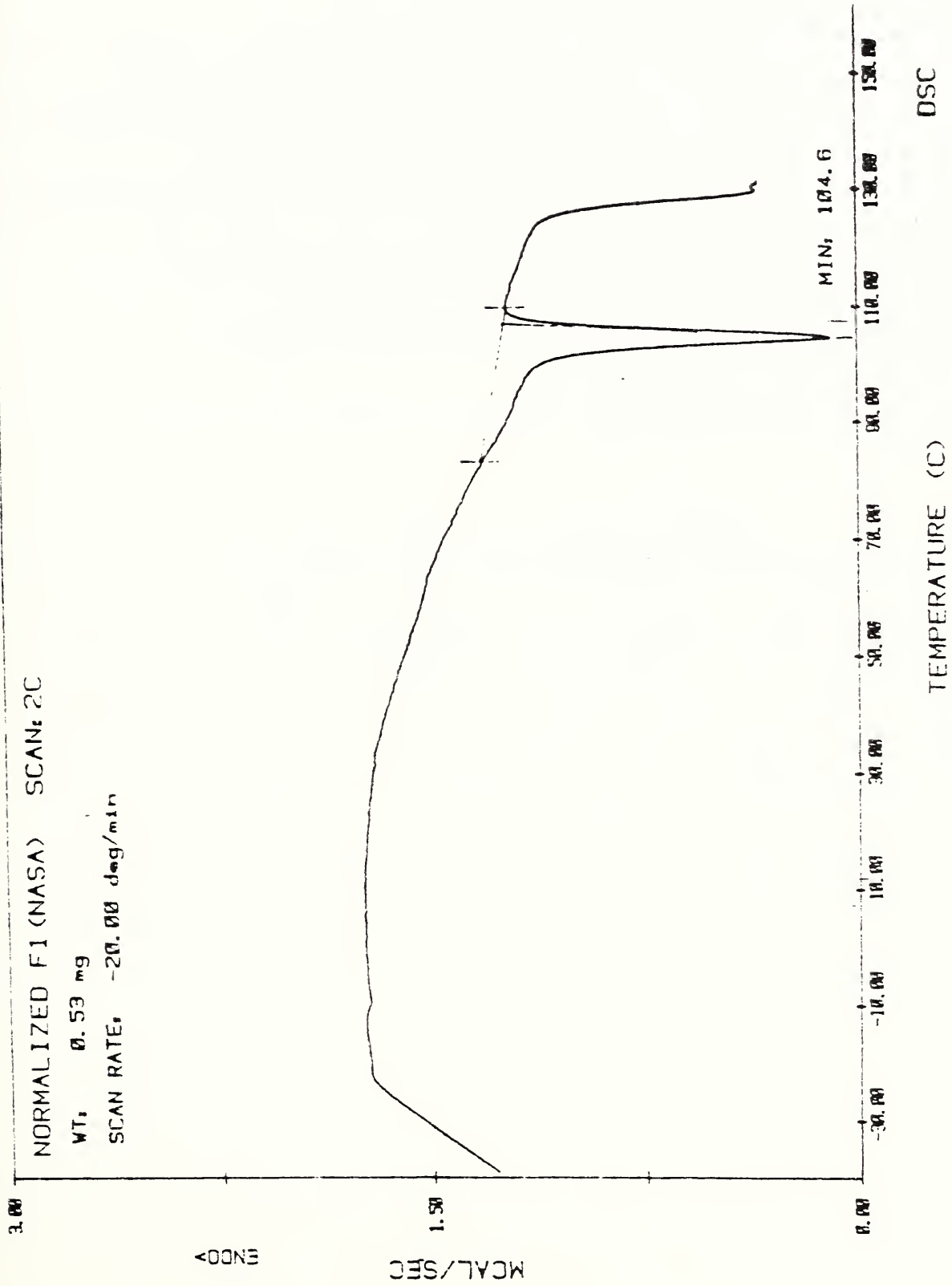
Fig. 39d. DSC scan of Film F1: Second cooling cycle

4. TITLE AND SUBTITLE

A Comparative Study of the Structure and Mechanical Properties of Polyethylene Films Used in Heavy Lift Balloons

5. AUTHOR(S) F. Khoury, J. M. Crissman, J. D. Barnes, B. M. Fanconi, H. L. Wagner, C. M. Guttman, J. R. Maurey, C. A. Harding, L. H. Bolz

11. ABSTRACT (A 200-word or less factual summary of most significant information. If document includes a significant bibliography or literature survey, mention it here)

Aspects of the mechanical properties and structure of three types of polyethylene film (I, III and Bl) used by NASA in helium filled heavy lift balloons have been investigated and compared. An additional film (Fl) which has as yet not been used in heavy lift balloons was also studied. The following are among the features which have been investigated:- Biaxial deformation behavior under inflation at 23°C and -73°C, biaxial creep under inflation at 23°C and -73°C, tensile properties at 23°C of unoriented specimens prepared by compression molding multilayers of the films, film shrinkage upon melting. The preferred orientation characteristics of the crystalline regions in the films were determined from pole figure coupled with small angle x-ray diffraction data. The possible morphological origins of the various orientation characteristics exhibited by the films are discussed with reference to three 'model' orientations and combinations thereof. Numerical simulations of the experimental pole figures of the films were attempted in an effort to compare differences in orientation among the films quantitatively. Finally, the following features which had been determined for films I, III and Bl in a previous study have been determined for the 'newer' film Fl: Chain branching, molecular weight and molecular weight distribution, intrinsic viscosity, melting/crystallization, density/crystallinity, birefringence, and tensile properties at 23°C (uniaxial extension in the machine and transverse directions).

12. KEY WORDS (Six to twelve entries; alphabetical order; capitalize only proper names; and separate key words by semicolons)

Balloon film; chain branching; density; intrinsic viscosity; molecular weight; orientation; polyethylene; tensile properties